Development of High-Throughput Fluorescence Polarization Immunoassay System by a Fluorescence Polarization Imaging Technique

蛍光偏光イメージングによる ハイスループット蛍光偏光イムノアッセイシステムの開発

Osamu Wakao

Graduate School of Chemical Sciences Engineering

Hokkaido University

Title Development of High-Throughput Fluorescence Polarization Immunoassay System by a Fluorescence Polarization Imaging Technique

Author Osamu Wakao

Degree Doctor of Philosophy (Engineering)

Supervisor Professor Manabu Tokeshi

CONTENTS

CHAPTER 1 General Introduction

1.1 Immunoassay

Immunoassays are widely used in clinical diagnoses, medical analyses, and food analyses, among others. The first immunoassay technique was reported by Berson et al. in 1956 as an analytical method utilizing a specific binding reaction between antigens and antibodies (antibody-antigen reaction) [1]. After Berson et al. reported a radioimmunoassay using radioactive iodine as a label, various immunoassays have been developed with the use of labeling reagents and measurement principles. Immunoassays are a highly sensitive, specific, and selective measurement technique for quantitative analyses because of the specific affinity of antibodies and antigens. For these reasons, immunoassays are widely used in fields such as medical, food, environment, and genome studies [2]. Additionally, owing to their versatility, commercially available immunoassay kits are sold, so those without specialized knowledge can use them.

Immunoassays are divided into heterogeneous immunoassays and homogeneous immunoassays depending on the reaction mechanism. Heterogeneous immunoassays are performed while immobilizing antibodies in the solid phase; on the other hand, homogeneous immunoassays are performed in solution from reaction to detection. A schematic illustration of a sandwich immunoassay, which is one of the most widely used heterogeneous immunoassays, is shown in Figure 1.1. In a sandwich immunoassay, an analyte is bound to an antibody, which is immobilized in the solid phase, and then the labeled antibody is bound to the analyte for quantification. In a heterogeneous immunoassay, an antibody immobilization process is necessary, so it is necessary to consider how to process the antibody immobilization and the influence of the immobilization. In addition, the separation of the analyte-antibody complex (bound) generated by the reaction from a free analyte/antibody (free) that is not bound to the antibody/analyte is necessary. The separation, namely bound/free (B/F) separation, is performed with several washings by inflowing and outflowing solution, so the operation procedure becomes complicated. Therefore, heterogeneous immunoassays typified by sandwich immunoassays may require tens of hours for all measurements [3]. However, since heterogeneous immunoassays are highly sensitive, they are used for analyses of very small amounts, and are conducted as the major immunoassay.

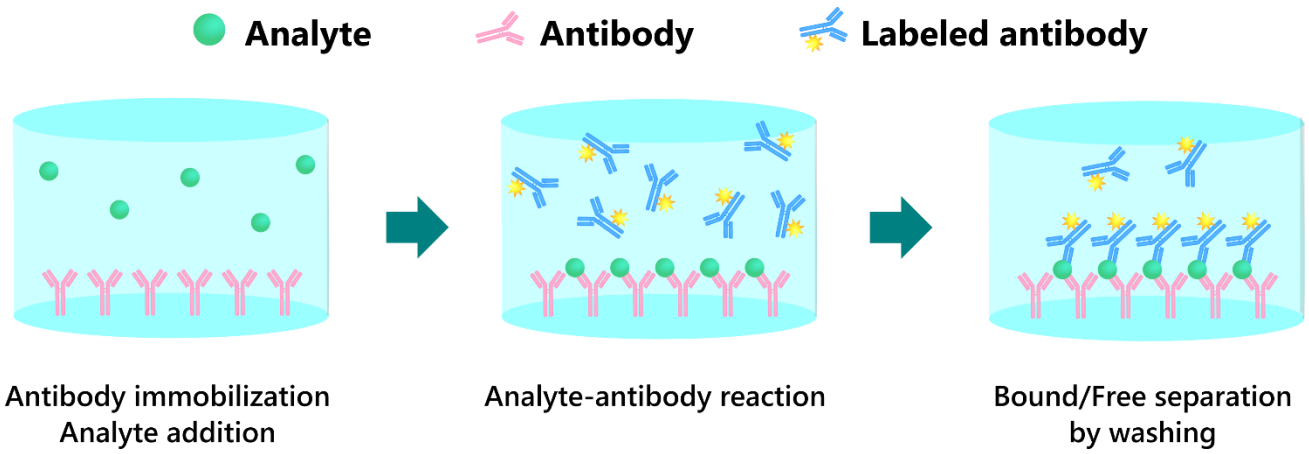

Figure 1.1 Schematic illustration of a sandwich immunoassay. Antibody immobilization onto a solid well is followed by analyte sample addition into the well. After washing, the labeled antibody is introduced into the well and the antibody-antigen reaction is conducted. Then, bound/free separation is performed with several washings by inflowing and outflowing solution and the measurement process is started. Washing is required between each step, so the operation procedure becomes complicated.

On the other hand, the homogeneous immunoassay does not require antibody immobilization or B/F separation, so the measurement operation is simple and faster. The homogeneous immunoassay is a solution-based immunoassay that is performed by analyte sample addition to the previously prepared antibody and labeled analyte solution. Generally, the sensitivity is lower than that of the heterogeneous immunoassay; however, its simplicity is suitable for on-site measurement and point-of-care testing (POCT) for small molecules [4].

1.1.1 Fluorescence Polarization

Fluorescence polarization (FP) is a versatile solution-based (homogeneous) method that enables the study of molecular interactions, such as protein-protein, protein-DNA, and protein-ligand binding interactions [5, 6]. Since this method is quick and easy to implement, it is expected to be applied as a high-throughput tool for protein-protein interaction and protein-DNA interaction analysis in drug discovery fields, among others. The basic principle of FP was reported by Perrin in 1926 [7], and it was first applied to immunoassays by

Dandliker et al. in 1961 [8]. They showed that FP immunoassays (FPIAs) could be directly measured by the antigen-antibody reaction using fluorescent-labeled ovalbumin and anti-ovalbumin antibodies. Since this study, FPIAs have been widely used mainly for low molecular detection [9, 10].

Fluorescent molecules are oriented in various directions in solution. If the fluorescent molecules stop moving when they are excited, then the direction of the dipole moment of the molecules is determined at the excitation state and the linear polarization of the excitation light is observed as FP. However, the fluorescent molecules rotate in Brownian motion in solution. When the fluorescent molecules rotate at a high speed in the excitation state, the direction of the moment becomes random and random FP is observed. This is called fluorescence depolarization, and the FP is affected by the motion condition of the molecules. In the FP measurement, *P*, namely the index of FP, is determined by the following equation:

$$P = (I_{\parallel} - I_{\perp})/(I_{\parallel} + I_{\perp}) \tag{1.1}$$

where $I_{\parallel}$ and $I_{\perp}$ are fluorescence intensities with parallel and perpendicular polarizations to the polarization of excitation light, respectively. According to Perrin (1926) [7], the value of *P* for a spherical molecule is given by the following equation:

$$\frac{1}{P} - \frac{1}{3} = \left(\frac{1}{P_0} - \frac{1}{3}\right)\left(1 + \frac{RT}{\eta V}\tau_0\right) \tag{1.2}$$

where R is the gas constant, *T* is the absolute temperature, η is the viscosity of the solvent, *V* is the molecular volume of the fluorescent molecule, and τ_0 is the lifetime of the excited state of the fluorescence. P_0 is the limit value of *P* when the viscosity is infinite. Acceding with Equation (1.2), the value of *P* is affected by the temperature and viscosity of the solvent. In addition, the value of *P* is affected by the size of the fluorescent molecule when the temperature and viscosity of the solvent are constant. Therefore, the molecular binding between the fluorescent-labeled molecule and target molecule (unlabeled) is observed as the FP difference between the free labeled molecule and complex molecule. Based on the FP method, an investigation method to determine the molecular binding constant between proteins and small molecules has been reported for the

first time by Laurence [11], and the FP method has been extended into the field of various biological interaction analyses [12-14].

1.1.2 Fluorescence Polarization Immunoassay

The FPIA based on the principle of the FP method, as mentioned in Section 1.1.1, was developed by Dandliker [8, 15, 16]. The FPIA is a homogeneous competitive immunoassay that is based on the competitive bind between hapten (target analyte) and a fluorescent-labeled target analyte (tracer) to antibodies. A standard curve is prepared from the changes in the degree of FP due to the competitive binding, and the target concentration is quantified from the calibration curve.

A schematic illustration of the change in FP by binding between tracer molecules and antibody molecules is shown in Figure 1.2. Unbound (free) tracer molecules and antibody molecules are free to rotate in solution, as shown in Figure 1.2(A). When polarized excitation light is irradiated, random FP is observed according to the dipole moment of the tracer molecules. On the other hand, when the tracers bind to the antibody molecules (tracer-antibody complex; Figure 1.2(B)), the whole molecular weight of the fluorescence molecules becomes larger and the rotational movement in the solution is suppressed compared to that of the free tracer. Therefore, FP is polarized to the direction of the excitation light polarization.

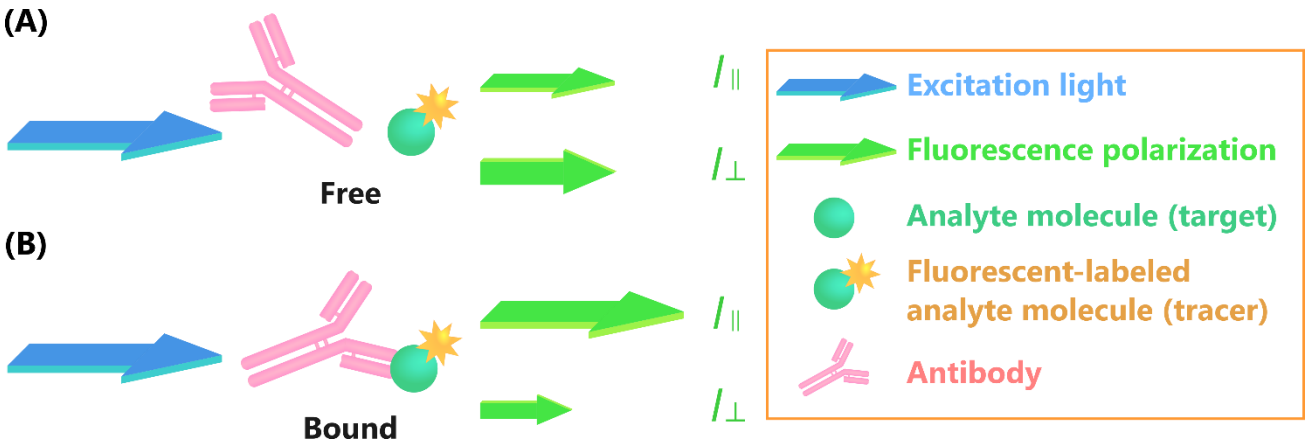

Figure 1.2 Schematic illustration of the change in fluorescence polarization (FP) by binding between the tracer molecules and antibody molecules. $I_{\parallel}$ and $I_{\perp}$ are the fluorescence intensities with parallel and perpendicular polarizations to the polarization of the excitation light, respectively. (A) The free tracer molecule and antibody molecule are free to rotate in solution. When polarized excitation light is irradiated, random FP is observed. (B) The bound tracer molecule rotates more slowly than the free tracer molecule, so FP is polarized to the excitation polarization.

Here, the concentration of the analyte present is considered, as shown in Figure 1.3. In FPIA, the amount of tracer molecules and antibody molecules are fixed as constant. The analyte molecules and tracer molecules competitively bind to the antibody molecules. When the analyte molecule concentration is low, as shown in Figure 1.3(A), most of the tracer molecules bind to the antibodies, so FP is polarized to the excitation polarization. On the other hand, when there is a high concentration of analyte, as shown in Figure 1.3(B), most of the analyte molecules bind to the antibodies, so free tracer molecules still exist and emit fluorescence with random polarization.

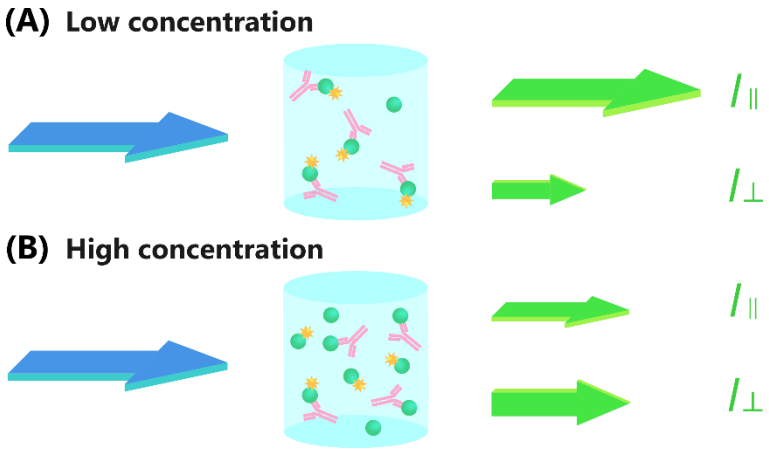

Figure 1.3 Schematic illustration of the fluorescence polarization (FP) immunoassay principle. $I_{\parallel}$ and $I_{\perp}$ are the fluorescence intensities with parallel and perpendicular polarizations to the polarization of excitation light, respectively. (A) When the analyte concentration is low, most of the tracer molecules bind to the antibodies, so FP is polarized to the excitation polarization. (B) When the analyte concentration is high, free tracers emit fluorescence with random polarization.

The *P* value, which is the degree of FP expressed by Equation (1.1), decreases as the analyte concentration increases. An example of a typical standard curve plotting FP against the analyte concentrations is shown in Figure 1.4 [17]. In FPIA, the analysis target is quantified using a sigmoidal calibration curve, as shown in Figure 1.4. The only required process for the quantification is mixing of the analyte, tracer, and antibody solutions. Because of its convenience, it is widely applied in research fields, such as the determination of drugs in blood in medical diagnoses [18], food analyses [19], and environmental hormone analyses [20]. According to Eremin [17], the measurable range of the FP is typically limited to a minimum of 30-60 mP to a maximum of 150-300 mP in the principle of FPIA. As a result, the measurable range is limited, so the analysis targets are sometimes limited. Based on this limitation of the FP response, FPIA is mainly used for the measurement of small molecules [5, 17, 21]. The reason for this is that the change in FP tends to be large by binding small molecules to large molecules.

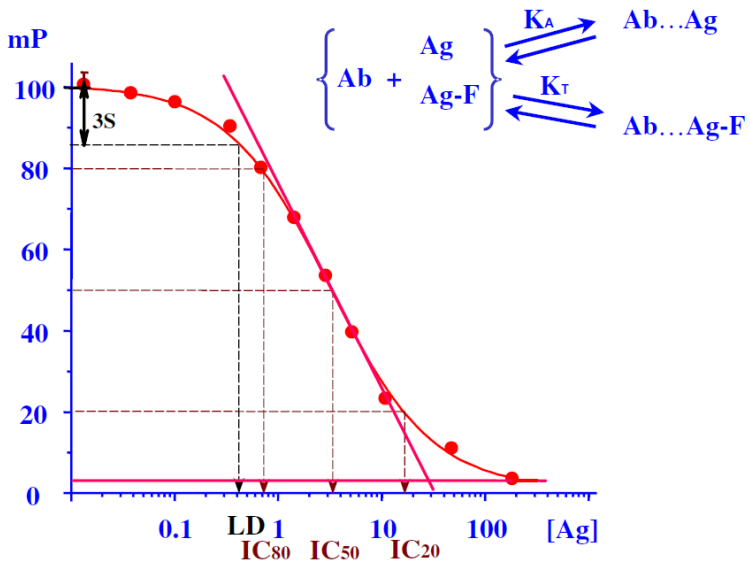

Figure 1.4 A typical standard curve plotting fluorescence polarization against the analyte concentrations (from Fig. 2. in Ref. 17). The unit of mP means one-thousandth of *P*. Ab, Ag, and Ag-F indicate antibody, analyte (target antigen), and fluorescent-labeled analyte (fluorescent-labeled antigen), respectively. IC_{80}, IC_{50}, and IC_{20} indicate 80%, 50%, and 20% inhibitory concentration, respectively. Limit of detection (LD) is identified from 3 standard division (3S) from the max value. *P* decreases as the analyte concentration increases, and the plot shows a sigmoidal curve.

FPIA does not require antibody immobilization, so it is able to measure antigen-antibody reactions in a sample solution as a direct signal. Additionally, it is extremely simple and the reaction and measurement times are very short. Moreover, FPIA is a ratio analysis that does not depend on the intensity of the excitation light and fluorescence; thus, in principle, *P* is constant regardless of the damage and photobleaching of fluorescence dyes. For these reasons, FPIA is expected to be applied to rapid analysis in various fields against the heterogeneous immunoassay, which is currently widely used as an analytical method and requires antibody immobilization. However, there are challenges; the optical system of the FP measurement system is complicated, the FP measurement apparatus is expensive, and simultaneous multi-sample FP measurement is not possible (for details see Chapter 2).

1.2 Microdevice

1.2.1 Micro Total Analysis System

Research on the integration of various chemical operations, such as mixing, reaction, separation, purification, and detection of samples and reagent solutions, onto a glass or plastic substrate chip, such as a semiconductor chip, has been rapidly developed in the past few decades [22]. Because a series of chemical manipulations are realized on the chip, it is called "lab on a chip." Because they handle microscale integration and microscale fluids, they are also called microdevices, microfluidics devices, integrated microchemical system, etc. Figure 1.5 provides the number of hits found from the search when the key word "lab-on-a-chip" was searched on Google Scholar for each corresponding year from 1990 to 2017. The increase in publications exemplified the increasing activity and interests in the research field.

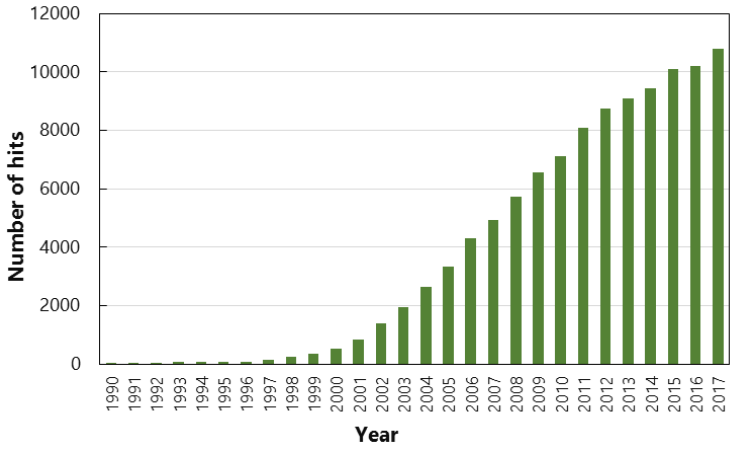

Figure 1.5 The number of hits found from the search "lab-on-a-chip" on Google Scholar for each corresponding year from 1990 to 2017. The increase in the number of hits of the key word exemplifies the increasing activity and interest in the research field.

The "lab-on-a-chip" research and developments are spread over all types of chemistry. In particular, in analytical chemistry, the application of analysis, separation, and measurement technology utilizing micro/nanotechnology is advanced in the fields of biochemistry, medical analysis, food analysis, and

environmental analysis. In 1990, Manz proposed the concept of a micro total analysis system (MicroTAS, μTAS), which micronizes the series of analysis operations [23]. MicroTAS is an analysis system for the micro reaction field, which is constructed by microstructures and microchannels on a substrate that is fabricated using semiconductor fabrication technologies. Figure 1.6 shows a schematic illustration of MicroTAS.

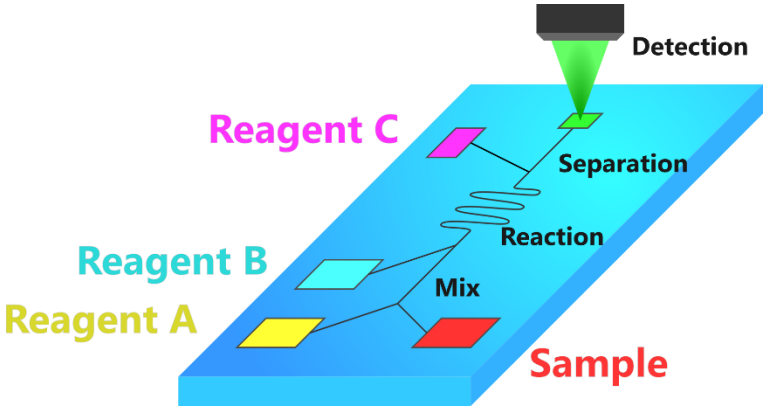

Figure 1.6 Schematic illustration of the micro total analysis system (MicroTAS).

The first study of a microscale analytical system was a gas chromatography system fabricated on a silicon substrate reported in 1979 [24]. Since then, various microdevices have been developed with the development of semiconductor fabrication technology and microfabrication technology. In the 1990s, the effectiveness in the field of biochemical analysis was recognized. Then, analysis using microdevices was significantly developed; analysis kits using microdevices are presently on the market. The features of the microscale space are related to the significant development of microdevices in analytical chemistry. The features include the reduction in consumption of samples and reagents, high reaction efficiency, rapidity by shortening the analysis/reaction time, low cost of the whole system, and versatility by simplification of operation, among others. These benefits are expected to contribute to environmental analyses, food analyses, and POCT diagnosis in clinical diagnoses [25]. For example, if biomarkers are detected at the bedside of patients using microdevices according to the measurement of body fluid samples of patients, such as blood, saliva, and tears,

then the burden on the patient will be alleviated. In environmental analyses, complex processes and long periods of time are required to detect dioxins and other harmful substances from natural samples. However, on-site collection and detection of natural samples is expected by using the microdevices.

1.2.2 Fluorescence Polarization Immunoassay on a Microdevice

Various analytical chemistry operations have been integrated onto microdevices that have microchannels of several micrometers to several hundred micrometers width as a reaction field. Typical semiconductor fabrication technology and microfabrication technology can easily use transparent materials, such as glass, silicon, and plastics, as substrates, so spectroscopic analysis is easily applied in analyses using microdevices. Since the sample to be measured exists in a microregion, microscopic spectroscopy is used. However, the sample volume enclosed in the three-dimensional space of the microchannel is of orders of approximately nanoliters to femtoliters, so highly sensitive microscopic spectroscopy is required for their signal detection. Therefore, innovative research on laser spectroscopy and fluorescence spectroscopy is conducted daily.

Some drug and protein detections by FPIA in microdevices have been reported [26-29]. Figure 1.7 provides the number of hits found from the search when the key words “fluorescence polarization” and “lab-on-a-chip” were searched on Google Scholar for each corresponding year from 1990 to 2017. The fluorescence polarization publications related to lab-on-a-chip increased as the number of publications related to lab-on-a-chip increased, as shown in Figure 1.5. They have developed measurement systems that combine the features of FPIA, where signals are generated only by mixing. The features of the microdevice include sample reduction, rapidity of analysis, highly reactive efficiency, and portability. These systems have the potential to contribute to clinical diagnoses, such as the measurement of drugs in blood and residual drug detection, environmental analyses, and food analyses. In opposition to the heterogeneous immunoassay, which has a complicated reaction process and operation, FPIA on microdevices is a simple, less costly, and

versatile measurement method. However, the optics of the measurement systems are complicated, and they cannot demonstrate simultaneous multi-sample measurement. Therefore, cost reduction and miniaturization of the whole system have not been achieved.

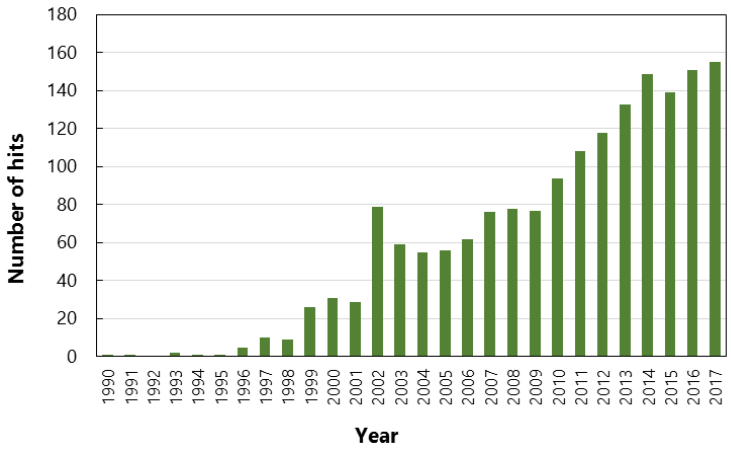

Figure 1.7 The number of hits found from the search "fluorescence polarization" and "lab-on-a-chip" on Google Scholar for each corresponding year from 1990 to 2017. The number of fluorescence polarization publications related to lab-on-a-chip increased as the number of publications related to lab-on-a-chip increased (Figure 1.5).

References

[1] S. A. Berson, R. S. Yalow, A. Bauman, M. A. Rothchild, and K. Newerly, *J. Clin. Invest.*, **35**, 170-190 (1956)

[2] G. H. W. Sanders and A. Manz, *Trends Anal. Chem.*, **19**, 364-378 (2000)

[3] K. Sato, M. Tokeshi, H. Kimura, and T. Kitamori, *Anal. Chem.*, **73**, 1213-1218 (2001)

[4] N. Kobayashi, H. Ueda, S. Miyake, and H. Arakawa, The Immunoassay: Basics and Applications (in Japanese), 3rd edition: Kodansha, pp. 17-18 (2016)

[5] W. A. Lea and A. Simeonov, *Expert Opin. Drug Discov.*, **6**, 17-32 (2012)

[6] D. M. Jameson and J. A. Ross, *Chem. Rev.*, **110**, 2685-2708 (2010)

[7] F. Perrin, *J. Phys. Radium*, **7**, 390-401 (1926)

[8] W. B. Dandliker and G. A. Feigen, *BBRC*, **5**, 299-304 (1961)

[9] M. E. Jolley, *JAT*, **5**, 236-240 (1981)

[10] M. E. Jolley, S. O. Stroupe, C. J. Wang, H. N. Panas, C. L. Keegan, R. L. Schmidt, and K. S. Schwenzer, *Clin. Chem.*, **27**, 1190-1197 (1981)

[11] D. J. R. Laurence, *Biochem J.*, **51**, 168-180 (1951)

[12] H. Zhang, P. Nimmer, S. H. Rosenberg, S. Ng, and M. Joseph, *Anal. Biochem.*, **307**, 70-75 (2002)

[13] M. S. Ozers, K. M. Ervin, C. L. Steffen, J. A. Fronczak, C. S. Lebakken, K. A. Carnahan, R. G. Lowery, and T. J. Burke, *Mol. Endocrinol.*, **19**, 25-34 (2004)

[14] C. V. Kumar and E. H. Asuncion, *J. Am. Chem. Soc.*, **115**, 8541-8553 (1993)

[15] W. B. Dandliker, M. Hsu, J. Levin, and B. R. Rao, *Methods Enzymol.*, **74**, 3-28 (1981)

[16] W. B. Dandliker, R. J. Kelly, J. Dandliker, J. Farquhar, and J. Levin, *Immunochemistry*, **10**, 219-227 (1973)

[17] D. S. Smith and S. A. Eremin, *Anal. Bioanal. Chem.*, **391**, 1499-1507 (2008)

[18] Z. Wang, S. Zhang, I. S. Nesterenko, S. A. Eremin, and J. Shen, *J. Agric. Food Chem.*, **55**, 6871-6878 (2007)

[19] R. Bhat, R. V. Rai, and A. A. Karim, *CRFSFS*, **9**, 57-81 (2010)

[20] T. Guan, Y. Sun, T. Zhang, T. Li, Z. Li, Y. Zhang, J. Zhang, and Y. Wang, *J. Soils. Sediments*, **18**, 845-851 (2018)

[21] J. A. Cruz-Aguado and G. Penner, *Anal. Chem.*, **80**, 8853-8855 (2008)

[22] E. K. Sackmann, A. L. Fulton, and D. J. Beebe, *Nature*, **507**, 181-189 (2014)

[23] A. Manz, N. Graber, and H. M. Widmer, *Sens. Actuators B*, **1**, 244-248 (1990)

[24] S. C. Terry, J. H. Jerman, and J. B. Engell, *IEEE Trans. Electron Device*, **26**, 1880-1886 (1979)

[25] P. Yager, T. Edwards, E. Fu, K. Helton, K. Nelson, M. R. Tam, and B. H. Weigl, *Nature*, **442**, 412-418 (2006)

[26] H. N. Joensson, C. Zhang, M. Uhlen, and H. Andersson-Svahn, *Electrophoresis*, **33**, 436-439 (2012)

[27] J. Choi, D. Kang, H. Park, A. J. deMello, and S. Chang, *Anal. Chem.*, **84**, 3849-3854 (2012)

[28] T. Tachi, N. Kaji, M. Tokeshi, and Y. Baba, *Lab. Chip.*, **9**, 966-971 (2009)

[29] T. Tachi, T. Hase, Y. Okamoto, N. Kaji, T. Arima, H. Matsumoto, M. Kondo, M. Tokeshi, Y. Hasegawa, and Y. Baba, *Anal. Bioanal. Chem.*, **401**, 2301-2305 (2011)

CHAPTER 2 Fluorescence Polarization Measurement System Using a Liquid Crystal Layer and Image Sensor

2.1 Introduction

Fluorescence polarization (FP) is a versatile solution-based (homogeneous) method that enables the study of molecular interactions, such as protein-protein, protein-DNA, and protein-ligand binding [1, 2]. Since this method is quick and easy to implement, it is widely used in clinical and biomedical applications. In particular, FP immunoassay (FPIA), which combines FP and competitive immunoassay, is a well-established technique for monitoring therapeutic drugs in the blood and quantitative analysis of drug residues in foods [3, 4].

Previously, FPIA on a microfluidic device was developed and realized the quantitative analysis of theophylline in serum in about 1 min [5]. Furthermore, the concentration of theophylline in sera of patients was measured using a microfluidic device-based-FPIA [6]. The combination of FPIA and a microfluidic device leads to rapid and easy-to-use low-cost analysis with low consumption of samples and reagents. In addition to this combination, a combination of FP and droplet-based microfluidic devices was used to analyze protein-protein interactions [7-9] and to apply FPIA [10]. These achievements demonstrate the usefulness of these combinations for small sample size analysis in medical and biological applications. However, they are all the result of a single analysis or assay, not multiple analyses or assays. This is because it is intrinsically difficult for the FP method to measure multiple samples simultaneously. In the FP measurement, P, namely the index of FP, is determined by the following equation:

$$P = (I_{\parallel} - I_{\perp})/(I_{\parallel} + I_{\perp}) \qquad (2.1)$$

where $I_{\parallel}$ and $I_{\perp}$ are the fluorescence intensities with parallel and perpendicular polarizations to the excitation plane, respectively. Therefore, to obtain P, $I_{\parallel}$ and $I_{\perp}$ must be measured separately. A schematic illustration of the components of a conventional FP system is shown in Figure 2.1, and a photo of a typical apparatus is shown in Figure 2.2. In the conventional FP measurement system, an excitation light from a light source is linearly polarized to one direction by a polarizer and then the excitation light enters a sample in a cuvette. Fluorescence from the sample is separated into parallel polarization and perpendicular polarization using a rotating polarizer. The fluorescence intensities with parallel ($I_{\parallel}$) and perpendicular ($I_{\perp}$) polarizations are

detected using a photodiode for each polarization. Therefore, two fluorescence intensity measurements are required for one sample measurement, so it is difficult to perform simultaneous measurements of multiple samples. In addition, a driver for the rotating polarizer is necessary, so the whole measurement system becomes large and expensive.

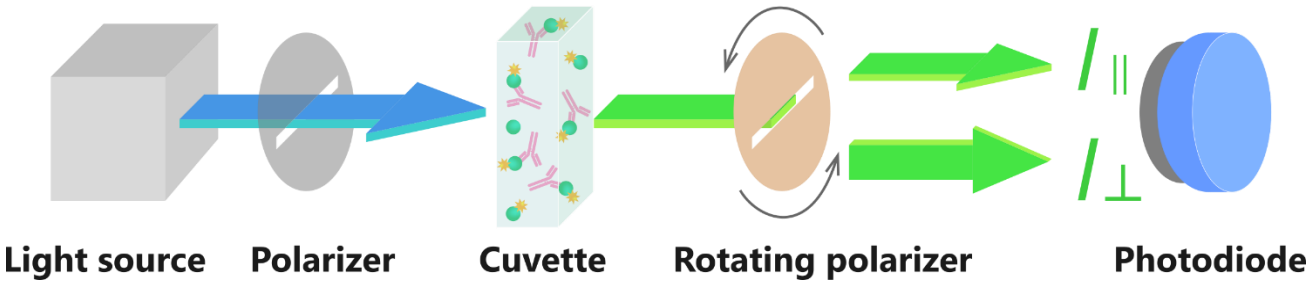

Figure 2.1 Schematic illustration of the components of a conventional fluorescence polarization system. Excitation light from a light source is linearly polarized by a polarizer, and then the excitation light enters a sample in a cuvette. Fluorescence from the sample is separated into parallel and perpendicular polarization by a rotating polarizer. The fluorescence intensities ($I_{\parallel}$ and $I_{\perp}$) are detected by a photodiode for each polarization.

Figure 2.2 Photo of a conventional commercial fluorescence polarization (FP) apparatus (FP-715, JASCO Co., Tokyo, Japan). A cuvette is used as the sample cell and the number of samples is limited to one for each measurement.

A combination of a polarizer and rotating polarizer [5, 6] or of a polarizer and polarizing beam splitter [7, 8] is usually used for the measurements. In order to measure multiple samples, it is necessary to scan the optical component including the polarizers or scan the samples. The scanning is required for both microfluidic

device-based FP measurement and FP measurement on microplates. Actual commercial microplate readers for high-throughput screening FP assays adopt an optical scanning method [11]. However, these are not suitable for the microfluidic device-based FP measurement because downsizing is not easy when there is a drive component.

Here, a unique FP measurement system based on the synchronization between the orientation of the liquid crystal (LC) molecules of a LC display (LCD) and the sampling frequency of an image sensor to realize simultaneous FP analysis or assay of multiple samples was developed. The system can acquire a two-dimensional image of FP. This feature allows the FP of multiple samples to be acquired for the image simultaneously. Therefore, the system can measure the FP of multiple samples simultaneously without scanning the optical component or samples, which is a significant advantage over conventional FP systems. In this chapter, first, a proof-of-concept demonstration of our FP measurement system for the viscosity dependence of FP of a fluorescein sample in water-ethylene glycol solution is presented. Second, the demonstration of simultaneous FPIA of multiple prostaglandin E2 (PGE2) samples is discussed. To the best of our knowledge, this was the first demonstration of simultaneous FP and FPIA of multiple samples. The performance of the system was compared with that of a commercial FP apparatus, and it was confirmed that the system had performance equal to that of the commercial apparatus. Furthermore, this system has great potential for apparatus downsizing and cost reduction.

2.2 Principle (Liquid Crystal-Charge Coupled Device Synchronization Detection)

A unique detection system for simultaneous FP analysis or assay of multiple samples was based on the synchronization between the LC layer orientation and the charge coupled device (CCD) sampling frequency (LC-CCD synchronization detection system). A concept illustration of the components of the developed FP system is shown in Figure 2.3. In a new FP measurement system, a LC layer, microdevice, and image sensor are used instead of a rotating polarizer, cuvette, and image sensor, respectively. The LC display (LCD) is disassembled into a LC layer and a polarizing filter. A set of a LC layer and polarizing filter can modulate the

value of FP. When the modulated signal is synchronously detected by an image sensor, *P* is measured in a single measurement. By synchronous detection using an image sensor, *P* is acquired as a two-dimensional image, namely *P* image; thus, the system can realize simultaneous multi-sample measurement. Simultaneous FP measurement of multiple samples is expected through image detection of multiple samples integrated in a microdevice, and the system is expected to apply a rapid and low-cost analysis. Additionally, by using an inexpensive compact LCD and image sensor, the complicated components of the conventional system are eliminated; thus, the whole system is expected to be constructed as a small and inexpensive system. Furthermore, the system realizes simultaneous FP measurements of multiple samples, so the total measurement time and total measurement cost decrease.

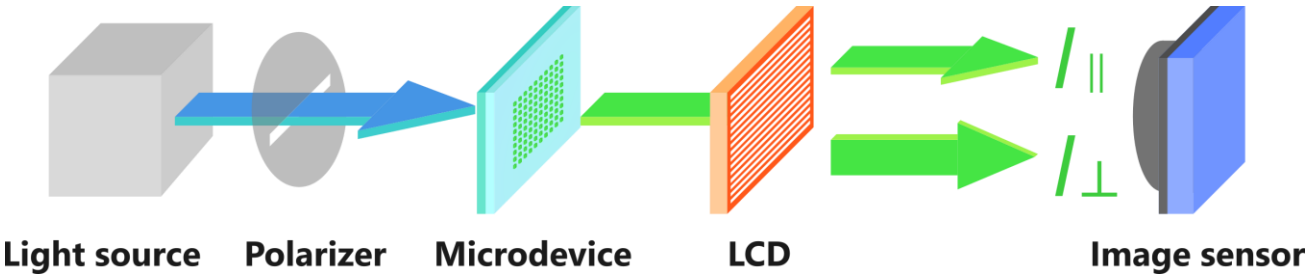

Figure 2.3 Concept illustration of the components of the developed fluorescence polarization system. Excitation light from a light source is linearly polarized by a polarizer, and then the excitation light enters a sample in a microdevice. Fluorescence from the sample is modulated by a liquid crystal display (LCD). The modulated fluorescence intensities ($I_{\parallel}$ and $I_{\perp}$) are synchronously detected by an image sensor.

2.2.1 Liquid Crystal Display

2.2.1.1 Overview of the liquid crystal display

LC material was reported as a thermotropic LC by Reinitzer in 1888 [12]. After the discovery that the phase change of LC can be controlled by the voltage applied to the LC [13], the world's first LCD was developed in 1968 [14]. The twisted nematic (TN) mode LCD, which has a lower power consumption, was developed in the 1970s [15]. The TN mode LCDs were mainly applied to the display parts of digital devices,

such as calculators, watches, and word processors, and they became popular. In Japan, in the early 1970s, LCDs were adopted as the display device of battery-driven calculators. LCDs became popular in the fields of television, and the first color television using a LCD was created in Japan by Seiko Epson Co. in 1984 [16]. During the 1990s, applications expanded not only to some devices for still images, but also to displays that handle moving photos, such as televisions, laptop computers, and car navigation systems. The LCD was significantly developed in the field of television displays instead of cathode ray tube displays, which were the mainstream at the time. In the 2000s, some industries in East Asia penetrated the LCD market, so the production cost decreased. Additionally, because of the development of small devices that employ LCDs, such as mobile phones, smart phones, and portable music players, the price of LCDs further decreased. According to Konoike's article from All About [17], the price of a 32-inch LCD television changed in Japan, as shown in Figure 2.4. Although Figure 2.4 provides the price trends for LCD televisions, price changes for small LCDs are very dynamic, and the price is currently a few hundred yen per inch.

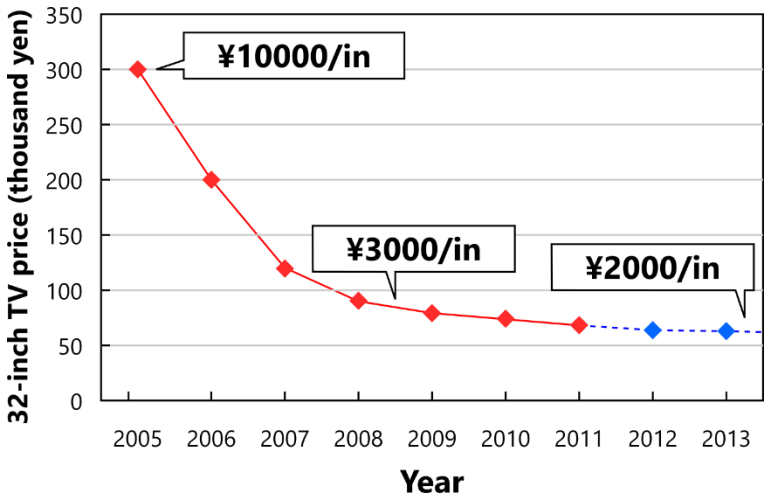

Figure 2.4 Price trends of 32-inch liquid crystal display televisions in Japan modified from the All About article "Material price soaring! Is the price of flat screen TVs as well?!" written by Konoike [17].

2.2.1.2 The operation principle of the liquid crystal display

Generally, LCDs consist of a light source, a driving and power supply circuit, a LC layer, and a polarizing filter. By changing the transmittance of the light from the backlight, a LCD changes its images. A schematic illustration of a typical LCD is shown in Figure 2.5. The LCD consists of four components, namely a backlight, first polarizing filter, LC layer, and second polarizing filter. The backlight, as the light source, has various polarizations. However, the first polarizing filter lets only parallel polarized backlight pass through, thereby absorbing other backlight that has other polarizations. After passing through the first polarizing filter, the backlight enters the LC layer as linearly polarized light. In the LC layer, the polarization of backlight is changed according to the state of the LC molecules because of its birefringence characteristics. To change the state of LC molecules, the voltage applied to the LC layer that changes the orientation direction of the LC molecules is controlled. According to the change in LC molecule orientation, the overall transmittance including the two polarizing filters and the LC layer changes, and then the brightness of the screen is changed. The LCD is based on the mechanism of an optical shutter. There are two types of LCD modes, namely normally white type and normally black mode. When a voltage is applied to the LC layer, normally white type displays a white, bright image. On the other hand, when a voltage is applied to the LC layer, normally black mode displays a black, dark image.

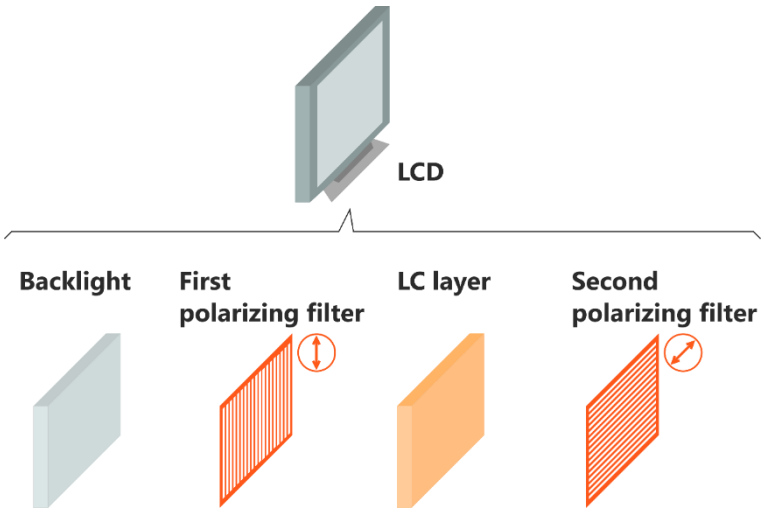

Figure 2.5 Schematic illustration of a liquid crystal display (LCD). The LCD consists of four components, namely a backlight, first polarizing filter, LC layer, and second polarizing filter.

A schematic illustration of the operation principle using the normally white type LCD employing a twisted nematic mode is shown in Figure 2.6. In the LCD mode, the transmission directions of the polarizing filters on the incident side and the outgoing side are placed orthogonal to each other. When a voltage is applied to the LC layer, the LC molecules align in the electric field direction so that the backlight passes through the LC layer without any polarization conversion. The transmitted polarization of the backlight is kept in the direction of the first polarizing filter and reaches the second polarizing filter, which blocks the backlight. As a result, when a voltage is applied to the LC layer, the backlight cannot pass through the second polarizing filter, so the LCD displays a black image. In contrast, when no voltage is applied to the LC layer, the orientation of the LC molecules is twisted by 90°. The twist causes the polarization conversion of the backlight by 90° while passing through the LC layer. As a result, when no voltage is applied to the LC layer, the backlight can pass through the second polarizing filter, so the LCD displays a white display. In the case of the TN type LCD, in order to orient the LC molecules without any damage, a square wave alternating current is applied to the LC layer at about 50-60 Hz when the applied voltage is turned on. Generally, the LC molecules are polarized when the frequency of the voltage is applied at the order of tens of microseconds, so the LC molecules in the LC layer are not affected at about 50-60 Hz. Therefore, the LC molecules are gradually oriented to the desired

arrangement while the applied voltage turns on to the LC layer. It is not clarified in detail how the individual LC molecules move owing to voltage changes in the LC mixture of the LC layer; however, it is well established that the transmittance polarization from the LC layer is controlled at the macro scale [18].

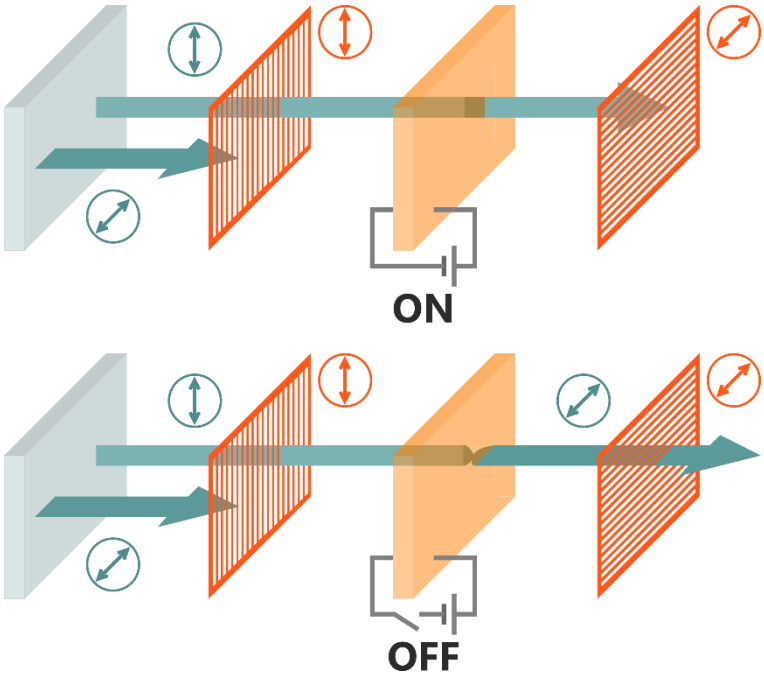

Figure 2.6 Schematic illustration of the operation principle using the normally white type liquid crystal display employing a twisted nematic mode.

2.2.2 Charge Coupled Device Synchronization Detection

2.2.2.1 Overview of charge coupled device synchronization detection

The CCD synchronization detection is a method of synchronizing the CCD image sensor with the signal frequency. The amplitude component (AC) of the signal is then calculated from the obtained image. Because of this method, it is possible to image the signal separated from the background and to acquire a two-dimensional image of the target signal with a short measurement time [19]. In the CCD synchronization detection, the AC and the direct component (DC) of the modulated target signal are separated and imaged, respectively.

Here, the concept illustration of the CCD synchronization detection utilizing four images in a period for light intensity modulated at f Hz is shown in Figure 2.7. A similar mathematical expression has been proposed to obtain optical beat images [19].

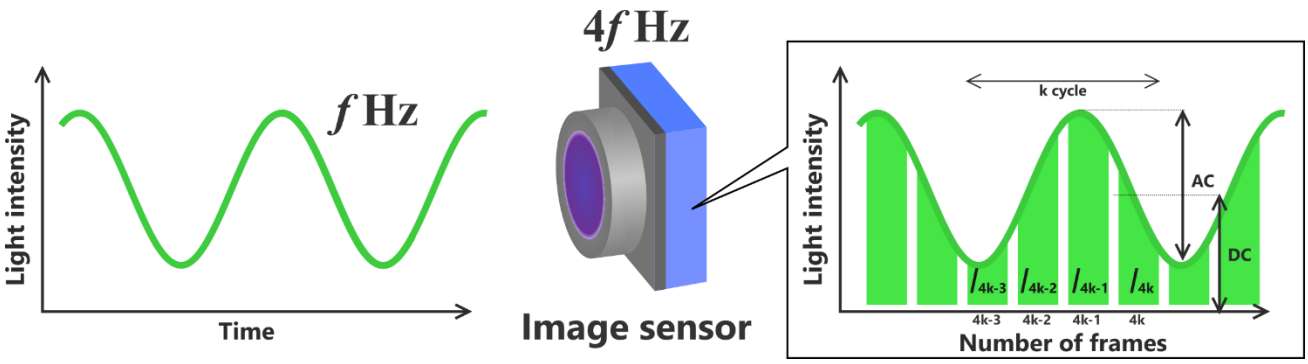

Figure 2.7 Concept illustration of the charge coupled device synchronization detection for light intensity modulated at f Hz. The image sensor is operated at 4f Hz sampling frequency and captures the images; four images are obtained in a single signal modulation cycle. The amplitude component (AC) and direct component (DC) are separated, respectively.

The light intensity at a certain pixel is denoted as follows:

$$F(t) = d + r\ sin(\theta_0 + \varphi t) \qquad (2.2)$$

where d and r are the direct and alternative amplitudes, respectively, and φ and θ_0 are the angular frequency ($\frac{2\pi}{T}$; T is the period) and the initial angle (phase shift), respectively. Each pixel of the image sensor accumulates the charge corresponding to the light intensity for the integration time. The integration time is set as one-fourth of the period T. The temporal sine waveform and parameters are shown in Figure 2.8.

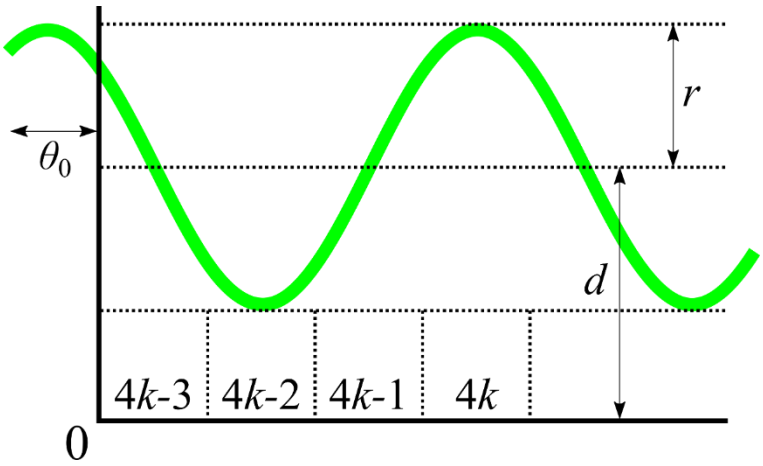

Figure 2.8 Temporal sine waveform and parameters at the *k*th cycle, where *d* and *r* are the direct and alternative amplitudes, respectively, and θ_0 is the initial angle (phase shift).

The accumulated charges of the quarter periods at the *k*th cycle of the wave are expressed as I_{4k-3}, I_{4k-2}, I_{4k-1}, and I_{4k} by the temporal integration of the light intensity. For example, I_{4k-3} is expressed as follows:

$$I_{4k-3} = \int_0^{T/4}\{d + r\sin(\theta_0 + \varphi t)\}dt = \left[dt - \frac{r}{\varphi}\cos(\theta_0 + \varphi t)\right]_0^{T/4}$$

$$= \frac{T}{4}d - \frac{r}{\varphi}\left\{\cos\theta_0 - \cos\left(\theta_0 + \frac{\pi}{2}\right)\right\} \qquad (2.3)$$

Here, the relationship $\frac{T}{4}\varphi = \frac{T}{4}\frac{2\pi}{T} = \frac{\pi}{2}$ is used. By utilizing the trigonometric function formula, the following equation is obtained:

$$I_{4k-3} = \frac{T}{4}d - \frac{r}{\varphi}\left\{\cos\left(\theta_0 + \frac{\pi}{2}\right) - \cos\theta_0\right\}$$

$$= \frac{T}{4}d + \frac{r}{\varphi}(\sin\theta_0 + \cos\theta_0) \qquad (2.4)$$

Similarly, I_{4k-2}, I_{4k-1}, and I_{4k} can be expressed as follows:

$$I_{4k-2} = \frac{T}{4}d - \frac{r}{\varphi}\left\{\cos(\theta_0 + \pi) - \cos\left(\theta_0 + \frac{\pi}{2}\right)\right\}$$

$$= \frac{T}{4}d + \frac{r}{\varphi}(-\sin\theta_0 + \cos\theta_0) \qquad (2.5)$$

$$I_{4k-1} = \frac{T}{4}d - \frac{r}{\varphi}\left\{\cos\left(\theta_0 + \frac{3\pi}{2}\right) - \cos(\theta_0 + \pi)\right\}$$

$$= \frac{T}{4}d + \frac{r}{\varphi}(-\sin\theta_0 - \cos\theta_0) \quad (2.6)$$

$$I_{4k} = \frac{T}{4}d - \frac{r}{\varphi}\left\{\cos(\theta_0 + 2\pi) - \cos\left(\theta_0 + \frac{3\pi}{2}\right)\right\}$$

$$= \frac{T}{4}d + \frac{r}{\varphi}(\sin\theta_0 - \cos\theta_0) \quad (2.7)$$

Then, the AC (amplitudes of signal) and DC (background) are defined and calculated as follows:

$$\text{AC} = \sqrt{(I_{4k-3} - I_{4k-1})^2 + (I_{4k-2} - I_{4k})^2}$$

$$= \frac{2r}{\varphi}\sqrt{(\cos\theta_0 + \sin\theta_0)^2 + (\cos\theta_0 - \sin\theta_0)^2}$$

$$= \frac{2r}{2\pi/T}\sqrt{(\cos\theta_0 + \sin\theta_0)^2 + (\cos\theta_0 - \sin\theta_0)^2}$$

$$= \frac{Tr}{\pi}\sqrt{2(\cos^2\theta_0 + \sin^2\theta_0)}$$

$$= \frac{\sqrt{2}T}{\pi}r \quad (2.8)$$

$$\text{DC} = \frac{I_{4k-3} + I_{4k-2} + I_{4k-1} + I_{4k}}{4} = \frac{1}{4} \times \frac{T}{4}d \times 4 = \frac{T}{4}d \quad (2.9)$$

The most important characteristic of Equations (2.8) and (2.9) is that they are independent of θ_0. This means that the initial angle (phase shift) of each pixel does not affect the calculation of the alternative amplitudes and DC. In other words, even with an initial angle difference between the pixels, or with a slow scan rate, the AC and DC can be obtained accurately.

2.2.2.2 Liquid crystal-charge coupled device synchronization detection

A unique principle for FP measurement based on the synchronization between the LC layer orientation and the image sensor sampling frequency (LC-CCD synchronization detection system) was developed. A concept illustration of the components of the developed FP system is shown in Figure 2.3. A set of LC layers and polarizing filters can modulate the value of the fluorescence intensities of each polarization ($I_{\parallel}$ and $I_{\perp}$). When the modulated FP signal is synchronously detected by an image sensor, *P* is measured as one single image.

By synchronous detection using an image sensor, *P* is acquired as a two-dimensional image, namely a *P* image; thus, the system can realize simultaneous measurement of multiple samples.

The LCD was disassembled to only use a LC layer and second polarizing filter. Figure 2.9 shows the operation principle of the normally white LCD employing a twisted nematic mode when the first polarizing filter was omitted. As mentioned above, the LC molecules are normally twist oriented by 90°. When no voltage is applied, the light passes through the second polarizing filter in the same way as that in Figure 2.6, but the light also passes through the second polarizing filter when the voltage is applied. When the voltage is applied, the light passing through the second polarizing filter has the same polarization direction as the second polarizing filter. On the other hand, the light passing through the second polarizing filter is the light with the polarization direction rotated by 90° before passing through the LC layer when no voltage is applied. Therefore, the polarization direction of the light that passes through the second polarizing filter can be controlled by on-off switching of the voltage applied to the LC layer.

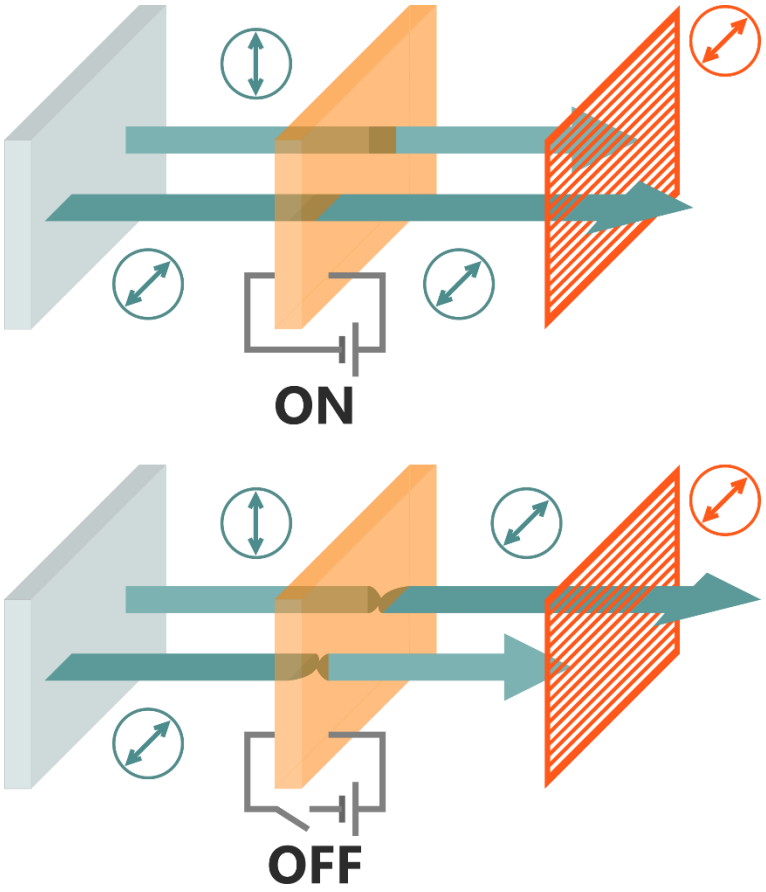

Figure 2.9 Schematic illustration of the operation principle of the normally white liquid crystal display employing a twisted nematic mode without the first polarizing filter.

In a commercially available LCD, the applied voltage that controls the LC molecule orientation is varied depending on the gray scale of the image to be displayed. For this reason, it is possible to modulate the polarization using cyclical grayscale gradation changes. When a low grayscale image is displayed, the voltage is applied to the LC layer and the polarization is maintained. Conversely, when a high grayscale image is displayed, no voltage is applied to the LC layer and the polarization is rotated. By cyclically changing the grayscale, as shown in Figure 2.10(A), the polarization that passes through the second polarizing filter is modulated, as shown in Figure 2.10(B).

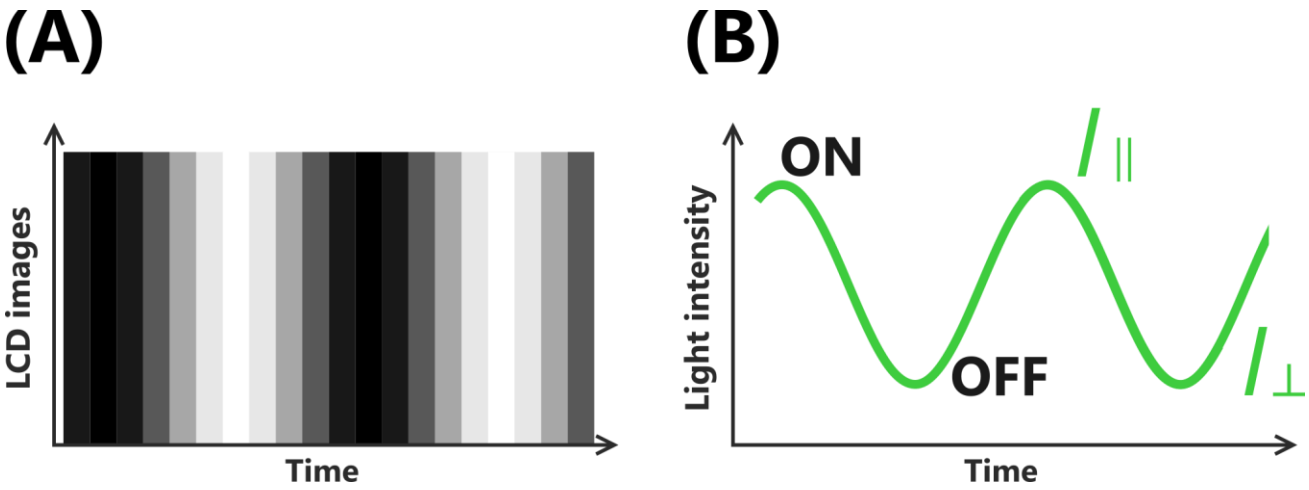

Figure 2.10 Temporal sine waveform by cyclical grayscale gradation changes. (A) The grayscale of the liquid crystal display (LCD) image is gradually changed. (B) Polarization that passes through the second polarizing filter is modulated depending on the grayscale gradation changes.

In this way, the polarization modulation method for FP using a set of a LC layer and polarizing filter was devised. The strategy for the FP measurement is shown in Figure 2.11. The polarization direction of fluorescence that is emitted from the sample changes as it passes through the polarizing filter owing to on-off switching of the voltage. When the voltage is on or off, fluorescence passing through the polarizing filter has parallel ($I_{\parallel}$) or perpendicular ($I_{\perp}$) polarization to the excitation plane, respectively. Then, fluorescence ($I_{\parallel}$ or $I_{\perp}$) passing through the polarizing filter is modulated on a certain frequency (f) by on-off switching of the voltage. When such fluorescence is detected by an image sensor (such as a CCD and CMOS sensor), which is operated at 4f Hz sampling frequency and captures the images, four images are obtained in a single modulation cycle.

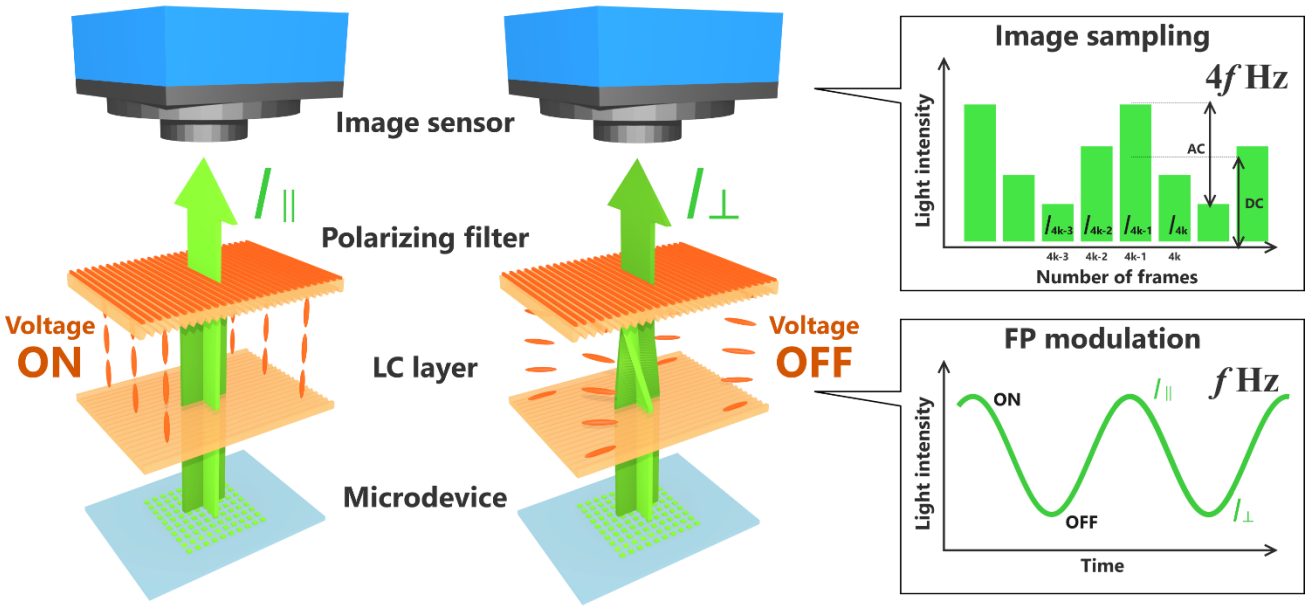

Figure 2.11 Strategy for the fluorescence polarization (FP) measurement. Schematic of the polarization direction of fluorescence that is emitted from the sample as it changes when passing through the polarizing filter owing to on-off switching of the voltage. Fluorescence ($I_{\parallel}$ and $I_{\perp}$) passing through the polarizing filter is modulated at f Hz by on-off switching of the voltage. An illustration of a histogram of the images captured at $4f$ Hz is shown in the balloon. The four images were obtained in a single modulation cycle.

By processing these four images, an AC and DC of the sinusoidal fluorescence intensities acquired at $4f$ Hz are obtained using Equations (2.8) and (2.9), respectively. Here, $2r$ is the amplitude of the signal and d is the mean value of the fluorescence intensities, so Equations (2.8) and (2.9) are transformed as follows:

$$\mathrm{AC} = \sqrt{(I_{4k-3} - I_{4k-1})^2 + (I_{4k-2} - I_{4k})^2} = \frac{\sqrt{2}T}{\pi} r = \frac{\sqrt{2}T}{2\pi}(I_{\parallel} - I_{\perp}) \quad (2.10)$$

$$\mathrm{DC} = \frac{I_{4k-3}+I_{4k-2}+I_{4k-1}+I_{4k}}{4} = \frac{T}{4} d = \frac{T}{8}(I_{\parallel} + I_{\perp}) \quad (2.11)$$

By modifying these equations, P is given as Equation (2.12).

$$P = \frac{I_{\parallel}-I_{\perp}}{I_{\parallel}+I_{\perp}} = \frac{2\mathrm{r}}{2\mathrm{d}} = \frac{\frac{\pi}{\sqrt{2}\mathrm{T}}}{\frac{4}{\mathrm{T}}} \frac{\mathrm{AC}}{\mathrm{DC}} = \frac{\pi}{4\sqrt{2}} \frac{\mathrm{AC}}{\mathrm{DC}} \quad (2.12)$$

Thus, P is obtained from each pixel of the image sensor regardless of the fluorescence intensity and phase delay. Therefore, it is possible to simultaneously obtain the P value of all the samples in the view of the image sensor as a two-dimensional image. The luminance value of the two-dimensional image, namely the P image, can directly reflect the P values of the multiple samples.

2.3 Experimental

2.3.1 Liquid Crystal-Charge Coupled Device Synchronization Detection System

Figure 2.12 shows a schematic illustration of the experimental setup of the FP detection system for FP measurements based on the LC-CCD synchronization detection principle.

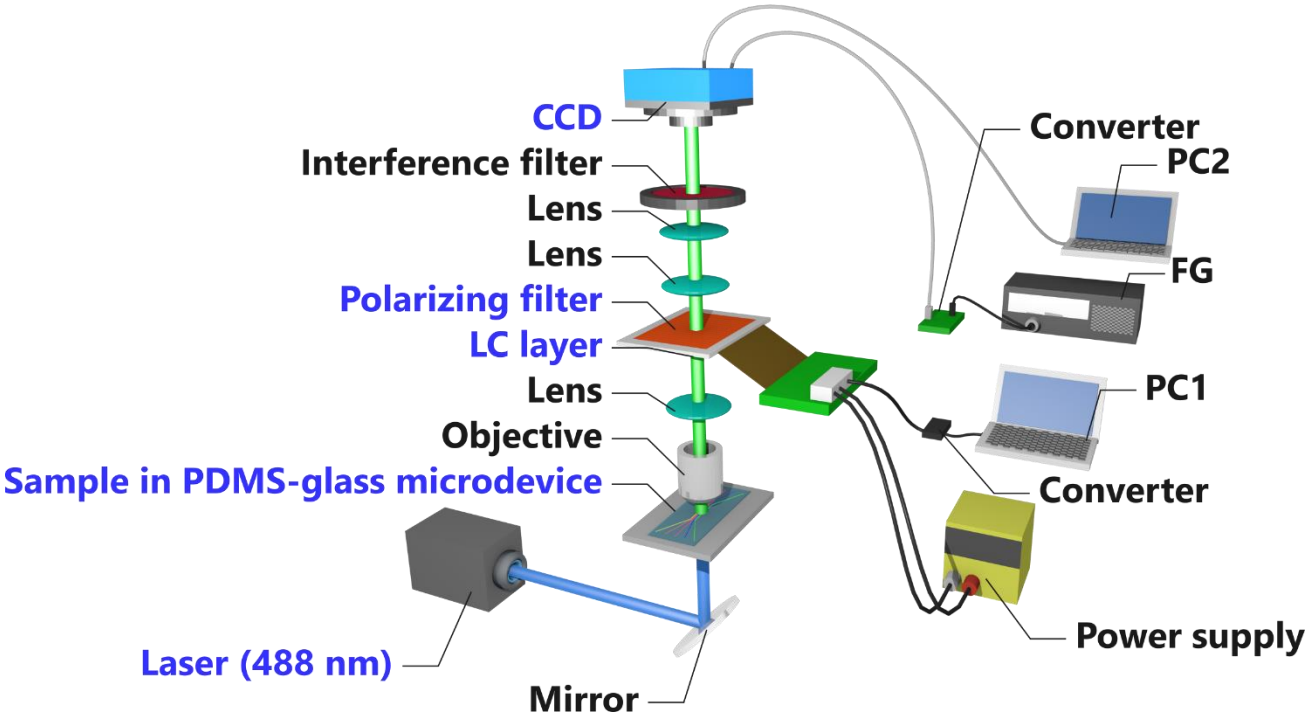

Figure 2.12 The experimental setup for fluorescence polarization measurements. A semiconductor laser with plane-polarized light was used as a light source. The orientation of the liquid crystal (LC) layer was modulated at 3 Hz using personal computer (PC) 1. The sampling frequency of the charge coupled device (CCD) was controlled at 12 Hz using a function generator (FG). The fluorescence images captured with the CCD were analyzed using a home-built image analysis software operating on PC 2. The samples were in the polydimethylsiloxane (PDMS)-glass microdevice.

As mentioned above, the LCD (3.5-inch color LCD, CLAA035QVA01, Chunghwa Photo Tubes Ltd., Taoyuan City, Taiwan) was disassembled and only a LC layer and a polarizing filter were used in the system. All optical components were purchased from Sigma Koki Co., Ltd. (Tokyo, Japan). A 488 nm semiconductor laser (20 mW, D488C-20-11, JUNO-Compact, Showa Optronics, Tokyo, Japan) was used as an excitation beam,

and the beam had parallel polarization to the polarizing filter on the LC layer (polarization ratio 1:100 <). The laser was controlled using an AC controller (JMD-12, Showa Optronics). After passing through a neutral-density (ND) filter and being reflected on a mirror, the excitation beam was irradiated onto a microdevice. Fluorescence was collected by an objective lens and focused on the LC layer by a lens. A 2× objective lens (NA 0.055) was used for the proof-of-concept demonstration and a 5× objective lens (NA 0.13) was used for the multi-sample FPIA. After passing through two lenses and an interference filter (YIF-BA510IFS, transmittance range wavelength (OD > 7): 517-700 nm), the fluorescence was detected by a CCD (Retiga EXi CCD, QImaging, Surrey, BC, Canada). A constant voltage (12 V, PMC18-3, Kikusui Electronics Co., Yokohama, Japan) was applied to the LC layer, and the orientation of the LC, i.e., polarization plane of the acquired fluorescence, was modulated at 3 Hz using a personal computer (PC 1). The video with grayscale changing made with Microsoft Windows Movie Maker was displayed on PC 1 and was converted into a LCD input signal using the USB display adapter (LDE-WX015U, Logitech, Japan) and down scan converter (DSE-002, ADE Techno, Japan). The grayscale was cyclically changed between 0 and 255 (0, 24, 88, 167, 231, 255, 231, 167, 88, and 24). The image was output to the LCD at *f* of 3 Hz. The sampling frequency of the CCD was controlled using a function generator (WF1947, NF Co., Yokohama, Japan) and was set to 12 Hz. The fluorescence images captured with the CCD at 12 Hz were acquired and analyzed using a home-built image analysis software operating on a second personal computer (PC 2). The images acquired by the software were analyzed using the free software Image J. Figures 2.13 and 2.14 show photos of the system and Figure 2.16 shows a photo of the LCD.

To compare the performance of the developed system, FP measurements were also taken using a conventional apparatus (FP-715, JASCO Co., Tokyo, Japan).

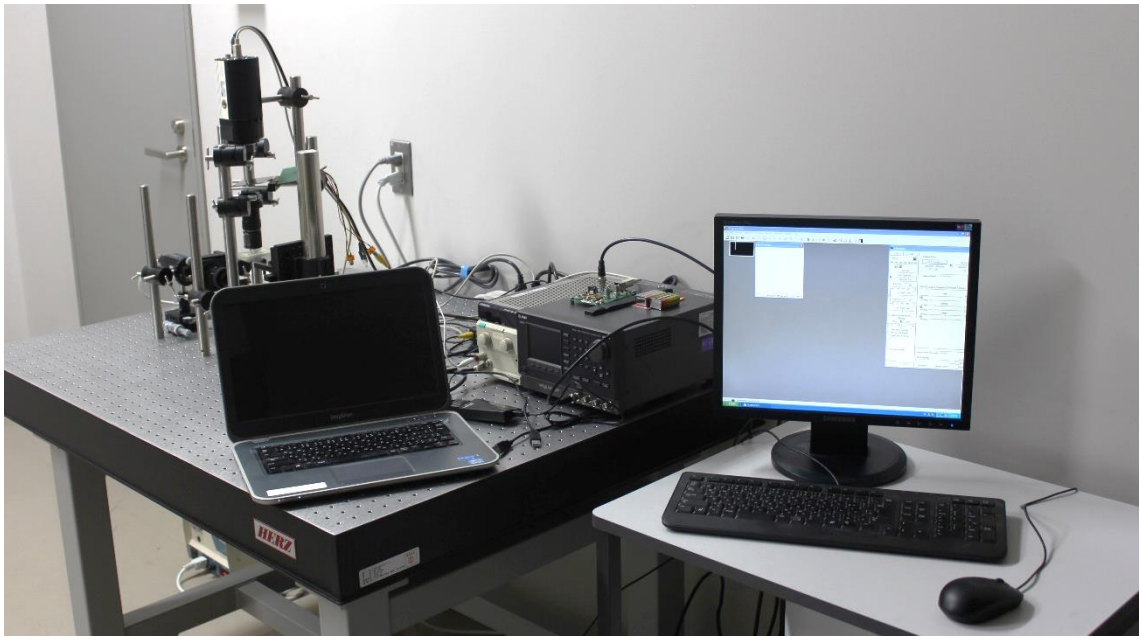

Figure 2.13 Photo of the whole experimental setup for fluorescence polarization measurements.

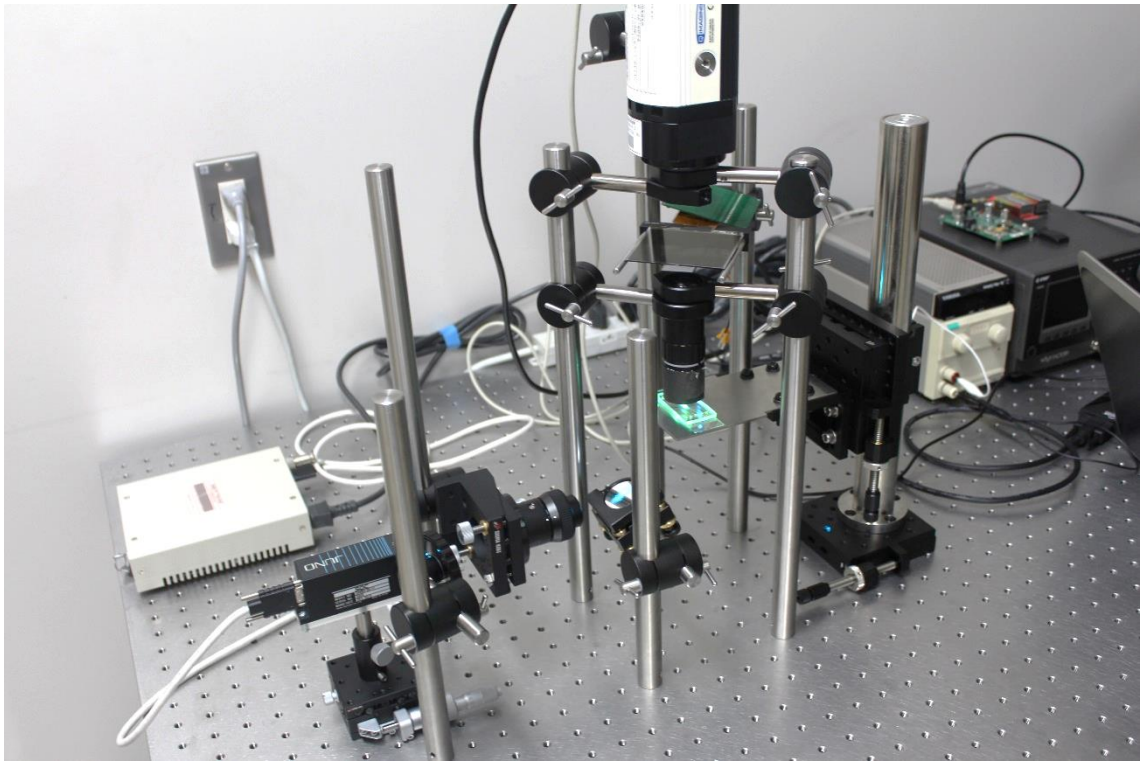

Figure 2.14 Photo of the optical components of the experimental setup for fluorescence polarization measurements.

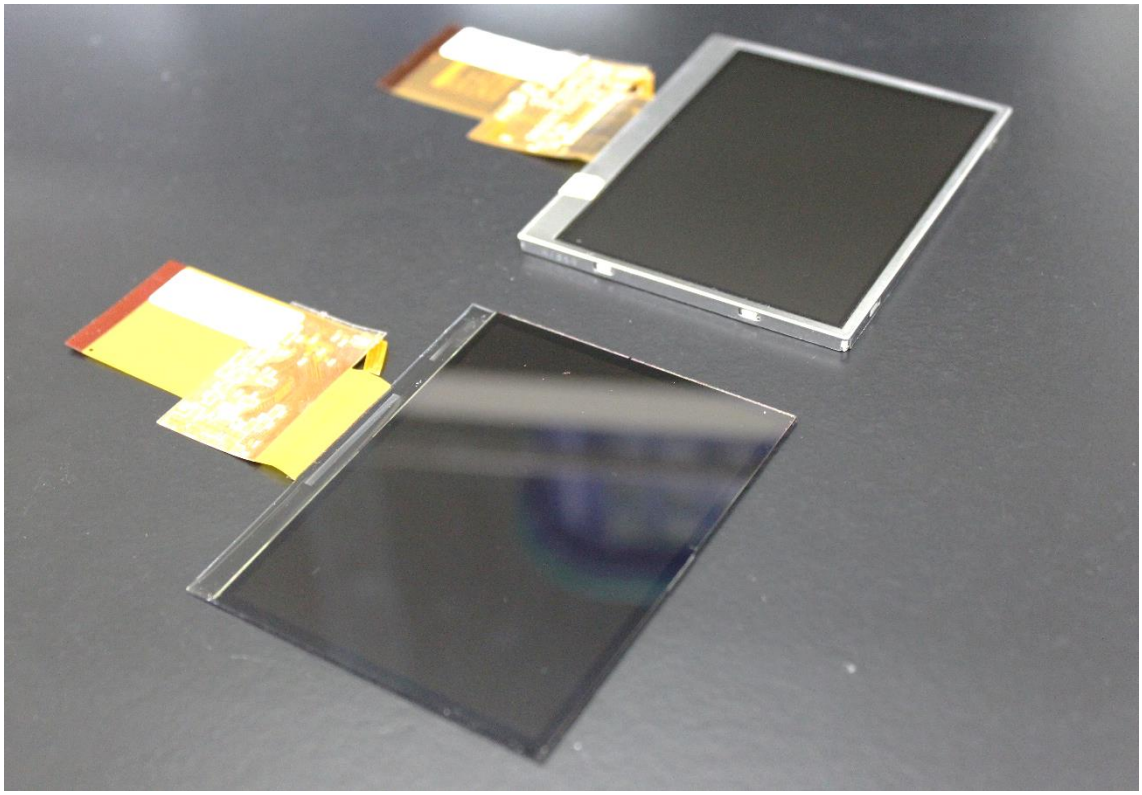

Figure 2.15 Photo of the liquid crystal display (LCD). A commercially available LCD (in the back) was disassembled, and only a set of a LC layer and polarizing filter (in the front) was used in the system.

2.3.2 Fabrication of a Polydimethylsiloxane-Glass Microdevice

A polydimethylsiloxane (PDMS)-glass microdevice was fabricated using the standard soft lithography process [20]. Figure 2.16 shows a schematic illustration of the fabrication of the PDMS-glass microdevice.

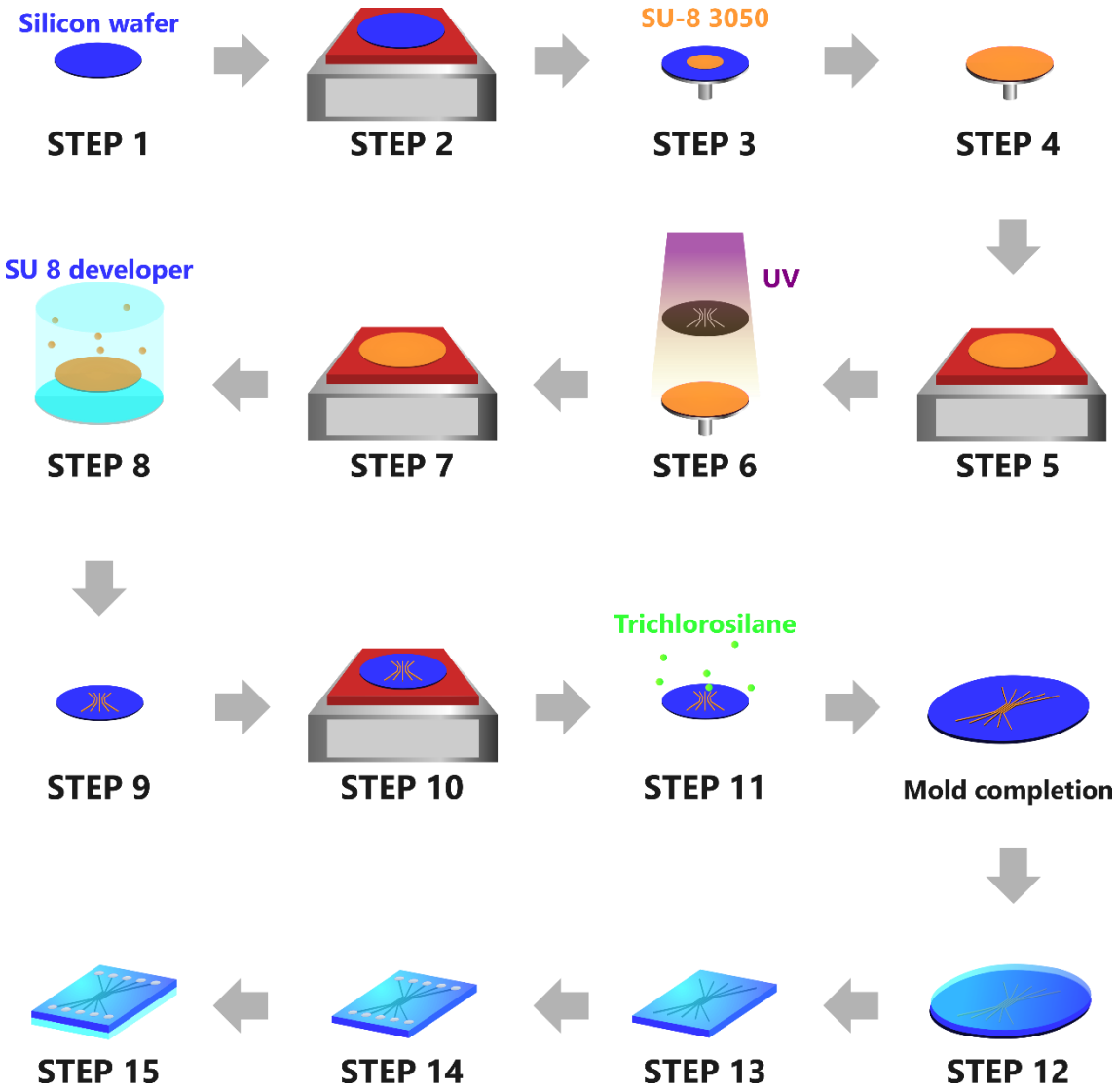

Figure 2.16 Procedure for microdevice fabrication using the standard soft lithography process [20].

First, a silicon wafer (Sumco Co., Tokyo, Japan), which was the substrate of the mold, was washed with acetone and isopropanol (STEP 1) and baked at 120 °C for 3 min on a hot plate (STEP 2). Negative photoresist SU-8 3050 was added on the silicon wafer (STEP 3) and spin-coated at 1090 rpm with a spin coater (STEP 4). After standing for 1 min, a soft bake was performed on a hot plate at 95 °C for 45 min (STEP 5). To make a mold for the microchannels, the wafer was exposed to UV light (approximately 8 mW/cm^2) that was passed through a designed film photomask using a mask aligner (M-1S, Mikasa Co., Ltd., Tokyo, Japan) for 35 s (STEP 6). After post-baking at 95 °C for 5 min (STEP 7), development was conducted using SU-8 Developer (STEP 8). After washing with isopropanol and spraying air (STEP 9), the mold was hard-baked at 150 °C for

3 min (STEP 10). Finally, the silicon wafer with a few drops of trichloro(1H, 1H, 2H, 2H-perfluorooctyl)silane was degassed in a desiccator and coated to prevent adhesion of PDMS to the mold (STEP 11). Silanization creates a silanized monolayer on the substrate surface, which prevents adhesion of PDMS [21, 22]. After mixing the PDMS prepolymer and the crosslinking curing agent, which was obtained from a commercially available PDMS kit (Sylgard® 184), at a weight ratio of 10:1, the PDMS was cast on the mold and cured at 70 °C for 60 min in an oven (DS 600, Yamato Science, Japan) (STEP 12). After curing, the PDMS was cut and peeled off from the mold (STEP 13) and inlets and outlets were punched out of the PDMS using a punching tool (Harris Uni-Core 2.00 mm, GE Healthcare Life Sciences) (STEP 14). The PDMS with the microchannels was bonded onto a glass slide (S1111, Matsunami Glass Ind., Ltd., Osaka, Japan) (STEP 15). A schematic illustration and photo of the PDMS-glass microdevice are shown in Figure 2.17(A) and Figure 2.17(B), respectively. The microdevice had five microchannels with five inlets and five outlets. Each microchannel was 300 μm wide and 110 μm deep with 300 μm of space between the microchannels.

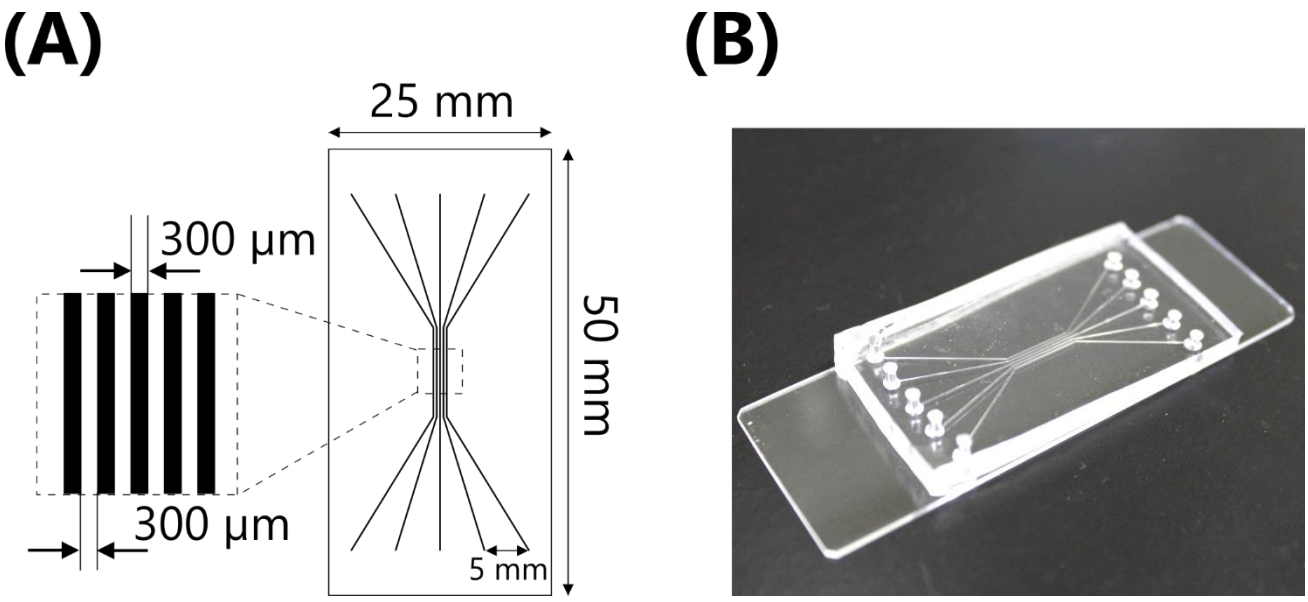

Figure 2.17 Schematic illustration of the polydimethylsiloxane-glass microdevice. (A) Design and dimensions and (B) photo of the microdevice.

2.3.3 Chemicals

Fluorescein and ethylene glycol used for the proof-of-concept demonstration were purchased from Kanto Chemical Co., Inc. (Tokyo, Japan) and Wako Pure Chemical Industries, Ltd. (Osaka, Japan), respectively. A FP immunoassay kit (Abnova Prostaglandin E2 FPIA Kit) containing fluorescein-conjugated PGE2 and control PGE2 solution was purchased from Abnova Corporation (Taipei, Taiwan). The fluorescein had a maximum absorption wavelength of 494 nm and maximum emission wavelength of 521 nm. A Sylgard® 184 Silicone Elastomer Kit for PDMS microdevice fabrication was purchased from Dow Corning Toray Co., Ltd. (Tokyo, Japan). The negative photoresist (SU-8 3050) for PDMS microdevice fabrication and SU-8 developer (1-methoxy-2-propyl acetate (98-100%) propylene glycol monomethyl ether acetate) were purchased from Nippon Kayaku Co., Ltd. (Tokyo, Japan). Ultrapure water was obtained using a Direct-Q® UV System (EMD Millipore Co., Billerica, MA, USA). Acetone and isopropanol for silicon wafer washing were purchased from Wako Pure Chemical Industries, Ltd.

2.4 Results and Discussion

2.4.1 Proof-of-Concept Experiment

To confirm that the LC-CCD synchronization detection system worked as expected, a proof-of-concept experiment was first conducted. For the proof-of-concept experiment, the viscosity dependence of the FP of the fluorophore was measured. Here, fluorescein was used as a model fluorophore. To vary the solvent viscosity, solvent mixtures were prepared at different solvent volume ratios (water-ethylene glycol: 0, 20, 40, 80, and 100%). The samples were prepared by dissolving 1 mM fluorescein in these solvent mixtures at a volume ratio of 1:100. For the FP measurement, these samples were introduced into the microchannels. The FP was influenced by the rotational motions of the fluorophore molecules. Their motions are slower in lower viscosity solvent [23, 24]. From Equation (1.2), at the same fluorophore molecule concentration and temperature, P depends on the solvent viscosity η. A schematic illustration of the FP change depending on

viscosity is shown in Figure 2.18. When the solvent had low viscosity, the molecules rotated rapidly and *P* decreased. On the other hand, when the solvent had high viscosity, the molecules rotated slowly and *P* increased.

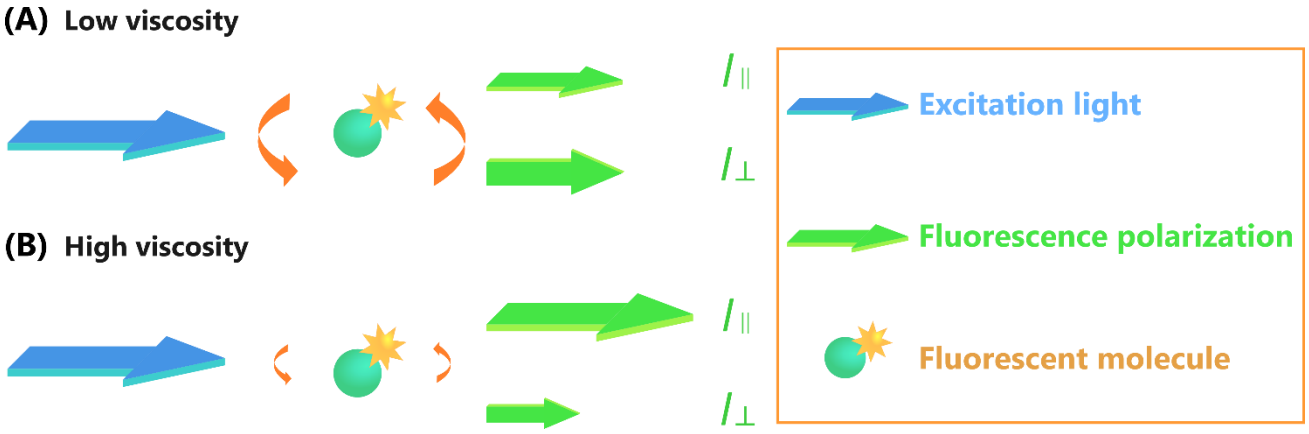

Figure 2.18 Schematic illustration of the change in fluorescence polarization (FP) according to viscosity. $I_{\parallel}$ and $I_{\perp}$ are the fluorescence intensities with parallel and perpendicular polarizations to the polarization of the excitation light, respectively. (A) When the viscosity of the solvent is low, the molecules rotate rapidly and random FP is observed. (B) When the viscosity of the solvent is high, the molecules rotate slowly and FP is polarized.

Figure 2.19 reproduces the images obtained by the LC-CCD synchronization detection system of the AC image, DC image, and *P* image of 1 mM fluorescein in water (water-ethylene glycol: 0%) with a bright field image.

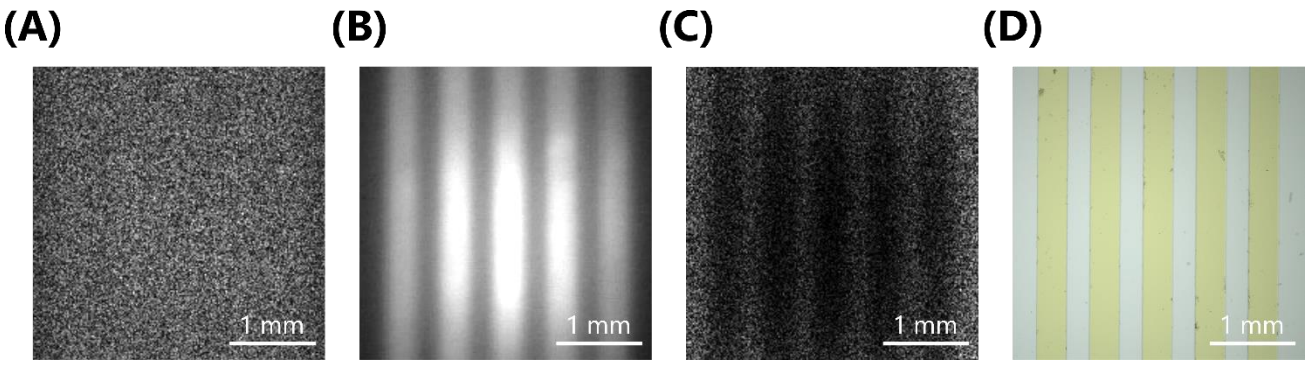

Figure 2.19 Images obtained by the liquid crystal-charge coupled device synchronization detection system of the (A) amplitude component, (B) direct component, (C) *P*, and (D) bright field of 1 mM fluorescein in water.

The AC image, DC image, and *P* image were observed, and corresponded to five microchannels in the respective images. In the *P* image, the noise signal of a location beside the microchannels was high because the DC signal was low. As shown in Figure 2.19, the system could measure the *P* value of multiple samples simultaneously. This was the most important advantage of the system. Prior to the proof-of-concept experiment, the FP measurement of these samples using a conventional FP apparatus and a standard 1 cm cuvette instead of the microdevice was demonstrated. The results are shown in Figure 2.20. *P* increased with increasing solvent viscosity, as expected. In order to compare the FP measurement performance, the results obtained using the LC-CCD synchronization detection system are also shown in Figure 2.20. Both sets of results agreed with each other. From these results, the *P* value could be obtained by processing the AC and DC images.

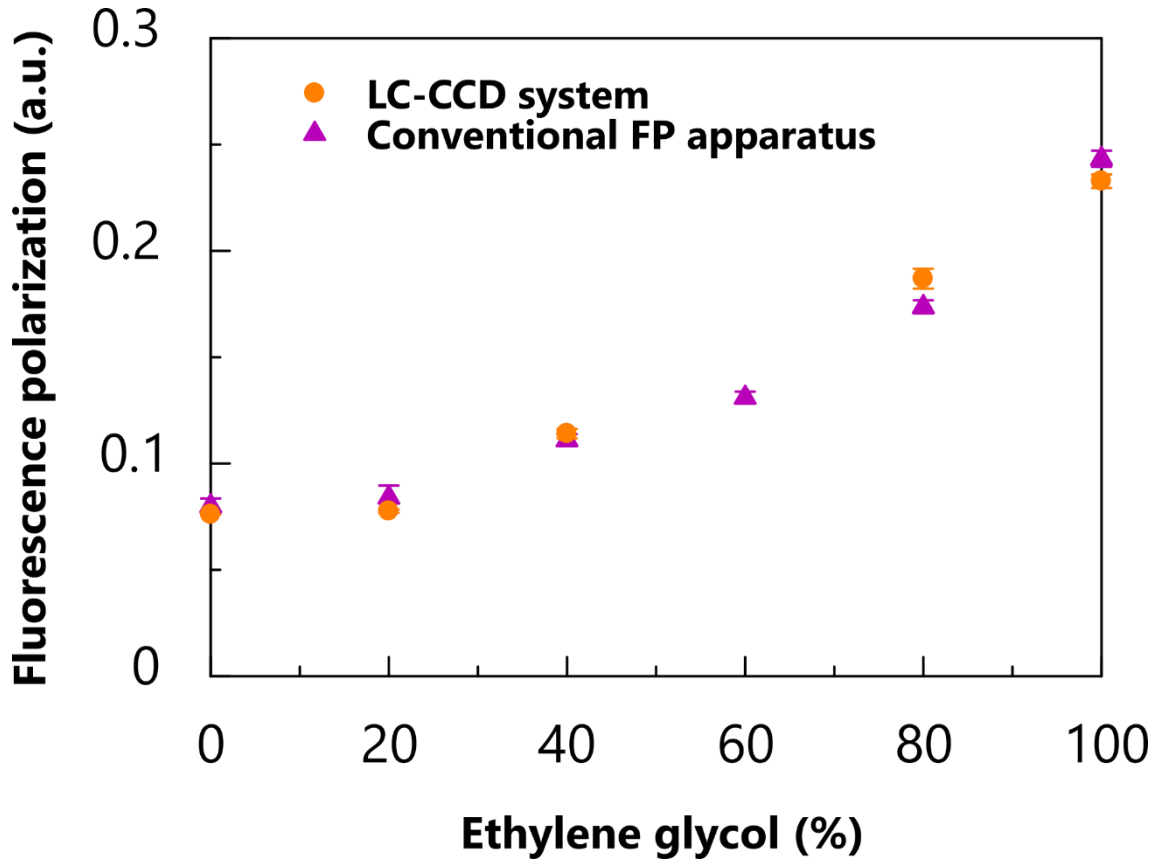

Figure 2.20 The viscosity dependence of the fluorescence polarization (FP) of fluorescein in water-ethylene glycol solution. The volume ratios of water and ethylene glycol (water-ethylene glycol solution) are 0, 20, 40, 60, 80, and 100%.

Therefore, the system developed here had the same FP measurement performance as the conventional FP apparatus. Moreover, the system could measure the FP of multiple samples simultaneously. The simultaneous FP measurement of multiple samples was successfully conducted for the first time. The system could easily acquire two-dimensional images of *P* without a complicated optical arrangement. This is a very advantageous feature for high-throughput screening in drug discovery, which is based on molecular interactions such as protein-protein and drug-protein interactions.

2.4.2 Multiple Sample Fluorescence Polarization Immunoassay

From the proof-of-concept experiment, the FP measurement performance of the system was confirmed. Next, an experiment on simultaneous FPIAs of multiple samples was conducted to show the usefulness of the system. PGE2 (Figure 2.21) was used as a model for simultaneous FPIAs of multiple samples.

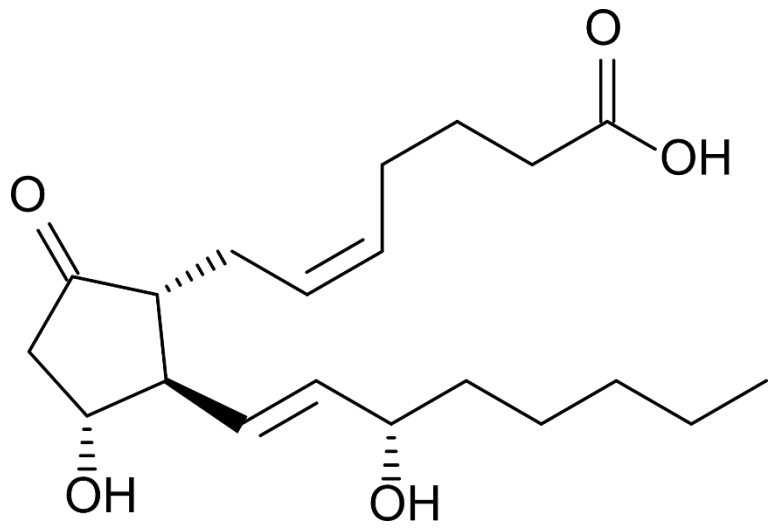

Figure 2.21 Prostaglandin E2 (M: 352.465).

The prostaglandins are members of the eicosanoids, which are formed via the conversion of arachidonic acid by cyclooxygenase [25-27]. PGE2 is a lipid mediator derived from the metabolism of arachidonic acid; it is a biologically active substance that is related to various phenomena, such as vasodilation [28], both pro-inflammatory and anti-inflammatory actions [29, 30], and sleeping and waking regulation [31]. In particular, because of its effect on excessive uterine contraction [32], it has been used as a labor-inducing and labor-accelerating agent called dinoprostone. However, pharmacokinetics information on PGE2 drugs by oral administration have not been elucidated. The main reason for this is that these clinical concentrations are low, so determination of concentrations from blood is difficult. Therefore, the determination of PGE2 concentrations in blood is widely demanded for drug discovery and clinical diagnosis.

To simplify the experiment, the samples that were assayed in test tubes were introduced into the microchannels of the microdevice. The assays were performed according to the instructions of the PGE2 assay kit manufacturer. In this experiment, a 5× objective lens was used to increase the sensitivity. Because of the narrow field of view when using higher magnification, the present setup could only measure three microchannels simultaneously. Thus, a simultaneous FP measurement of three samples with different PGE2 concentrations was conducted. First, three samples with different concentrations of PGE2 (control, 12.5 ng/mL, and 25.0 ng/mL) were measured. Then, the samples with different sample concentrations (control, 50 ng/mL, and 100 ng/mL) were measured. Both results were normalized to the control value. Figure 2.22 shows a standard curve plotting FP against the PGE2 concentrations (12.5, 25.0, 50.0, and 100 ng/mL). As expected, the relaxation of FP was observed with increasing PGE2 concentration, which is typical for the FPIA. The results obtained using the conventional FP apparatus are also plotted in Figure 2.22. Both sets of results correlated well; thus, the simultaneous FPIA of multiple samples was possible with the system.

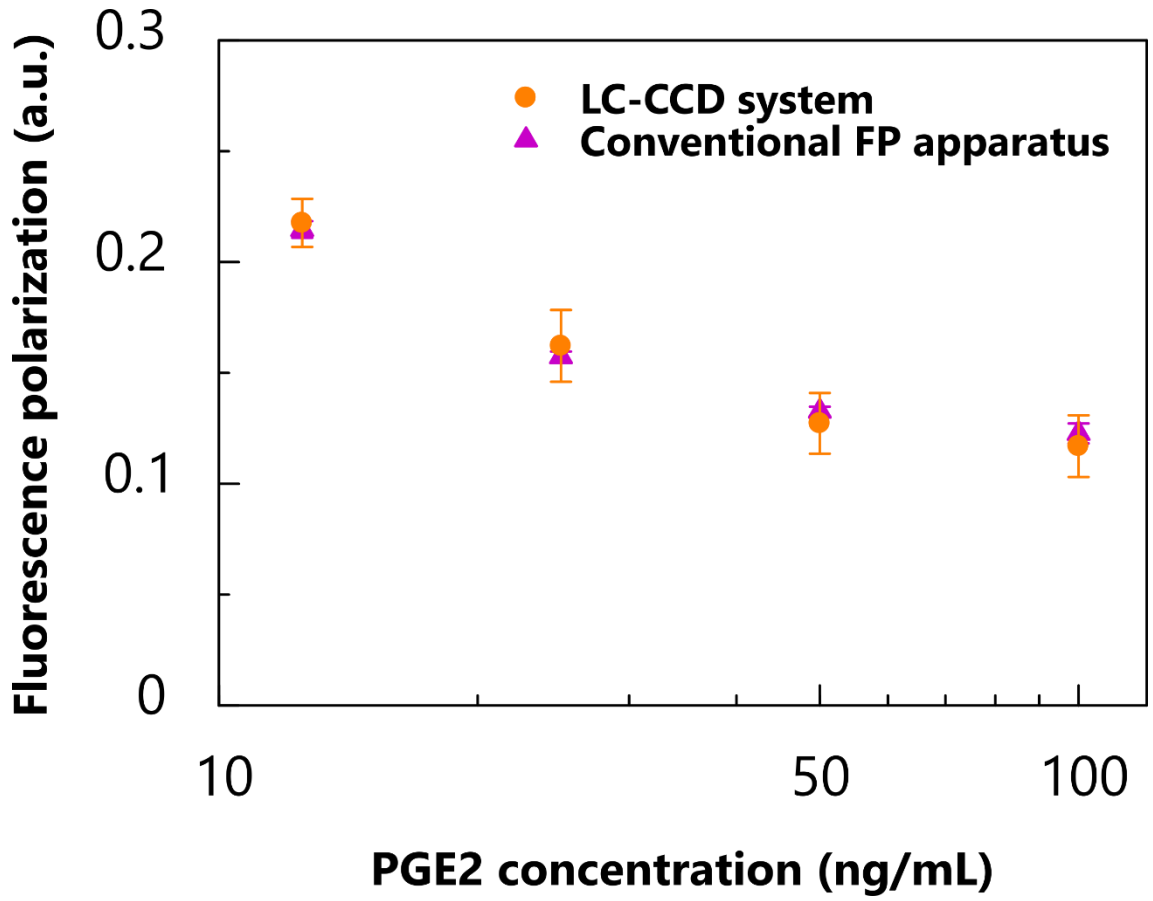

Figure 2.22 Standard curve plotting of fluorescence polarization (FP) against the prostaglandin E2 (PGE2) concentration in the range of 12.5-100 ng/mL.

The larger error bars of the results obtained with the system compared with those of the results obtained with the conventional FP apparatus were attributed to the relatively low detection sensitivity of the current system. Through further optimization of the optics (lenses and filters), microdevice, electronics, and optical arrangement, improvement in the detection sensitivity is possible.

Only three samples could be measured simultaneously by the current system, but changing the microdevice design should make it possible to increase the number of samples that can be measured simultaneously. Twenty-five FPIA samples for PGE2 were demonstrated using a microchamber array with a volume of 9 nL using on-off LC switching (not synchronization) [33]. Typical fluorescence images for 25 microchambers filled with fluorescence samples are shown in Figure 2.23. Figure 2.24 shows a standard curve

plotting of P against the PGE2 concentration. The P values were directly calculated from $I_{\perp}$ and $I_{\parallel}$ using Equation (1.1). In this situation, the same samples were introduced in the 25 microchambers; however, the results showed that simultaneous detection of 25 samples was conducted for the first time and that reagent consumption decreased compared with that of the previous work in Figure 2.22.

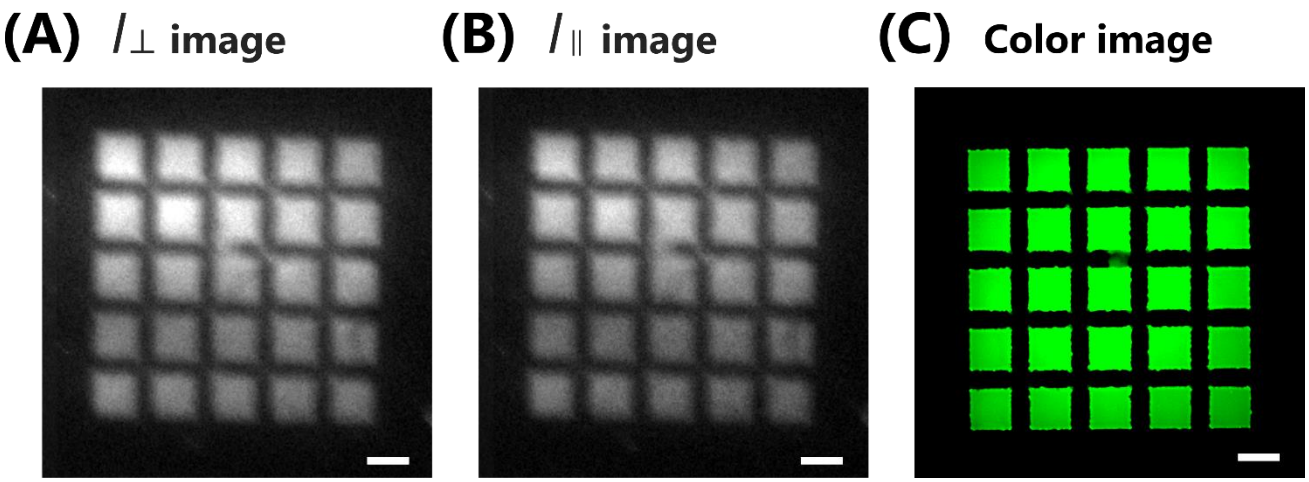

Figure 2.23 Typical fluorescence images for a microchamber array. (A) $I_{\perp}$, (B) $I_{\parallel}$, and (C) color fluorescence images of 1 mM fluorescein in water obtained by the fluorescence polarization (FP) detection system. The FP signals were calculated from each of the 25 chambers. Each microchamber was a square with sides of 300 μm length. The scale bars are 300 μm.

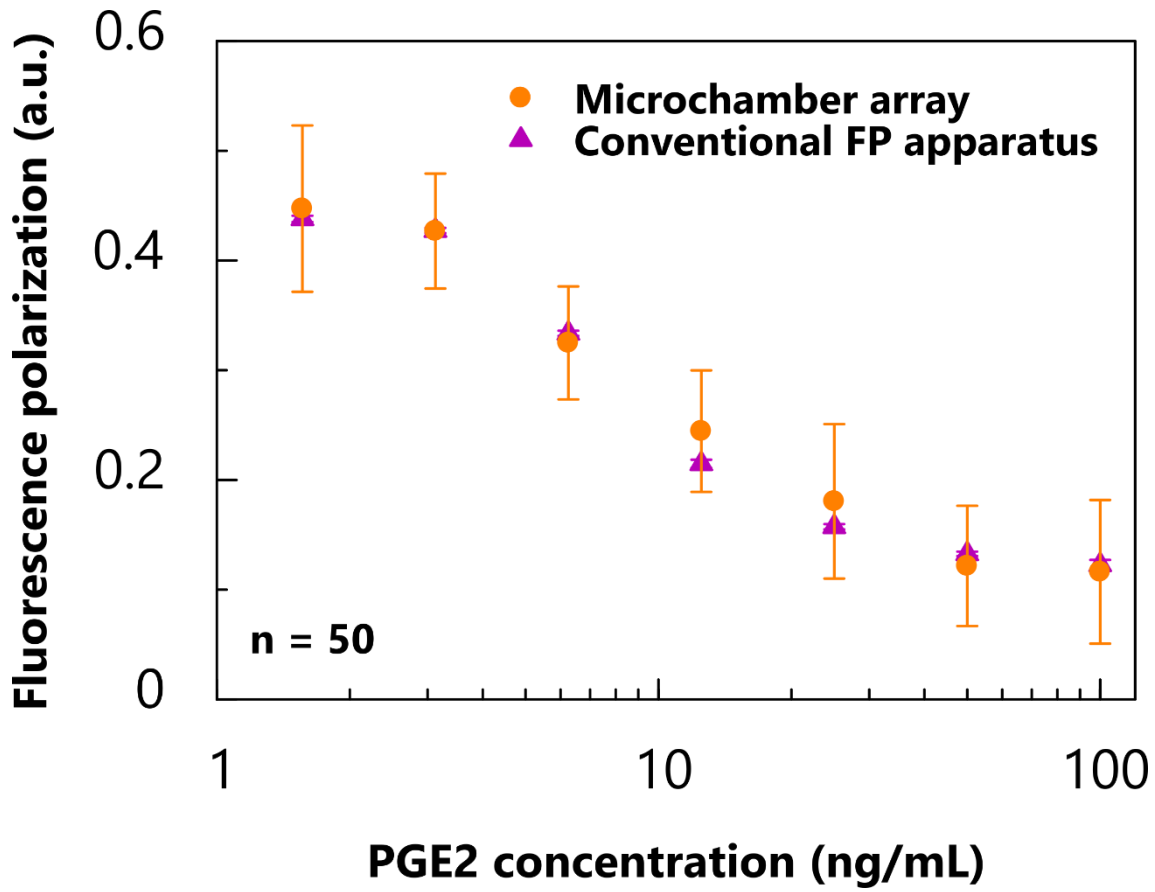

Figure 2.24 Standard curve plotting of fluorescence polarization (FP) against the prostaglandin E2 (PGE2) concentration in the range of 12.5-100 ng/mL. The plots show two times detection using an array of 25 microchambers.

When the system was optimized with the items mentioned above, the detection sensitivity was improved and the number of samples that could be measured simultaneously was easily increased. Furthermore, the system has great potential for miniaturization and price reduction as well as simultaneous FP measurement of multiple samples. Actual image sensors, such as the CCD and CMOS sensor, are steadily being downsized and lowered in price, and the system should be able to use an light emitting diode (LED) as a light source instead of a laser.

2.5 Conclusions

A unique FP measurement system to realize simultaneous FP analysis or assay of multiple samples was developed. The system was based on the synchronization between the orientation of the LC layer and the sampling frequency of an image sensor. As a proof-of-concept experiment, the viscosity dependence of FP of fluorescein in water-ethylene glycol solution was measured. In the experiment, simultaneous FP measurement of multiple samples was successfully demonstrated for the first time [34]. Moreover, simultaneous FPIA of multiple samples of PGE2 was also successfully demonstrated. The results obtained with the developed system were compared with those of a conventional apparatus. As a result, the measurement performance of the system was equal to that of the conventional apparatus. In principle, the system could be miniaturized and become less expensive to fabricate. An inexpensive, small system for FP measurement with high-throughput could be achieved in the near future. Recently, Cheow et al. [35] reported a microfluidic platform-based system for fluorescence anisotropy measurement to analyze protein-ligand interactions. Although FP measurement is superior to fluorescence anisotropy measurement from the viewpoint of detection sensitivity, the system of Cheow et al. is advantageous in terms of its simplicity. Although FP and fluorescence anisotropy are well established, by combining a new idea and new techniques it is expected that they will become even more useful in measurement systems with unprecedented characteristics for protein-ligand interactions, such as FPIA.

References

[1] W. A. Lea and A. Simeonov, *Expert Opin. Drug Discov.*, **6**, 17-32 (2012)

[2] D. M. Jameson and J. A. Ross, *Chem. Rev.*, **110**, 2685-2708 (2010)

[3] D. S. Smith and S. A. Eremin, *Anal. Bioanal. Chem.*, **391**, 1499-1507 (2008)

[4] P. A. Routledge and A. D. Hutchings, The Immunoassay Handbook: Theory and Applications of Ligand Binding, ELISA and Related Techniques, 4th edition, D. Wild: Elsevier, pp. 945-962 (2013)

[5] T. Tachi, N. Kaji, M. Tokeshi, and Y. Baba, *Lab. Chip.*, **9**, 966-971 (2009)

[6] T. Tachi, T. Hase, Y. Okamoto, N. Kaji, T. Arima, H. Matsumoto, M. Kondo, M. Tokeshi, Y. Hasegawa, and Y. Baba, *Anal. Bioanal. Chem.*, **401**, 2301-2305 (2011)

[7] J.-W. Choi, S. Lee, D.-H. Lee, J. Kim, A. J. deMello, and S.-I. Chang, *RSC Adv.*, **4**, 20 341-20 345 (2014)

[8] J.-W. Choi, D.-K. Kang, H. Park, A. J. deMello, and S.-I, Chang, *Anal. Chem.*, **84**, 3849-3854 (2012)

[9] H. N. Joensson, C. Zhang, M. Uhlén, and H. Andersson-Svahn, *Electrophoresis*, **33**, 436-439 (2012)

[10] J.-W. Choi, G.-J. Kim, S. Lee, J. Kim, A. J. deMello, and S.-I Chang, *Biosens. Bioelectron.*, **67**, 497-502 (2015)

[11] J. Inglese, C. E. Shamu, and R. K. Guy, *Nat. Chem. Biol.*, **3**, 438-441 (2007)

[12] F. Reinitzer, *Monatsh. Chem.*, **9**, 421-441 (1888)

[13] E. R. Wooding, *Nature*, **199**, 273-274 (1963)

[14] G. H. Heilmeier, J. A. Castellano, and L. A. Zanoni, *Mol. Crystals*, **8**, 293-304 (1969)

[15] J. Fergason, US3731986A (1971)

[16] Seiko Epson Corp., History of Epson ET-10, https://www.epson.jp/ms/1984_8.htm (2018/12/13)

[17] Kenzo Konoike, All About (March 5, 2008), Material price soaring! Is the price of flat screen TVs as well?!, http://allabout.co.jp/gm/gc/51216/2/ (2018/12/13)

[18] K. Yoshino and M. Ozaki, Fundamental of Liquid Crystal and Display (in Japanese), 1st edition: Corona Publishing, pp. 118-119 (1994)

[19] S. Grauby, B. C. Forget, S. Holé, and D. Fournier, *Rev. Sci. Instrum.*, **70**, 3603-3608 (1999)

[20] J. C. McDonald and G. M. Whitesides, *Acc. Chem. Res.*, **35**, 491-499 (2002)

[21] J. Chen, F. Ko, K. Hsieh, C. Chou, and F. Chang, *J. Vac. Sci. Technol.*, **22**, 3233-3241 (2004)

[22] P. Silberzan, L. Leger, D. Ausserre, and J. J. Benattar, *Langmuir*, **7**, 1647-1651 (1991)

[23] G. Weber, *Adv. Protein Chem.*, **8**, 415-459 (1953)

[24] J. R. Lakowicz, Principles of Fluorescence Spectroscopy, 3rd edition: Springer, pp. 17-18 (2006)

[25] P. Needleman, J. Turk, B. A. Jakschik, A. R. Morrison, and J. B. Lefkowith, *Ann. Rev. Biochem.*, **55**, 69-102 (1986)

[26] W. L. Smith, L. J. Marnett, and D. L. Dewitt, *Pharmac. Ther.*, **49**, 153-179 (1991)

[27] W. L. Smith, *Biochem. J.*, **259**, 315-324 (1989)

[28] P. D. I. Richardson and P. G. Withrington, *Br. J. Pharmacol.*, **57**, 581-588 (1976)

[29] J. Raud, S. E. Dahlén, A. Sydbom, L. Lindbom, and P. Hedqvist, *Proc. Natl. Acad. Sci. U.S.A.*, **85**, 2315-2319 (1988)

[30] J. W. Christman, R. Abdolrasulinia, V. L. Shepherd, and J. E. Rinaldo, *Prostaglandins*, **41**, 251-262 (1991)

[31] O. Hayaishi, *J. Biol. Chem.*, **263**, 14 593-14 596 (1988)

[32] K. Bremme, P. Eneroth, C. Gottlieb, H. Kindahl, K. Svanborg, B. Nilsson, M. Olsson, and M. Bygdeman, *Prostaglandins Leukot. Essent. Fatty Acids*, **37**, 169-176 (1989)

[33] O. Wakao, M. Maeki, A. Ishida, H. Tani, A. Hibara, and M. Tokeshi, *Proc. of Micro TAS 2016*, 1400-1401 (2016)

[34] O. Wakao,Y. Fujii, M. Maeki, A. Ishida, H. Tani, A. Hibara, and M. Tokeshi, *Anal. Chem.*, **87**, 9647-9652 (2015)

[35] L. F. Cheow, R. Viswanatha, C.-S. Chin, N. Jennifer, R. C. Jones, E. Guccione, S. R. Quake, and W. F. Burkholder, *Anal. Chem.*, **86**, 9901-9908 (2014)

CHAPTER 3 Sensitive Fluorescence Polarization Immunoassay by Optimizing the Synchronization Mismatch Condition

3.1 Introduction

Fluorescence polarization (FP) is a unique tool for studying molecular interactions. Since FP measurement is not difficult and valuable information can be obtained, it is widely used in biological and clinical applications [1-6]. Recently, interaction assays with nucleic acids adopted the FP measurement technique to analyze the interactions with DNA or RNA [7-9]. FP immunoassay (FPIA), which is a competitive immunoassay, is applied to quantitative analysis of mycotoxins, pesticides, and antibiotics in foods and monitoring of therapeutic drugs in blood [10-13]. The greatest advantage of FPIA is the simplicity of its measurement protocol. In the measurement protocol, only fluorescent-labeled target molecules, namely tracer molecules, target molecules, and antibodies, which bind to the target and tracer molecules, are mixed in a liquid. In FP measurement, the fluorescence intensities of parallel and perpendicular polarizations to the excitation polarization are detected for calculation of the degree of polarization, namely P. P reflects the concentration of a target molecule and is calculated by the following equation:

$$P = (I_{\parallel} - I_{\perp})/(I_{\parallel} + I_{\perp}) \tag{3.1}$$

where $I_{\parallel}$ and $I_{\perp}$ are the fluorescence intensities with parallel and perpendicular polarizations to the excitation plane, respectively. Therefore, each polarization measurement is necessary to calculate the P value, which reflects the target concentration.

As mentioned in Chapter 2, a unique FP measurement system based on a liquid crystal-charge coupled device (LC-CCD) synchronization detection method was developed, where the acquisition frequency should be set 4 times higher than that of the LC [14, 15]. By processing the acquired fluorescence images, the P value for each image sensor pixel was calculated straightforwardly. The P image enabled simultaneous measurement of multiple samples in the view field. The FPIA method was advantageous for the development of inexpensive mobile measurement systems, which are potentially applicable to various important analyses, such as on-site therapeutic drug monitoring [16, 17] and on-site analysis of food samples [18, 19].

In the proof-of-concept detection system [14], a video output from a personal computer (PC) controlled the LC, and a function generator (FG) triggered image acquisition of the CCD. Although the LC and CCD

were controlled by independent frequency sources and there was a certain frequency mismatch, the image-based FPIA of prostaglandin E2 (PGE2) was successfully demonstrated. However, to develop a more precise, accurate, and sensitive apparatus, the effect of the frequency mismatch should be clarified and a method for its optimization should be established.

In Chapter 3, experimental and theoretical investigations on the influence of the synchrony between LC switching and CCD image sampling for measured values were demonstrated for synchronization optimization. The theoretical values with several synchronization mismatches at certain numbers of measurement cycles were calculated. In the presence of synchronization mismatches, the timings of the synchronization between LC switching and CCD image sampling were intentionally unsynchronized to reveal their respective influences. Then, a comparison of the measured values with theoretical values to validate the theoretical model was conducted. Finally, to establish a prediction method for the optimum condition, FPIAs for PGE2 as model samples under some synchronization mismatch conditions were demonstrated.

3.2 Experimental

3.2.1 Measurement Principle

The measurement principle of the FP system was based on the LC-CCD synchronization detection method [14]. A schematic illustration of the synchronization detection method is shown in Figure 3.1.

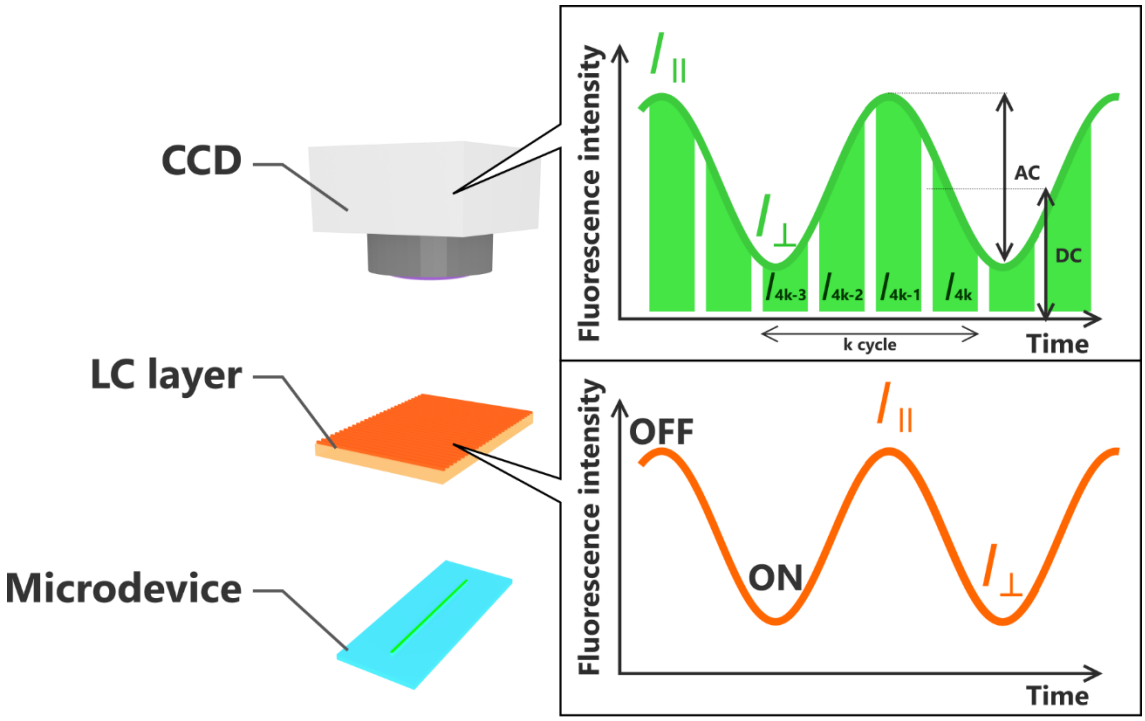

Figure 3.1 Schematic illustration of the synchronization detection method. When fluorescence from samples in the microdevice passes through the liquid crystal (LC) layer, the fluorescence polarization (FP) direction ($I_{\parallel}$ or $I_{\perp}$) is switched at a certain frequency (f_{LC} Hz) by on-off switching of the voltage applied to the LC layer. The charge coupled device (CCD) image sensor operated at f_{CCD} ($4f_{LC}$ Hz) captures four images during each cycle. An amplitude component (AC) image includes the difference in intensities of the FPs and a direct component (DC) image includes the summed intensities of the FPs. When the number of measurement cycles is *k* cycles, images are captured until *k* cycles are integrated and image processed.

The LC layer can switch the polarization direction of the transmitted light through on-off switching of the voltage applied to the LC layer. Thus, FP is switched at a certain frequency (f_{LC} Hz) by modulation of the voltage applied to the LC layer. Such fluorescence is obtained by a CCD image sensor operated at f_{CCD} ($4f_{LC}$ Hz) sampling frequency for synchronization with LC modulation (LC-CCD synchronization detection). Then, four images with FP signals are captured during the period of a single LC modulation frequency cycle. An amplitude component (AC) image and direct component (DC) image of FP modulation are obtained by image processing. The luminance values of the AC and DC images include the difference in intensities of the FPs and the summed intensities of the FPs, respectively. Thus, a *P* image is obtained as a single two-dimensional image by image calculation using the AC and DC images, and the *P* value is obtained by reading out the

luminance of the *P* image. In the theoretical calculation, the sine function modulation is considered an ideal FP switching by LC modulation and calculation of the theoretical AC and DC image luminance values.

3.2.2 Fluorescence Polarization Measurement System

A FP measurement setup using the LC-CCD synchronization detection method was built, as shown in Figure 3.2. It was modified from the earlier experimental setup [14].

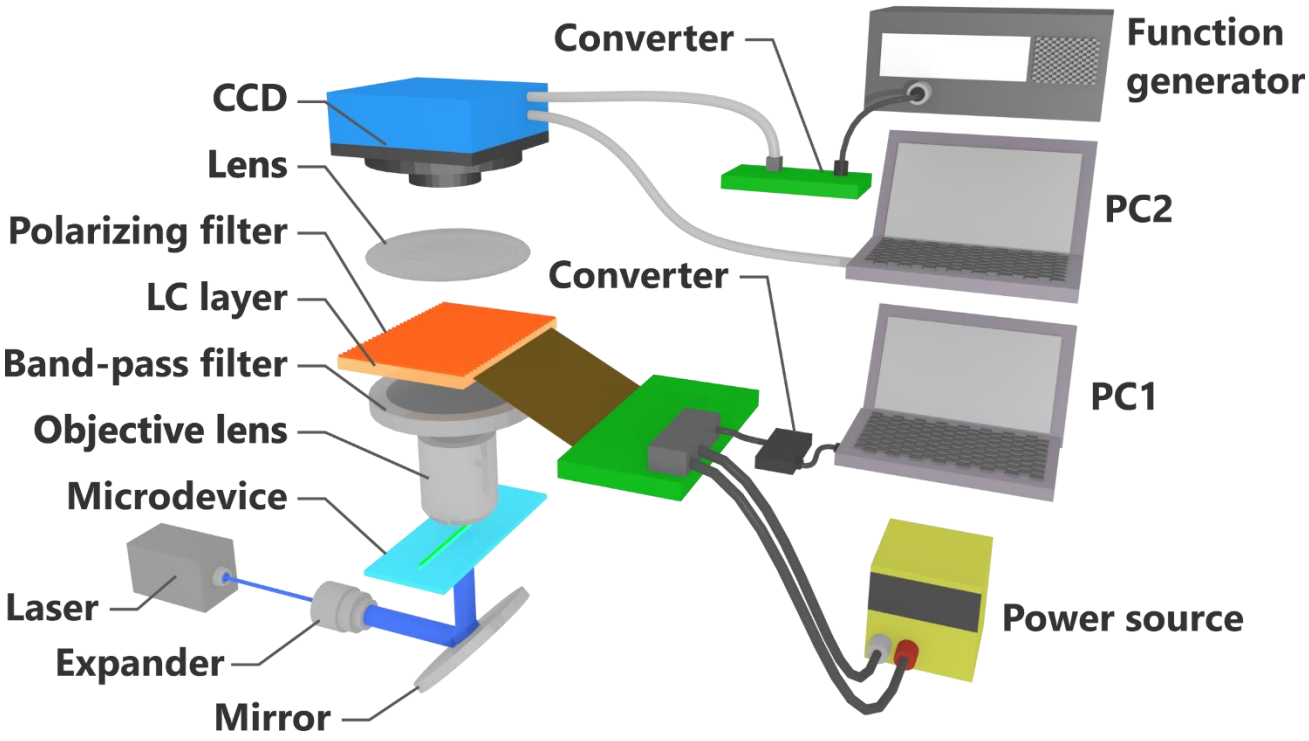

Figure 3.2 Schematic illustration of the experimental setup for fluorescence polarization (FP) measurement. The modulation frequency of the liquid crystal (LC) layer (f_{LC}) was controlled by personal computer (PC) 1. The charge coupled device (CCD) sampling frequency (f_{CCD}) was controlled by the function generator. Amplitude component and direct component images were processed using a home-built image processing software operated on PC 2.

A 488 nm semiconductor laser (200 mW, D488C-200, JUNO-Compact, Showa Optronics, Tokyo, Japan) was used as a polarized excitation light source. The excitation beam was parallel polarized to the

polarizing filter on the LC layer. The intensity of the excitation beam was adjusted with a neutral-density (ND) filter (NDHN-50, Sigma Koki, Tokyo, Japan). The excitation beam was introduced into a microdevice after being expanded by an expander (LBED-5, Sigma Koki). Fluorescence was collected by a 4× objective lens (UPlan Apo, NA 0.16, Olympus, Tokyo, Japan) and passed through a bandpass filter (YIF-BA510-550S; transmittance range wavelength of 517-742 nm; Sigma Koki). After passing through the LC layer, fluorescence was focused on a CCD (Retiga EXi CCD, QImaging, Surrey, BC, Canada) by a plano-convex lens (SLB-30-40PM, Sigma Koki) to obtain a sample plane image. The LC display (Chunghwa Picture Tubes, Ltd., Taoyuan City, Taiwan) was disassembled into a LC layer and a polarizing filter. A constant voltage (12 V; PMC18-3, Kikusui Electronics Co., Yokohama, Japan) was used as a power source for the LC controller. The frequency of the polarizations after passing through the LC layer was modulated by a gray movie, which gradually changed its own gray scales according to the control by a PC (PC 1; f_{LC}). A FG (WF1947, NF Co., Yokohama, Japan) triggered the CCD sampling (f_{CCD}). The microdevice was fabricated using the standard soft-lithography method with polydimethylsiloxane and a glass slide [20]. The microdevice had five microchannels, as previously described [14]; however, in this experiment, only a single microchannel that was 300 μm wide and 100 μm deep was used. The samples were introduced into the microchannel by a syringe pump (Kd Scientific, Holliston, MA) at a flow rate of 1 μL/min. The captured fluorescence images were processed using a home-built image processing software operating on a second PC (PC 2). The experimental AC values and DC values were obtained by reading out the luminance of the microchannel area in the AC and DC images.

3.2.3 Theoretical Calculation of Amplitude Component and Direct Component Values

The theoretical values of the AC and DC with several synchronization mismatches at certain numbers of measurement cycles were calculated. In the synchronization cases, the CCD sampling frequency (f_{CCD}) was four times larger than the LC modulation as a base frequency (f_{LC}). For comparison of these synchronization cases, unsynchronization cases in which f_{CCD} was around four times larger than f_{LC} was taken into consideration.

Ideal FP modulation by the LC layer was fixed as a sine function. Here, the light intensity at a certain time was denoted as follows:

$$F(t) = d + r\ \sin(\varphi t) + \text{random numbers} \qquad (3.2)$$

where d and r are the direct and alternative amplitudes, respectively, and φ is the angular frequency ($\frac{2\pi}{T}$; T is the period). In consideration of the irregular noise from the measurement system, random numbers were employed in Equation (3.2) using the RAND function [21]. In the investigation, random noise mainly from the image sensor was considered. The integration time was set to one-fourth of the LC modulation frequency cycle. The AC and DC values were calculated from four integral values of $F(t)$ within the CCD sampling time Δt. As a model situation, the exact AC and DC values calculated from the ideal FP modulation without synchronization mismatches were fixed to 2 and 10, respectively. Additionally, in consideration of the synchronization mismatch, the LC modulation frequency and CCD sampling frequency were intentionally unsynchronized, and the unsynchronized frequencies were applied to the calculation of the AC and DC values. The mean values of 10 random number trials were used as the calculated values.

3.2.4 Reagents and Chemicals

Fluorescein (Kanto Chemical Co., Inc., Tokyo, Japan) and ethylene glycol (Wako Pure Chemical Industries, Ltd., Osaka, Japan) were used for the experimental measurements of the AC and DC values. The FPIA kit (Abnova Prostaglandin E2 FPIA Kit, Abnova Co., Taipei, Taiwan) containing standard PGE2, fluorescein-conjugated PGE2, and anti-PGE2 antibody solutions was used for the FPIA demonstration. Fluorescein has a maximum absorption wavelength of 494 nm and a maximum emission wavelength of 521 nm.

3.3 Results and Discussion

3.3.1 Theoretical Amplitude Component and Direct Component Values for Synchronization Mismatches

First, the theoretical AC and DC values were calculated. The CCD sampling frequency (f_{CCD}) and LC modulation frequency (f_{LC}) were intentionally unsynchronized. The synchronization mismatch was defined as $f_{CCD}/4f_{LC}$. In this theoretical investigation, the AC and DC value responses at several mismatches (mismatch = 0.90, 0.99, 1.00, 1.10, and 1.20) in the range of 1 to 300 measurement cycles were calculated. Here, the LC modulation frequency cycles were set as the measurement cycles. The synchronization mismatches are shown in Table 3.1 with each frequency of LC modulation (f_{LC}) and CCD sampling (f_{CCD}).

Table 3.1. Liquid crystal (LC) modulation frequency (f_{LC}) and charge coupled device (CCD) sampling frequency (f_{CCD}) at each synchronization mismatch.

Mismatch	f_{LC}**/Hz**	f_{CCD}**/Hz**
0.90	$3.33 = \frac{10}{3}$	12.00
0.99	$2.78 = \frac{25}{9}$	11.00
1.00	$2.78 = \frac{25}{9}$	$11.11 = \frac{100}{9}$
1.10	2.50	11.00
1.20	2.50	12.00

The calculated AC and DC values in the range of 1 to 300 measurement cycles are shown in Figure 3.3(A) and 3.3(B), respectively. Although they had some fluctuations in several initial cycles, the calculated DC values were within 300 cycles of the targeted values. On the other hand, the calculated AC values decreased within 300 cycles, except for mismatches 1.00 and 0.99. The results showed that the AC values without synchronization mismatches (namely mismatch 1.00) were kept at the targeted values. However, when there were some synchronization mismatches, the AC values decreased with some fluctuation as the number of measurement cycles increased. The decreasing behaviors differed according to the degree of

synchronization mismatches. When the synchronization mismatch was relatively large, such as mismatches 0.90, 1.10, and 1.20, the AC values rapidly decreased within several cycles with some fluctuation. On the other hand, when the synchronization mismatch was relatively small, such as mismatch 0.99, the AC values decreased slightly within 300 cycles with some fluctuation. In particular, for mismatch 0.99, the AC value recovered at 150 cycles after the value decreased at 100 cycles. The results meant that the number of cycles significantly affected the AC values for mismatch 0.99, while the number of cycles did not affect the DC values. Therefore, for the synchronization mismatch, measurement cycle optimization was necessary to obtain more accurate *P* values.

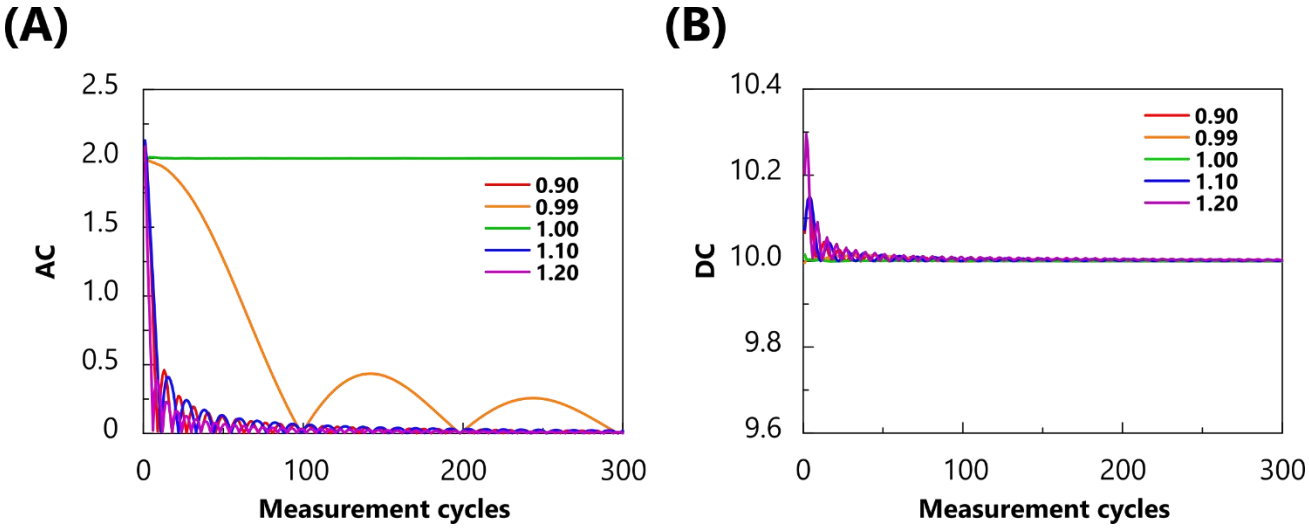

Figure 3.3 Theoretical (A) amplitude component (AC) values and (B) direct component (DC) values for synchronization mismatches in the range of 1 to 300 measurement cycles. The exact AC and DC values calculated from the ideal fluorescence polarization modulation were fixed to 2 and 10, respectively. The legends indicate mismatches ($f_{CCD}/4f_{LC}$).

3.3.2 Experimental Amplitude Component and Direct Component Values for Synchronization Mismatches

Second, the AC and DC values of a model sample were measured using the FP system for comparison with the calculated values. Fluorescein ethylene glycol solution, as a model sample, was prepared by

dissolving 1 mM fluorescein in ethylene glycol at a volume ratio of 1:100. The measured AC and DC values in the range of 1 to 300 measurement cycles are shown in Figure 3.4(A) and 3.4(B), respectively.

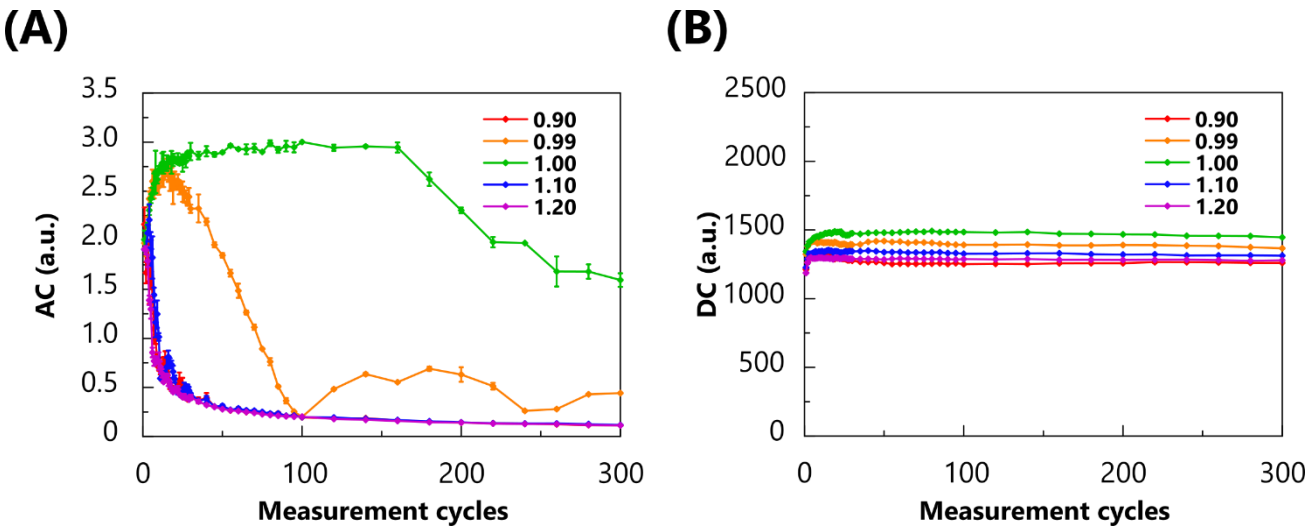

Figure 3.4 Experimental (A) amplitude component (AC) values and (B) direct component (DC) values for synchronization mismatches in the range of 1 to 300 measurement cycles. The legends indicate mismatches ($f_{CCD}/4f_{LC}$).

The measured DC values remained at certain values within 300 cycles and were not affected by the number of cycles, similar to the calculated values. The measured AC values under the synchronization mismatches decreased within 300 cycles, as expected. In particular, the recovery of the AC values was measured for mismatch 0.99, which was the same as that with the calculated values. These sets of results for synchronization mismatches almost agreed with the calculated AC and DC values within 150 cycles. However, the measured AC values for mismatch 0.99 and mismatch 1.00 were different from the calculated values when the number of measurement cycles was more than 160. In the case of mismatch 0.99, the second decline in AC values was observed at around 250 cycles, while the calculated value was around 200 cycles. In the case of mismatch 1.00, the AC values decreased from more than 160 cycles, while the calculated values were constant. The way that the frequencies synchronized to each other was considered the cause of the phenomena. In the FP system, the LC switching mechanism and CCD sampling mechanism were independent, so there was a possibility of

some synchronization mismatches. In order to measure the actual f_{LC}, the modulated excitation beam after passing through the LC layer was detected by a photodetector instead of the CCD. The LC modulation frequency was obtained using excitation light measurements taken with a photodetector (ET-2030, Electro-Optics Technology, Traverse, MI) connected to an oscilloscope (TBS 1062, Tektronix, Beaverton, OR). As a result, the actual f_{LC} was slightly different form the target f_{LC}. Therefore, there were some lags between the actual mismatches and the target mismatches, so the experimental AC values differed from the calculated AC values. Additionally, there were some synchronization mismatches under mismatch 1.00, as shown in Table 3.2. Because of the influence of these few synchronization mismatches, the measured AC values for mismatch 1.00 decreased at the large number of cycles. Although there were some small disagreements, the system generally worked ideally and the AC and DC values measured by the system were almost the same as the theoretical values.

Table 3.2. Measured liquid crystal (LC) modulation frequency (f_{LC}) and actual synchronization mismatches.

Target mismatch	**Target f_{LC}/Hz**	**Measured f_{LC}/Hz**	**Actual mismatch**
0.90	$3.33 = \frac{10}{3}$	3.330 ± 0.006	0.901 ± 0.002
0.99	$2.78 = \frac{25}{9}$	2.787 ± 0.101	0.987 ± 0.036
1.00	$2.78 = \frac{25}{9}$	2.787 ± 0.101	0.997 ± 0.037
1.10	2.50	2.495 ± 0.087	1.102 ± 0.039
1.20	2.50	2.495 ± 0.087	1.202 ± 0.042

3.3.3 Fluorescence Polarization Immunoassay of a Physiologically Active Substance for Synchronization Mismatches

Finally, FPIAs for PGE2 for the synchronization mismatches were demonstrated. To simplify the experiment, sample solutions that were reacted in a test tube were introduced into the microchannel using a syringe pump. The assays were performed according to the manual of the FPIA kit manufacturer. Standard

curves of *P* values against the PGE2 concentration for each synchronization mismatch at 50, 100, and 150 measurement cycles are shown in Figure 3.5.

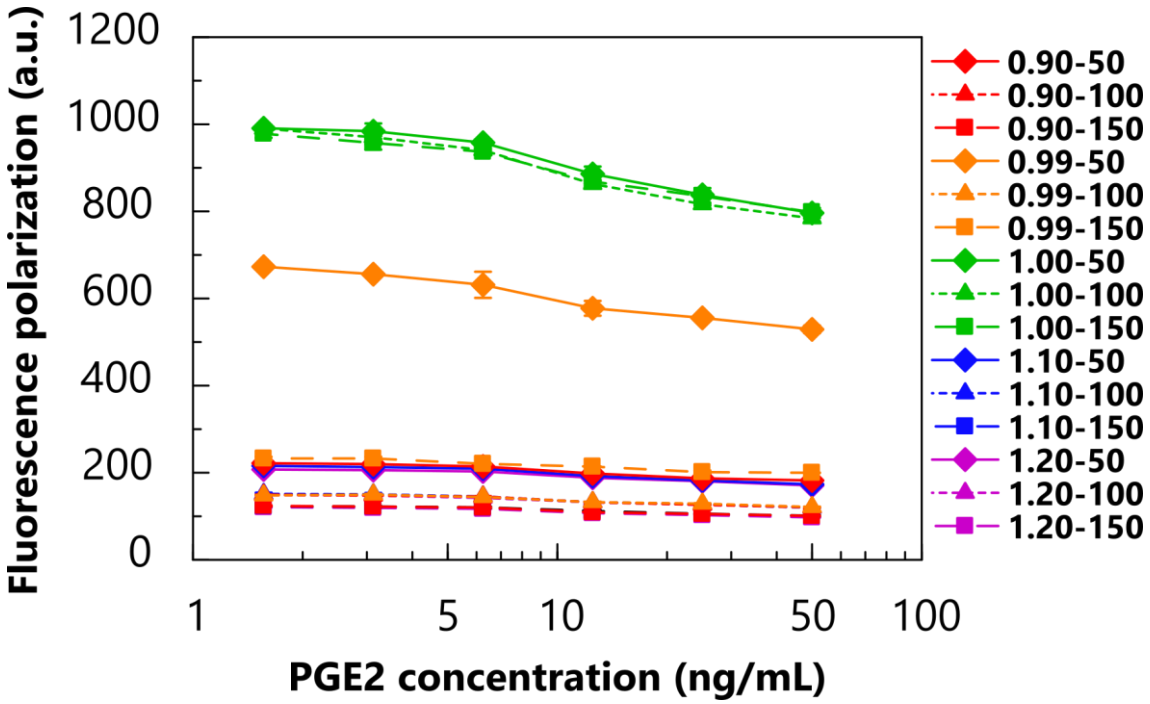

Figure 3.5 Standard curves of fluorescence polarization against the prostaglandin E2 (PGE2) concentration in the range of 1.56-50 ng/mL for each synchronization mismatch at 50 (diamonds), 100 (triangles), and 150 (squares) measurement cycles. The legends indicate mismatches and measurement cycles as mismatches - cycles.

Under the condition without synchronization mismatches, the *P* values remained at almost the same values at each cycle. On the other hand, with synchronization mismatches, the *P* values decreased as the number of measurement cycles increased. However, for mismatch 0.99, the recovery of the *P* values was observed. The *P* values increased at 150 cycles after decreasing at 100 cycles for mismatch 0.99. To obtain a better understanding, standard curves of *P* values against the PGE2 concentration for mismatch 0.99 at 50, 100, and 150 measurement cycles are shown in Figure 3.6(A), (B), and (C), respectively. The standard curves calculated from the Rodbard function ($y = d + \frac{a+d}{1+\left(\frac{x}{c}\right)^b}$) are also shown in Figure 3.6. The parameters, R^2 values, and dynamic ranges of the standard curves are summarized in Table 3.3.

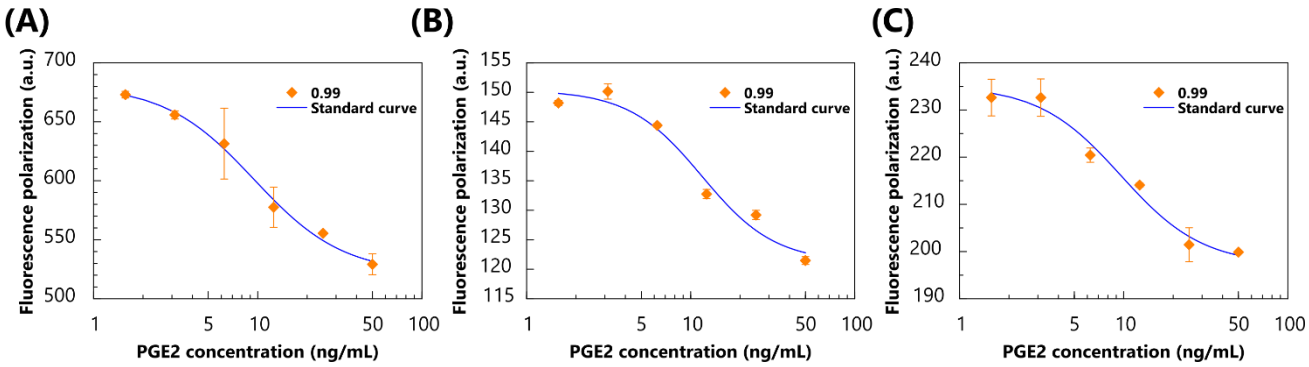

Figure 3.6 Standard curves of fluorescence polarization against the prostaglandin E2 (PGE2) concentration for mismatch 0.99 at (A) 50, (B) 100, and (C) 150 measurement cycles. The standard curves were calculated using the Rodbard function.

Table 3.3. The standard curve parameters, R^2 values, and dynamic ranges of FP calculated using the Rodbard function ($y = d + \frac{a+d}{1+\left(\frac{x}{c}\right)^b}$)) for each measurement cycle.

Number of measurement cycles	**50 cycles**	**100 cycles**	**150 cycles**
Standard curve parameters	a = 681.1 b = 1.596 c = 9.485 d = 521.2	a = 150.4 b = 1.955 c = 11.70 d = 121.2	a = 235.1 b = 1.738 c = 9.591 d = 197.1
R^2	0.9935	0.9711	0.9804
Dynamic range of FP* (a.u.)	159.90	29.20	37.98

*The dynamic ranges were calculated from the standard curve parameters (a-d).

The *P* values for mismatch 0.99 were significantly affected by the number of measurement cycles. Judging from the R^2 values, the measurement variation was small at 50 cycles compared to the large variation at 100 cycles. However, at 150 cycles, the measurement variation was small again. Similarly, the dynamic ranges of FP were dependent on the number of measurement cycles. The dynamic range was the largest at 50 cycles; however, the minimum range appeared at 100 cycles. Then, the dynamic range was large again at 150

cycles. As a result, the measurement performance of the system was dependent on the number of measurement cycles for the synchronization mismatches. In the case of mismatch 0.99, the measurement performance at 150 cycles was better than that at 100 cycles. Therefore, optimization of the number of measurement cycles was necessary to obtain *P* values with more accurate measurement performance.

3.4 Conclusions

Experimental and theoretical investigations on the influence of synchrony for synchronization measurements were conducted. First, the theoretical FP values of our FP measurement system based on the synchronization measurement between LC operation and CCD image sampling were calculated. When there were some synchronization mismatches between the LC operation and the image sampling, the calculated AC values decreased as the number of measurement cycles increased. In particular, when there was a relatively small synchronization mismatch, the AC values recovered at a certain number of cycles after the value decreased. The results meant that measurement cycle optimization was necessary to obtain more accurate *P* values for the synchronization mismatch. After an experimental confirmation using a model sample, FPIAs for PGE2 samples at several measurement cycles for the synchronization mismatch were conducted. The *P* values for mismatch 0.99 were significantly affected by the number of measurement cycles. Judging from the R^2 values and the dynamic range of the standard curve of PGE2, the measurement performance at 150 cycles was better than that at 100 cycles. Measurement performance recovery was observed for the relatively small synchronization mismatch, such as the 1% mismatch (mismatch 0.99). As a result, the measurement performance was dependent on the number of measurement cycles for the synchronization mismatches, thereby indicating the need for measurement cycle optimization. However, the behavior may potentially be applicable as a frequency filter. For example, at 150 measurement cycles, only the *P* values for mismatch 0.99 maintained high values, while the other *P* values for synchronization mismatches were cut off. In other words, only the frequency at mismatch 0.99 could pass through the band-pass frequency filter. The frequency filter could decrease the background from the excitation light by excitation light modulation and decrease the background

from other light sources that have their own frequency. Therefore, further investigation of the operation frequency and number of measurement cycles may demonstrate potential ways to improve the system sensitivity and measurement performance. A system with high sensitivity and high measurement performance is expected to contribute to high-throughput interaction analysis, such as protein-nucleic acids binding assays. Additionally, the information is useful not only for the FP system, but also for fluorescence imaging technology based on a synchronous detection system. A combination of the FP imaging system and a microfluidic device led to rapid and easy-to-use analysis with low consumption of samples, so the information will contribute to a wide range of applications.

References

[1] J. R. Lundblad, M. Laurance, and R. H. Goodman, *Mol. Endocrinol*., **10**, 607-612 (1996)

[2] K. Kakehi, Y. Oda, and M. Kinoshita, *Anal. Biochem*, **297**, 111-116 (2001)

[3] D. M. Jameson and S. E. Seifried, *Methods*, **19**, 222-233 (1999)

[4] Q. Wan and X. C. Le, *Anal. Chem.*, **72**, 5583-5589 (2000)

[5] J. Choi, D. Kang, H. Park, A. J. deMello, and S. Chang, *Anal. Chem.*, **84**, 3849-3854 (2012)

[6] J. A. Cruz-Aguado and G. Penner, *Anal. Chem.*, **80**, 8853-8855 (2008)

[7] M. M. Makowski, C. Gräwe, B. M. Foster, N. V. Nguyen, T. Bartke, and M. Vermeulen, *Nat. Commun.*, **9**, 1653 (2018)

[8] B. Wang, D. Ren, Z. You, Y. Yalikun, and Y. Tanaka, *Analyst*, **148**, 3560-3569 (2018)

[9] L. Qi, Y. Fan, H. Wei, D. Zhang, and Z. Zhang, *Sens. Actuators B*, **257**, 666-671 (2018)

[10] C. Li, K. Wen, T. Mi, X. Zhang, H. Zhang, S. Zhang, J. Shen, and Z. Wang, *Biosens. Bioelectron*., **79**, 258-265 (2016)

[11] M. Ma, M. Chen, L. Feng, H. You, R. Yang, A. Boroduleva, X. Hua, S.A. Eremin, and M. Wang, *Food Anal. Methods*, **9**, 2471-2478 (2016)

[12] T. Tachi, N. Kaji, M. Tokeshi, and Y. Baba, *Lab. Chip*., **9**, 966-971 (2009)

[13] T. Tachi, T. Hase, Y. Okamoto, N. Kaji, T. Arima, H. Matsumoto, M. Kondo, M. Tokeshi, Y. Hasegawa, and Y. Baba, *Anal. Bioanal. Chem.*, **401**, 2301-2305 (2011)

[14] O. Wakao, Y. Fujii, M. Maeki, A. Ishida, H. Tani, A. Hibara, and M. Tokeshi, *Anal. Chem.*, **87**, 9647-9652 (2015)

[15] O. Wakao, K. Satou, A. Nakamura, K. Sumiyoshi, M. Shirokawa, C. Mizokuchi, K. Shiota, M. Maeki, A. Ishida, H. Tani, K. Shigemura, A. Hibara, and M. Tokeshi, *Rev. Sci. Instrum.*, **89**, 024103 (2018)

[16] M. E. Jolley, S. D. Stroupe, C. H. Wang, H. N. Panas, C. L. Keegan, R. L. Schmidt, and K. S. Schwenzer, *Clin. Chem.*, **27**, 1190-1197 (1981)

[17] M. Winkler, G. Schumann, D. Petersen, M. Oellerich, and K. Wonigeit, *Clin. Chem.*, **38**, 123-126 (1992)

[18] T. Mi, Z. Wang, S. A. Eremin, J. Shen, and S. Zhang, *Agric. Food Chem.*, **61**, 9347-9355 (2013)

[19] D. S. Smith and S. A. Eremin, *Anal. Bioanal. Chem.*, **391**, 1499-1507 (2008)

[20] N. Kimura, M. Maeki, Y. Sato, Y. Note, A. Ishida, H. Tani, H. Harashima, and M. Tokeshi, *ACS Omega.*, **3**, 5044-5051 (2018)

[21] The RAND function is one of the functions in Microsoft Excel (https://www.microsoft.com/). The function returns a random real number greater than 0 but less than 1. A new random real number is returned every time the worksheet is calculated.

CHAPTER 4 A Cost-Reduced Compact Fluorescence Polarization System with a High-Transmittance Liquid Crystal Layer

4.1 Introduction

Understanding systematic biological systems and phenomena is important to obtain fundamental knowledge in biology and drug discovery applications [1-2]. Biophysics attempts to elucidate biological systems and functions using physicochemical, reactive mechanics, and statistical approaches. Molecular interactions are pivotal in understanding the functions of biological systems and phenomena. Analyzing specific molecular interactions is one of the major challenges in biophysics. Fluorescence imaging [3], transmission electron microscopy [4], and fluorescence resonance energy transfer [5] are typically employed to analyze molecular interactions, such as protein-protein interaction, protein-ligand interaction, and protein-DNA interaction. However, these techniques require complex and expensive equipment as well as several time-consuming technical processes for sensitive molecular interaction analysis. Therefore, a simple, rapid, and high-throughput technique for molecular interaction analysis is required. Fluorescence polarization (FP) is a solution-based method that is widely used to study molecular interactions [6-12]. In FP measurements, P, namely the degree of polarization, is determined by the following equation:

$$P = (I_{\parallel} - I_{\perp})/(I_{\parallel} + I_{\perp}) \qquad (3.1)$$

where $I_{\parallel}$ and $I_{\perp}$ are the fluorescence intensities parallel and perpendicular to the excitation polarization, respectively. Therefore, it is necessary to select each polarization to determine P. Conventional FP measurement apparatuses employ a rotating polarizer [6-10] or a polarizing splitter [11, 12] to select the polarizations and detect their intensities with a photodiode [6, 7, 8, 11] or an image sensor [9, 10, 12]. FP measurements with this mechanism are limited to single sample analysis and low throughput. Although commercial fluorescence spectrometers present microplate-based FP measurements to improve the throughput, sample scanning is necessary, which requires additional complex optical components [13, 14].

Previously, a unique FP measurement system with a liquid crystal (LC) layer and a charge coupled device (CCD) image sensor, which enables simultaneous FP imaging for multiple samples, was developed [15]. The FP measurement system was based on the synchronized detection between the switching rate of the LC layer and the sampling rate of the CCD. This system consists of a semiconductor laser, CCD camera, LC layer,

and optical components, such as an objective lens, filters, and mirror. Using this system, simultaneous detection of molecular interactions between antigens and antibodies in multiple samples using FP immunoassay (FPIA) was successfully demonstrated. However, the measurement precision of the system was lower than that of the conventional FP apparatus. The main reason for this low precision was that only a fraction of the incident light was transmitted by the LC layer, which was obtained by disassembling a commercially available LC display (LCD). Moreover, the control system for synchronization between the switching rate of the LC layer and the sampling rate of the CCD needed to be improved.

In this chapter, an improved system addressing the problems of the previous system was developed. First, in order to design a suitable LC layer, the wavelength dependence of LC transmittance was considered. A FPIA for a model sample was conducted using long-pass or band-pass filters to compare each FP measurement performance. As a result of the comparison between the long-pass and band-pass filters, it was confirmed that the filtration of the wavelength affected the FP performance. Based on these results, an improved system using a twisted nematic (TN) mode LC and dichroic block including an excitation and emission filter was developed. By using a homebuilt high-transmittance LC suitable for the purpose, the performance of the system was significantly improved. Additionally, cost reduction was achieved by using an inexpensive CCD and a light emitting diode (LED) instead of an electronically cooled CCD and a laser, respectively. In order to evaluate the performance of the developed system, simultaneous FPIA of multiple samples of prostaglandin E2 (PGE2) was performed and compared with a conventional FP apparatus.

4.2 Experimental

4.2.1 Measurement Principle

The detection principle was based on LC-CCD synchronization detection, as mentioned in Ref. 15. In a FP imaging system, the FP signal passing through the LC layer is modulated at a certain frequency (f Hz) by on-off switching of the voltage applied to the LC layer. When such a fluorescence signal is captured by the

CCD, which is operated at 4*f* Hz to synchronize with the LC switching, four images with FP signals are sampled. By processing these four images, the system obtains an amplitude component (AC) image, which includes different components of FP, and a direct component (DC) image, which includes a sum of the components of FP. Thus, the *P* values of multiple samples are obtained as a single two-dimensional image through image analysis.

4.2.2 Consideration of the Wavelength Dependence of Liquid Crystal Transmittance

The wavelength dependence of LC layer transmittance was considered by comparison of the FP measurement performance using two kinds of optical filters. Figure 4.1 shows a schematic illustration of the setup for the FPIA to compare the FP measurement performance. A band-pass filter (YIF-BA510-550S; transmittance range wavelength (OD > 7) of 517-542 nm; Sigma Koki, Tokyo, Japan) or a long-pass filter (YIF-BA510IFS; transmittance range wavelength (OD > 7) of 517 < nm; Sigma Koki, Tokyo, Japan) were used. The TN mode LC layer for development (Tianma Japan, Kawasaki, Japan) was directly controlled by a function generator (FG) (WF1948, NF, Yokohama, Japan). The LC layer for development did not include a color filter. The frequency of the LC layer for development orientation and that of image sampling for the CCD were synchronized by a FG with a ratio of 1:4. The FPIA for PGE2 as a model target was conducted to evaluate the performance. The reactions were performed according to the instructions of the commercial PGE2 assay kit manufacturer (Abnova Prostaglandin E2 FPIA Kit, Abnova, Taipei, Taiwan). A made-to-order quartz glass cell (Shin-Etsu Chemical Co., Tokyo, Japan), which had a depth of 500 μm, was used as the sample cell.

To compare the performance depending on the condition, the FP measurements were also taken using a previous combination of a color LC layer (disassembled from a 3.5-inch color LCD; CLAA035QVA01, Chunghwa Photo Tubes Ltd., Taoyuan City, Taiwan) and a long-pass filter (YIF-BA510IFS, Sigma Koki).

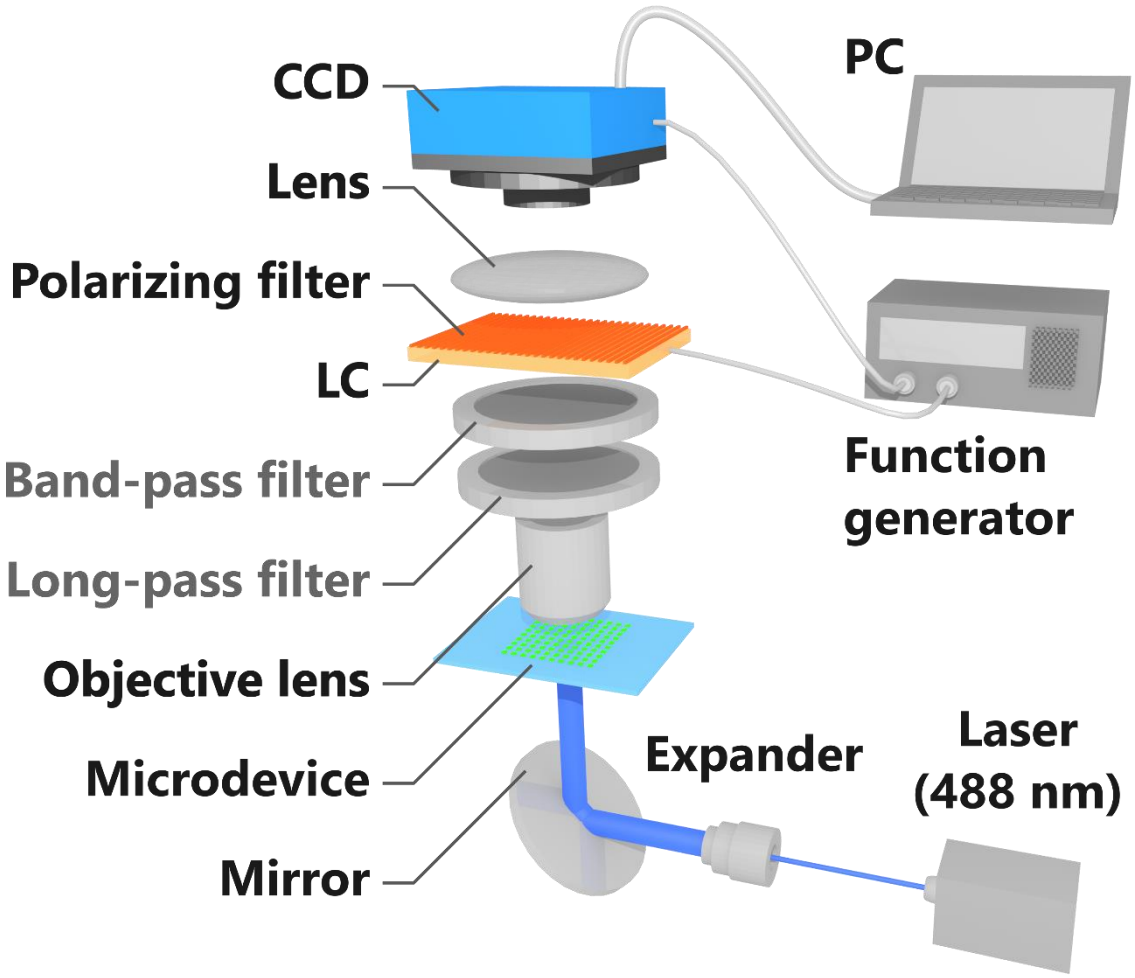

Figure 4.1 Schematic illustration of the setup for the fluorescence polarization immunoassay to compare the fluorescence polarization measurement performance between band-pass and long-pass filters.

4.2.3 Development of a Cost-Reduced Compact Fluorescence Polarization System with a Suitable High-Transmittance Liquid Crystal Layer

A FP measurement system with a suitable high-transmittance LC layer and LED allowing multi-sample processing was built. A concept illustration of the setup using an LED and high-transmittance LC layer is shown in Figure 4.2.

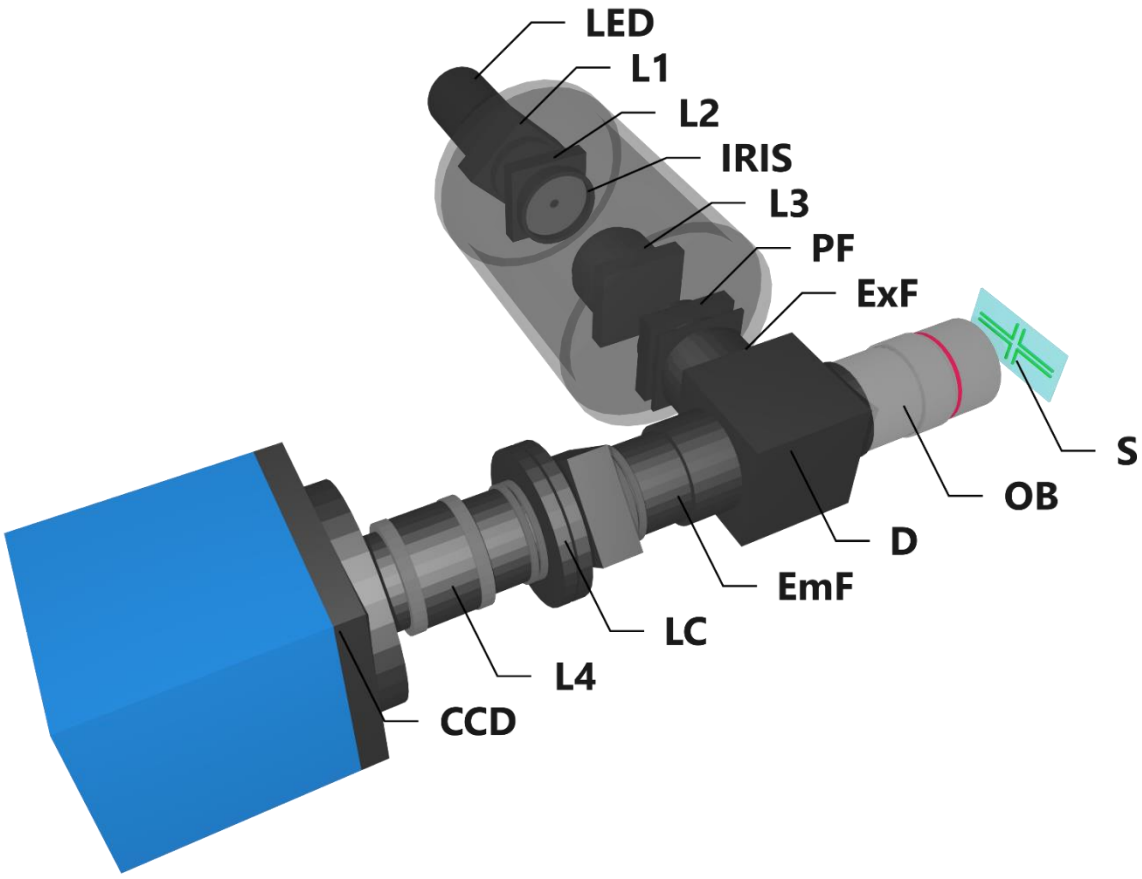

Figure 4.2 Schematic illustration of the experimental setup for fluorescence polarization imaging (L: lens; PF: polarizing filter; ExF: excitation filter; D: dichroic mirror; OB: objective lens; S: sample; and EmF: emission filter).

A 470 nm wavelength LED (M470L3, Thorlabs, Newton, NJ) was employed as the excitation source. In order to collimate the beam, an aspheric condenser lens (ACL5040U-A, Thorlabs) was used. The excitation beam was introduced into plano-convex lenses (SLB-25.4-35P, Sigma Koki) and focused on the blades of an iris diaphragm (SM1D12, Thorlabs). The iris diaphragm removed the unnecessary beam to create a uniform beam profile. After passing through the iris diaphragm, the beam was collimated again by an achromatic lens (ATL-30-40PY2, Sigma Koki). The collimated beam was introduced into a linear glass polarizing filter (Edmund Optics, Barrington, NJ). The polarized excitation beam entered a dichroic block (A11214, Hamamatsu Photonics, Hamamatsu, Japan) with an excitation filter (ET470/10x, Chroma Technology, Bellows Falls, VT) and a dichroic mirror (DM505, Olympus, Tokyo, Japan). The dichroic mirror reflected the

excitation beam, and the beam passed through the objective lens (M Plan Apo 5×, Mitutoyo, Kawasaki, Japan). The excitation beam was focused onto a microdevice, which held the samples to be imaged. The microdevice, a photo of which is shown in Figure 4.3, was fabricated using standard soft-lithography techniques with polydimethylsiloxane (PDMS) including India ink and a glass slide [16]. The microdevice had microchannels with individual inlets and outlets to hold four different samples. Each microchannel was 300 μm wide and 1 mm deep with < 1 μL sample volume. The microdevice was designed to obtain four samples in the same field of view. The sample had an emission wavelength of approximately 520 nm. The fluorescence signals were collected by the objective lens and then introduced into the dichroic block including the emission filter (ET520/10x, Chroma Technology). After passing through the dichroic mirror and emission filter, the fluorescence passed through a high-transmittance LC layer (MS-β14A, Tianma Japan, Kawasaki, Japan) with a polarization filter while polarization modulation occurred. The high-transmittance LC layer, which employed the TN mode, was designed as a single pixel and did not include a color filter to increase the transmittance. The transmittance increased from approximately 7% to 40%. This addressed one of the main drawbacks of the previous FP system. The fluorescence signals were focused on the CCD image sensor (Retiga R1, QImaging, Surrey, BC, Canada) by an achromatic lens (ATL-30-40PY2, Sigma Koki) and were captured as images. The captured images were processed by the homebuilt software designed using Microsoft Visual Studio. The frequency of the high-transmittance LC layer orientation and that of image sampling for the CCD were synchronized using a FG (WF1948) with a ratio of 1:4. The applied voltage to the high-transmittance LC layer was designed to fit the measurement conditions (60 Hz; < 8 V).

FPIA is a popular FP measurement technique [17, 18] for detecting molecular interactions. FPIA is based on the competitive binding reaction of an unlabeled target molecule and a fluorescent-labeled target molecule (tracer) to an antibody. A simultaneous multi-sample FPIA for PGE2 as a model target was demonstrated to evaluate the performance of the developed compact system. The mixture of PGE2, fluorescein-conjugated PGE2, and anti-PGE2 antibodies was incubated before sample measurement. The reactions were performed according to the instructions of the commercial PGE2 assay kit manufacturer. The

microdevice was designed to obtain four samples with different target concentrations in the same field of view. Four simultaneous FP measurements of seven different PGE2 concentrations (1.56, 3.13, 6.25, 12.5, 25, 50, and 100 ng/mL) were demonstrated. The measurements were performed in triplicate. FP measurement of a similar sample was also performed with a commercial conventional FP apparatus (FP-715, JASCO Co., Tokyo, Japan) to compare their performance.

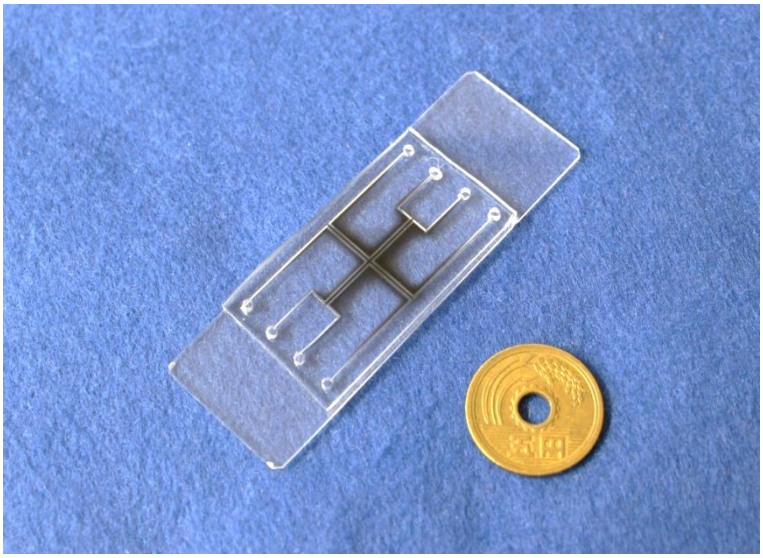

Figure 4.3 Photo of the microdevice for fluorescence polarization measurements. The polydimethylsiloxane (PDMS) of the microdevice included India ink to decrease the background from the excitation light.

4.3 Results and Discussion

4.3.1 Consideration of the Wavelength Dependence of Liquid Crystal Transmittance

First, in order to design a suitable LC layer, the wavelength dependence of LC transmittance was considered. FPIAs for model samples of different PGE2 concentrations (1.56, 6.25, 25, and 100 ng/mL) were conducted using long-pass or band-pass filters to compare each FP measurement performance. Each sample was introduced into the 500 μm depth pool cell. Standard curves of *P* values against the PGE2 concentration obtained by the system using the LC layer for development and each filter are shown in Figure 4.4. Standard

curves of *P* values against the PGE2 concentration obtained from the system using the previous LC layer are also shown in Figure 4.4.

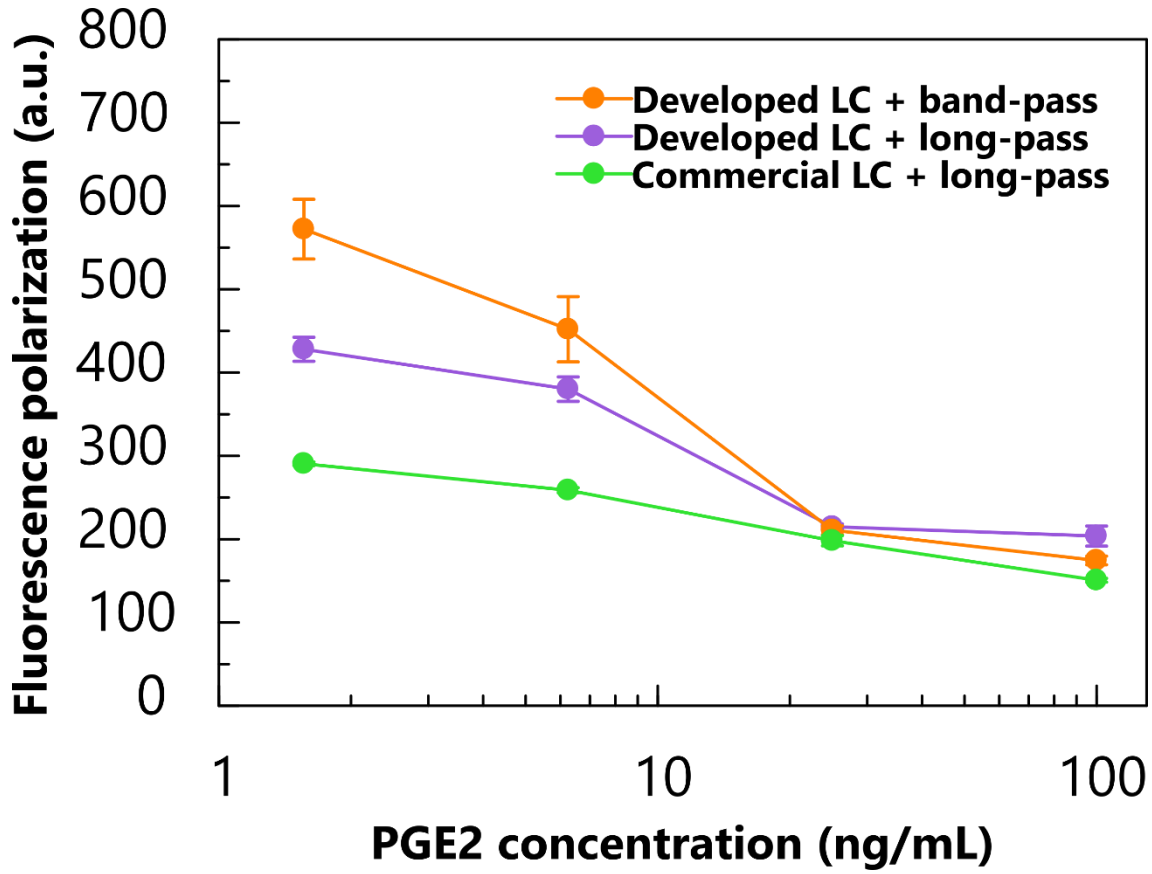

Figure 4.4 Standard curves of *P* values against the prostaglandin E2 (PGE2) concentration obtained by the system with a liquid crystal (LC) layer for development and a band-pass filter (orange), those with a LC layer for development and a long-pass filter (purple), and those with the previous commercial LC layer and a long-pass filter (green).

Compared to the dynamic range of the result using the previous LC layer, which included a color filter, that of the results using the LC layer for development was wider. This was because the LC layer for development did not include a color filter, so transmittance increased. As the transmittance increased, the FP signal appeared significantly. The dynamic ranges of FP were dependent on the type of filter used. The dynamic range of FP was narrow with the system using the long-pass filter. However, the dynamic range of

FP was wide with the system using the band-pass filter. Generally, it is known that LC transmittance is dependent on the wavelength. Figure 4.5 shows the typical transmittance of a TN mode LC layer against wavelengths when the voltage is on (A) and off (B).

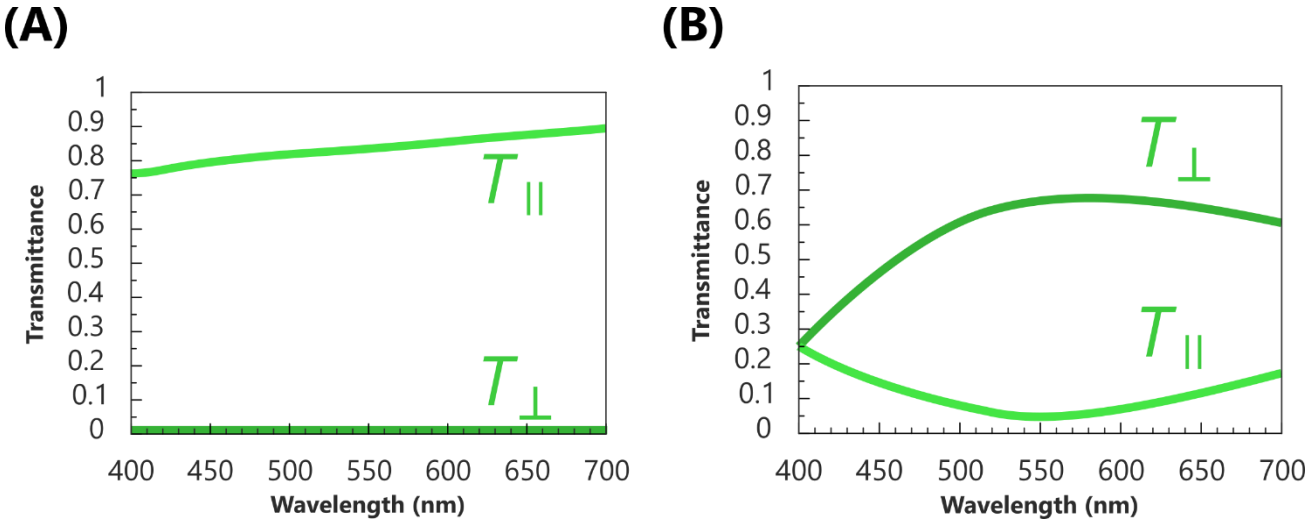

Figure 4.5 Typical transmittance of a twisted nematic (TN) mode liquid crystal layer against wavelengths when the voltage is on (A) and off (B), where $T_{\parallel}$ and $T_{\perp}$ are the transmittances parallel and perpendicular to the base polarization, respectively.

As shown in Figure 4.5, the transmittance of a LC layer depends on the wavelength, and the polarization ratio ($T_{\parallel}/T_{\perp}$) also depends on the wavelength. Therefore, the filtration of wavelengths affects the FP performance, which is controlled by the transmittance (S/N ratio) and polarization ratio. For these reasons, the dynamic range and sensitivity of FP measurements with the system using the band-pass filter were better than those with the system using the long-pass filter. Based on these results, the selection of the filter is important for system improvement, so the improved system employed a dichroic block including an excitation and emission filter.

4.3.2 Development of a Cost-Reduced Compact Fluorescence Polarization System with a Suitable High-Transmittance Liquid Crystal Layer

Figure 4.6 and Figure 4.7 show photos of the whole developed system and optics system, respectively. Figure 4.8 shows the LC layer designed to adjust depending on its purpose. The designed LC layer that was designed as a single pixel without a color filter increased the transmittance from approximately 7% to 40%. This addressed one of the main drawbacks of the previous FP system. The suitable designed voltage was applied to the LC layer, and the transmittance FP from the LC layer was modulated as a sine function, which was experimentally conformed.

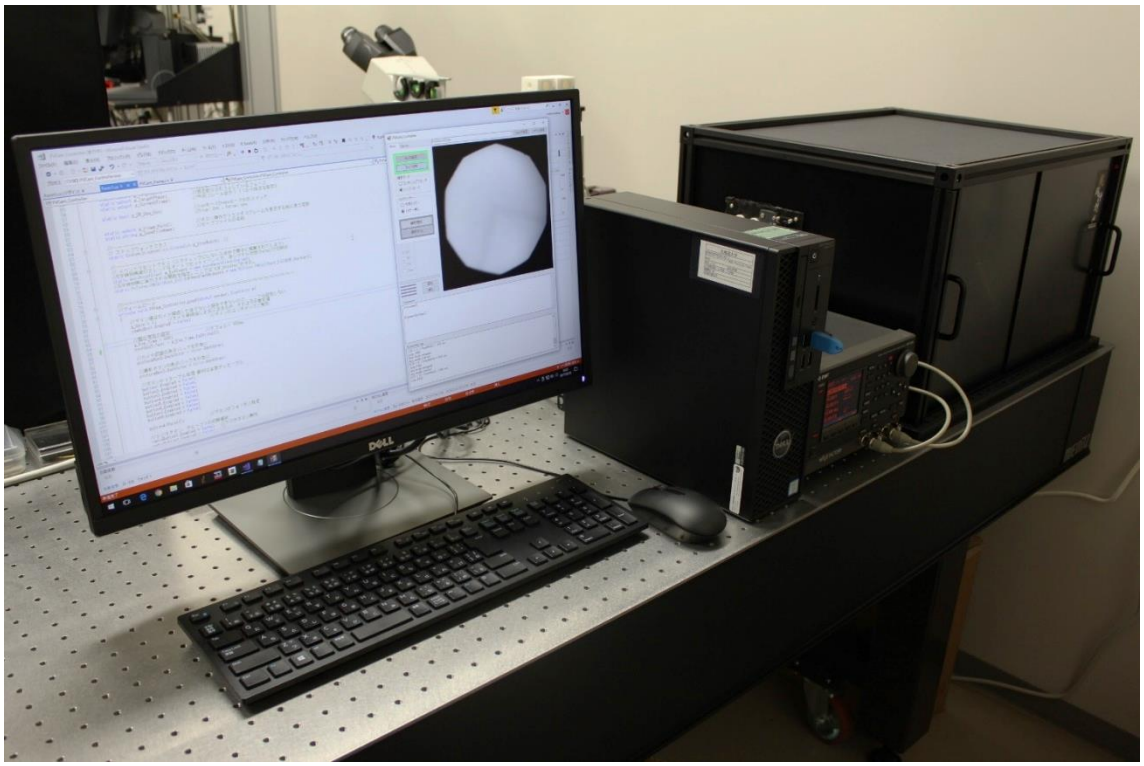

Figure 4.6 Photo of the whole setup for fluorescence polarization measurements.

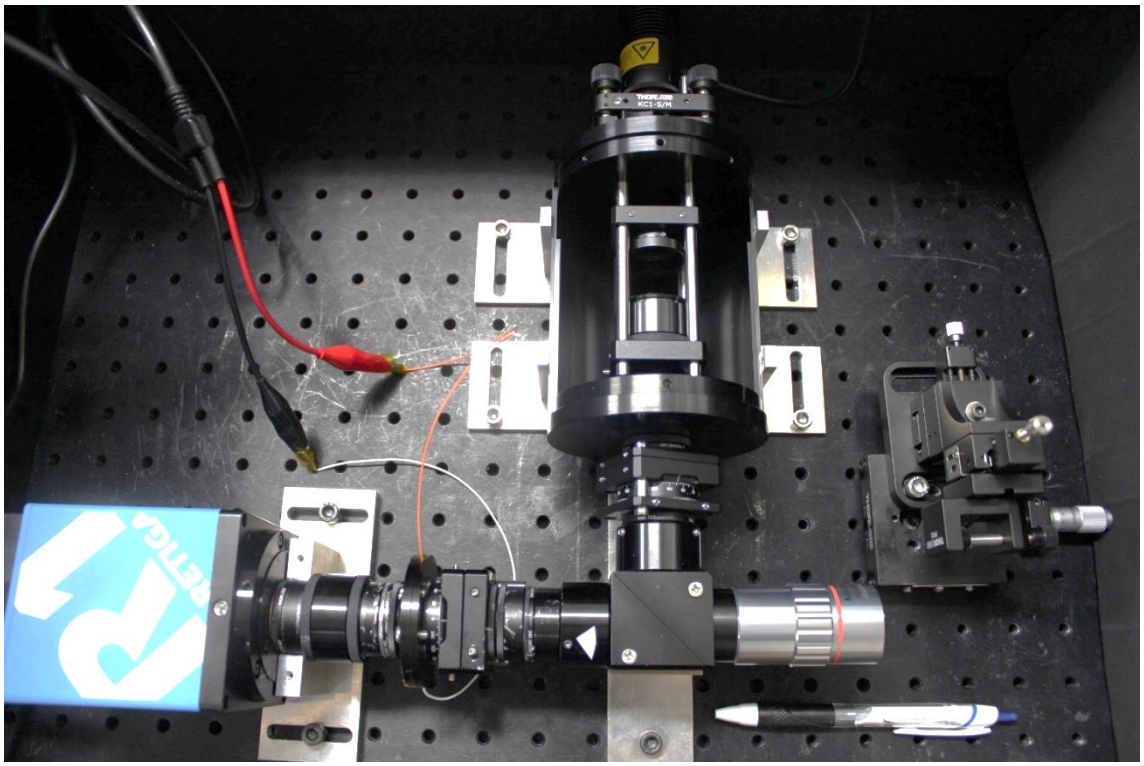

Figure 4.7 Photo of the optical part of the fluorescence polarization measurement setup.

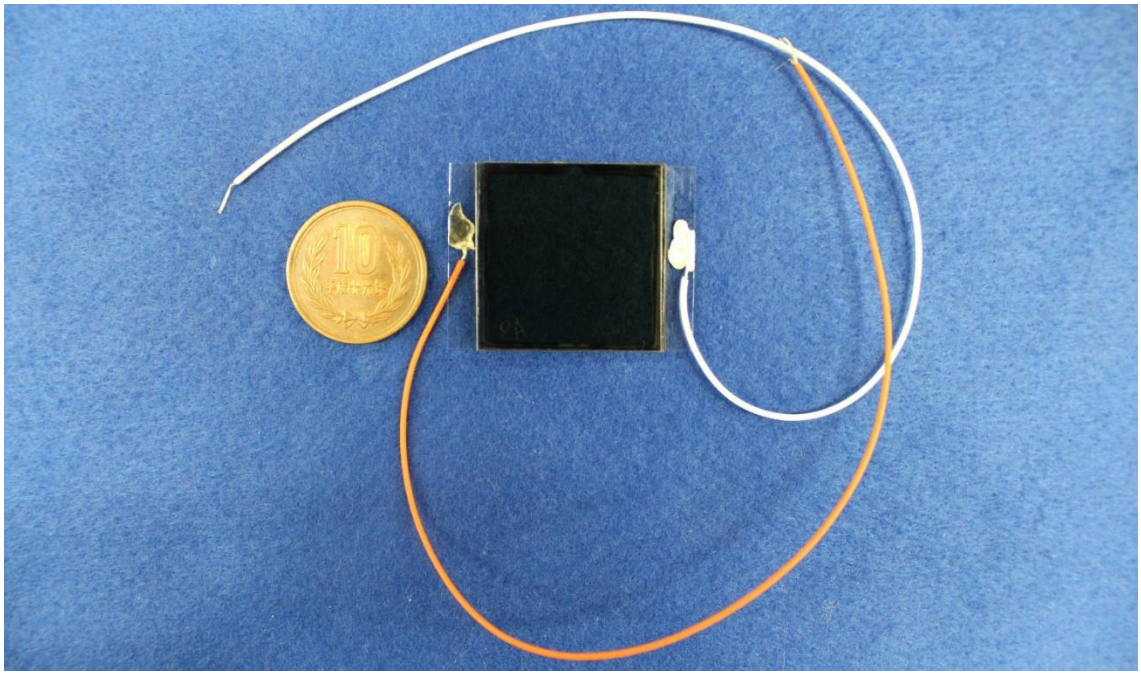

Figure 4.8 The liquid crystal layer designed to adjust depending on its purpose. The transmittance increased from approximately 7% to 40%. This addressed one of the main drawbacks of the previous fluorescence polarization system.

A simultaneous multi-sample FPIA for PGE2 as the model target was demonstrated to evaluate the performance of the developed compact FP system. PGE2, which is the lipid metabolite of arachidonic acid, is an endogenous mediator and modulator of innate immunity, inflammatory effects [19], and sleeping and waking regulation [20]. The mixture of PGE2, fluorescein-conjugated PGE2, and anti-PGE2 antibodies was incubated before sample measurement. Four simultaneous FP measurements of seven different PGE2 concentrations (1.56, 3.13, 6.25, 12.5, 25, 50, and 100 ng/mL) were demonstrated using the microdevice. Figure 4.9 shows a typical *P* image obtained by the developed FP system. The standard curve was obtained from the luminescence of microchannels in these *P* images, as shown in Figure 4.10. For performance comparison, the standard curves obtained from the previous system, which employed a commercially available LC layer and conventional instruments, are also shown in Figure 4.10. The coefficient of variations (CVs) from these results are shown in Table 4.1.

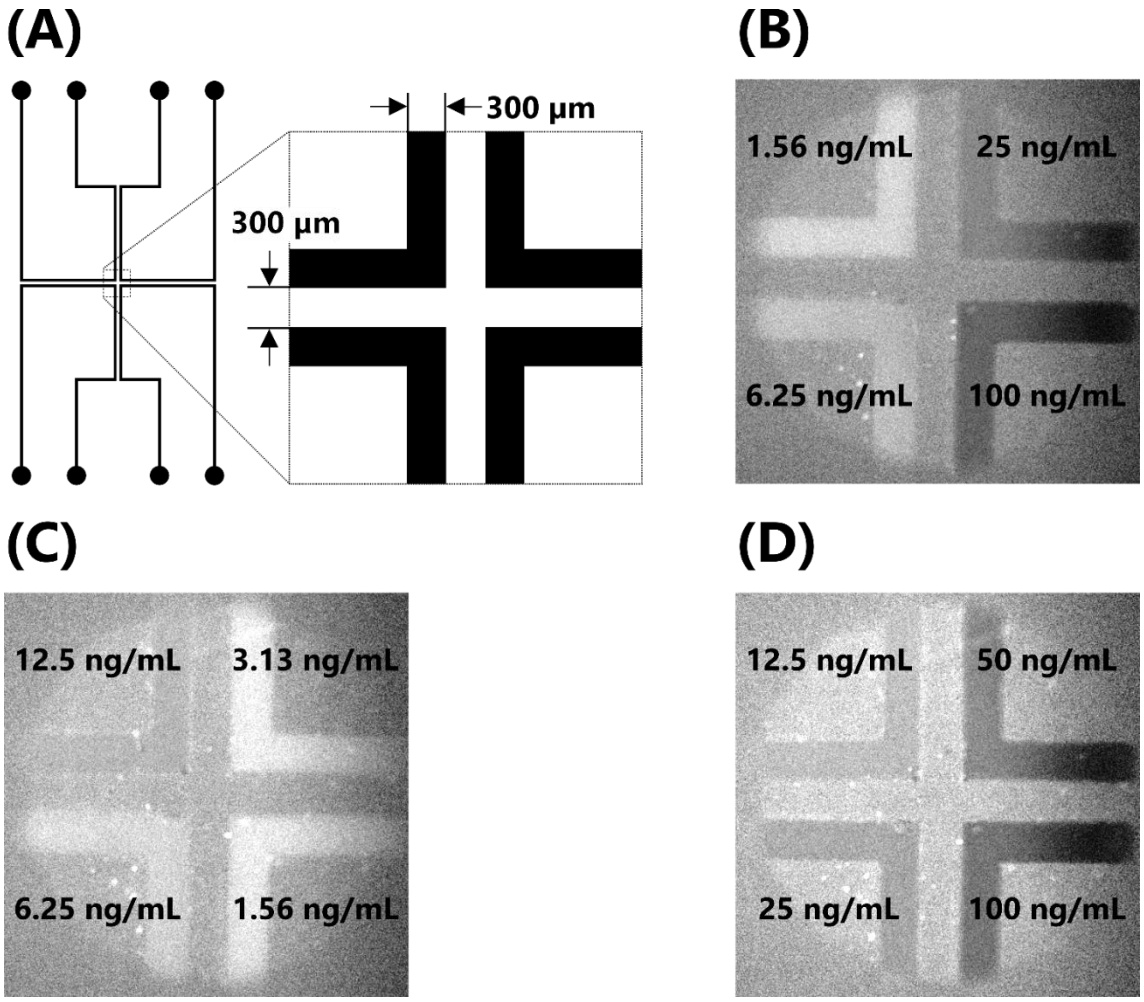

Figure 4.9 Images obtained by the developed fluorescence polarization (FP) imaging system. (A) Design and dimensions of the microdevice. FP imaging of four samples with several prostaglandin E2 concentrations, namely (B) 1.56, 6.25, 25, and 100 ng/mL; (C) 1.56, 3.13, 6.25, and 12.5 ng/mL; and (D) 12.5, 25, 50, and 100 ng/mL.

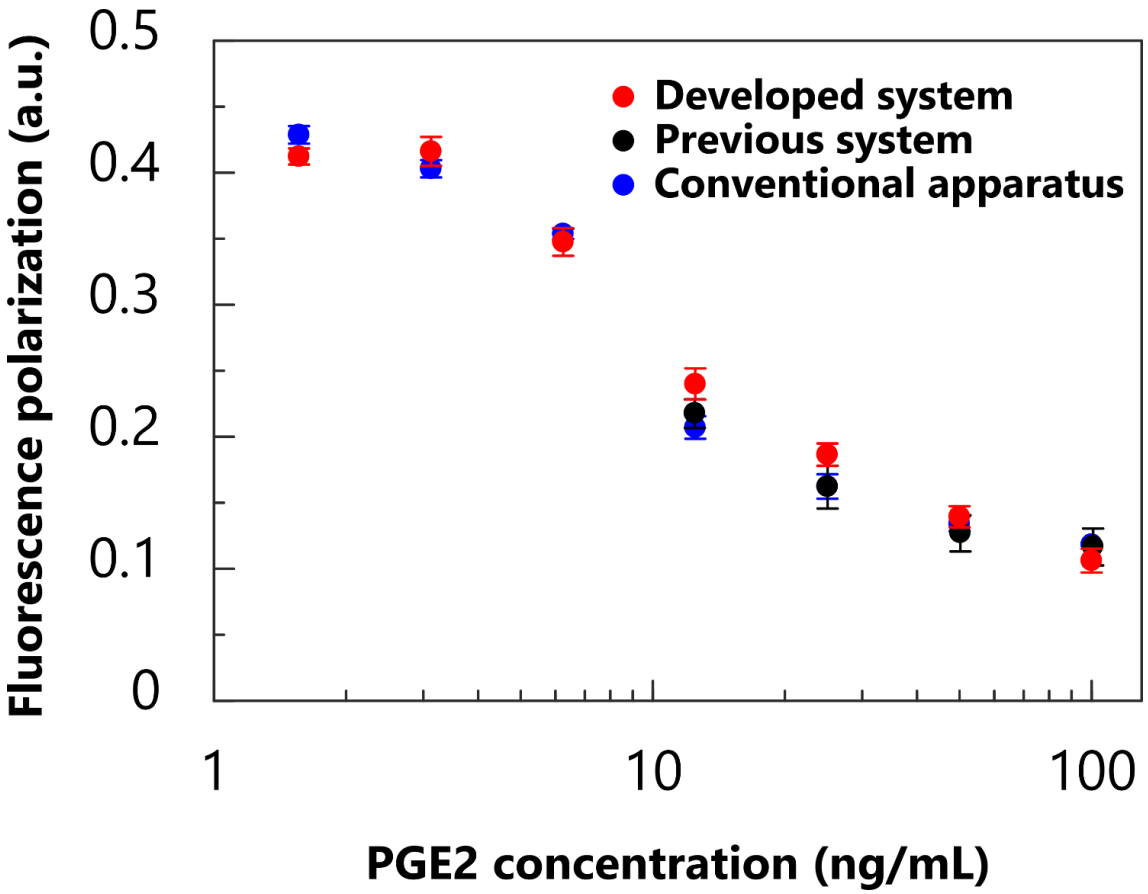

Figure 4.10 Standard curve of fluorescence polarization against prostaglandin E2 (PGE2) concentration in the range of 1.56-100 ng/mL obtained from the developed compact system, previous system, and conventional apparatus.

Table 4.1 Percentages of coefficient of variations from the standard curve in Figure 4.10.

PGE2 (ng/mL)	Developed system (%)	Previous system[15] (%)	Conventional apparatus (%)
100	7.73	10.36	0.49
50	5.32	9.45	4.16
25	4.30	9.01	5.72
12.5	4.72	4.61	4.13
6.25	2.93	*1	1.07
3.125	2.57	*1	1.63
1.5625	1.43	*1	1.55

*1The results could not to be obtained because of a lack of fluorescence intensities.

A decrease in *P* values was observed with increasing PGE2 concentration, as expected. Additionally, these sets of results were correlated with each other, thereby confirming that FP imaging is possible with the developed system. The error bars of the results obtained from the developed system were smaller than those obtained with the previous system because of increased LC layer transmittance and improved synchronization. While the maximum standard deviation against *P* deviation of the conventional FP apparatus was 3.0%, those of the developed and previous systems were 3.9% and 16.1%, respectively. Therefore, the measurement precision of the developed system was almost the same as that of the conventional FP apparatus. By altering the microdevice design, it will be possible to increase the number of samples detected simultaneously. The increased throughput is an advantageous feature for the field of molecular interaction analysis.

4.4 Conclusions

A new, improved FP measurement system with simultaneous sample processing ability was developed. Simultaneous FPIAs of multiple samples for PGE2 were performed to evaluate the measurement performance of the system. From the results, the measurement performance of the developed system was comparable with that of the conventional FP apparatus, thereby improving from the previous system. Table 4.2 summarizes and compares the abilities of the three apparatuses (the developed compact FP system, previously developed FP system, and conventional FP system) in terms of the number of samples processed simultaneously, measurement precision, and cost.

Table 4.2 Comparative table of the abilities of the developed system, previous system, and conventional apparatus.

	Developed system	**Previous system[15]**	**Conventional apparatus**
Number of samples	Multiple	Multiple	Single
Precision (%)	3.9	16.1	3.0
Cost ($)	13000	57000	10000

The developed system could conduct simultaneous FP measurements of multiple samples, and the measurement precision of the system was comparable with that of the conventional FP apparatus designed for single sample analysis. Additionally, cost reduction was achieved by using an inexpensive CCD and an LED. Theoretically, the compact system has the potential for further price reduction by optimizing the optical components (lenses and filters), optical arrangement, and electronics. Moreover, an increase in the number of samples processed at the same time is possible by changing the microdevice design. If the inexpensive high-throughput FP measurement system is developed, then its wide usage in molecular interaction studies is expected.

References

[1] S. Boccaletti, V. Latora, Y. Moreno, M. Chavez, and D.-U. Hwang, *Phys. Rep.*, **424**, 175 (2006)

[2] H. Kitano, *Science*, **295**, 1662 (2002)

[3] J. L. Schwartz, E. Snapp, and A. Kenworthy, *Nature. Rev. Mol. Cell. Biol.*, **2**, 444 (2001)

[4] M. Cohen, Y. B. Tzur, E. Neufeld, N. Feinstein, M. R. Delannoy, K. L. Wilson, and Y. Gruenbaum, *J. Struct. Biol.*, **140**, 232 (2002)

[5] E. A. Jares-Erijman and T. M. Jovin, *Nat. Biotechnol.*, **21**, 1387 (2003)

[6] J. R. Lundblad, M. Laurance, and R. H. Goodman, *Mol. Endocrinol.*, **10**, 607 (1996)

[7] K. Kakehi, Y. Oda, and M. Kinoshita, *Anal. Biochem.*, **297**, 111 (2001)

[8] D. M. Jameson and S. E. Seifried, *Methods*, **19**, 222 (1999)

[9] T. Tachi, N. Kaji, M. Tokeshi, and Y. Baba, *Lab. Chip.*, **9**, 966 (2009)

[10] T. Tachi, T. Hase, Y. Okamoto, N. Kaji, T. Arima, H. Matsumoto, M. Kondo, M. Tokeshi, Y. Hasegawa, and Y. Baba, *Anal. Bioanal. Chem.*, **401**, 2301 (2011)

[11] Q. Wan and X. C. Le, *Anal. Chem.*, **72**, 5583 (2000)

[12] J. Choi, D. Kang, H. Park, A. J. deMello, and S. Chang, *Anal. Chem.*, **84**, 3849 (2012)

[13] J. C. Owicki, *Biomol. Screen.*, **5**, 297 (2000)

[14] J. A. Cruz-Aguado and G. Penner, *Anal. Chem.*, **80**, 8853 (2008)

[15] O. Wakao, Y. Fujii, M. Maeki, A. Ishida, H. Tani, A. Hibara, and M. Tokeshi, *Anal. Chem.*, **87**, 9647 (2015)

[16] M. Maeki, T. Saito, Y. Sato, T. Yasui, N. Kaji, A. Ishida, H. Tani, Y. Baba, H. Harashima, and M. Tokeshi, *RSC Adv.*, **5**, 46 181 (2015)

[17] N.V. Beloglazova and S.A. Eremin, *Talanta*, **142**, 170 (2015)

[18] J. Choi, G. Kim, S. Lee, J. Kim, A. J. deMello, and S. Chang, *Biosens. Bioelectron.*, **67**, 497 (2015)

[19] D. M. Aronoff, C. Canetti, and M. Peters-Golden, *J. Immunol*., **173**, 559 (2004)

[20] O. Hayashi, *J. Biol. Chem.*, **263**, 14 593 (1988)

CHAPTER 5 High-Throughput Immunoassay Using a Portable Fluorescence Polarization Analyzer with a Microdevice

5.1 Introduction

Fluorescence polarization (FP) is a solution-based method that is widely used to study molecular interactions [1-7]. In FP measurements, *P*, namely the degree of polarization, is determined using the following equation:

$$P = (I_{\parallel} - I_{\perp})/(I_{\parallel} + I_{\perp}) \quad (3.1)$$

Where $I_{\parallel}$ and $I_{\perp}$ are the fluorescence intensities parallel and perpendicular to the excitation polarization, respectively. For this reason, it is necessary to select each polarization and detect each fluorescence intensity to determine *P*. Conventional FP measurement apparatuses employ a rotating polarizer [1-5] or a polarization splitter [6, 7] to separate the polarizations. Additionally, the detection part of the FP apparatus employs a photodiode [1, 2, 3, 6] or an image sensor [4, 5, 7] to detect the intensities. FP measurement using this mechanism is limited to single sample analysis, so the throughput of the measurement is low. Although commercial microplate-based FP measurement apparatuses attempt to improve the throughput, scanning for all wells including samples is necessary, so additional complex optical components are required [8, 9].

Previously, a unique FP measurement principle with a liquid crystal (LC) layer and a charge coupled device (CCD) image sensor, which enables simultaneous FP imaging for multiple samples, was developed [10]. The FP measurement principle was based on the synchronized detection between the switching rate of the LC layer and the sampling rate of the CCD. Based on this principle, a compact FP system with an inexpensive LED and suitable high-transmittance LC layer was developed [11]. The developed system could conduct simultaneous FP measurements of multiple samples, and the measurement precision of the system was comparable with that of the conventional FP apparatus designed for single sample analysis. However, from the viewpoint of general utility, further downsizing, cost reduction, and throughput increase are necessary.

In this chapter, a high-throughput portable FP analyzer that was improved from the previous compact system [11] was developed. Previously, a high-power laser-based FP system demonstrated simultaneous FP immunoassays (FPIAs) of 100 samples [12]. However, the system was expensive and large because it used an electronically cooled CCD and a laser. Here, in order to downsize and reduce the cost, an improved FP

measurement analyzer was developed by changing its form and components. An inexpensive complementary metal-oxide semiconductor (CMOS) sensor was used as a detector instead of a CCD camera, and the optical arrangement was changed. First, to confirm the measurement performance, simultaneous FPIAs of 96 mycotoxin samples were conducted using a suitably designed microdevice with the FP analyzer. Additionally, to prove the potential for high-throughput analysis, FPIAs for more than 500 samples were conducted. The results indicated that high-throughput FPIA measurements for mycotoxins were achieved.

5.2 Experimental

5.2.1 Development of a Portable Fluorescence Polarization Analyzer with a Complementary Metal-Oxide Semiconductor Sensor

A portable FP analyzer with a CMOS sensor was built. The detection principle was based on LC-CCD synchronization detection, as mentioned in Ref. 10. It was based on the design of the compact FP system setup [11]. A concept illustration of the setup using the CMOS sensor is shown in Figure 5.1.

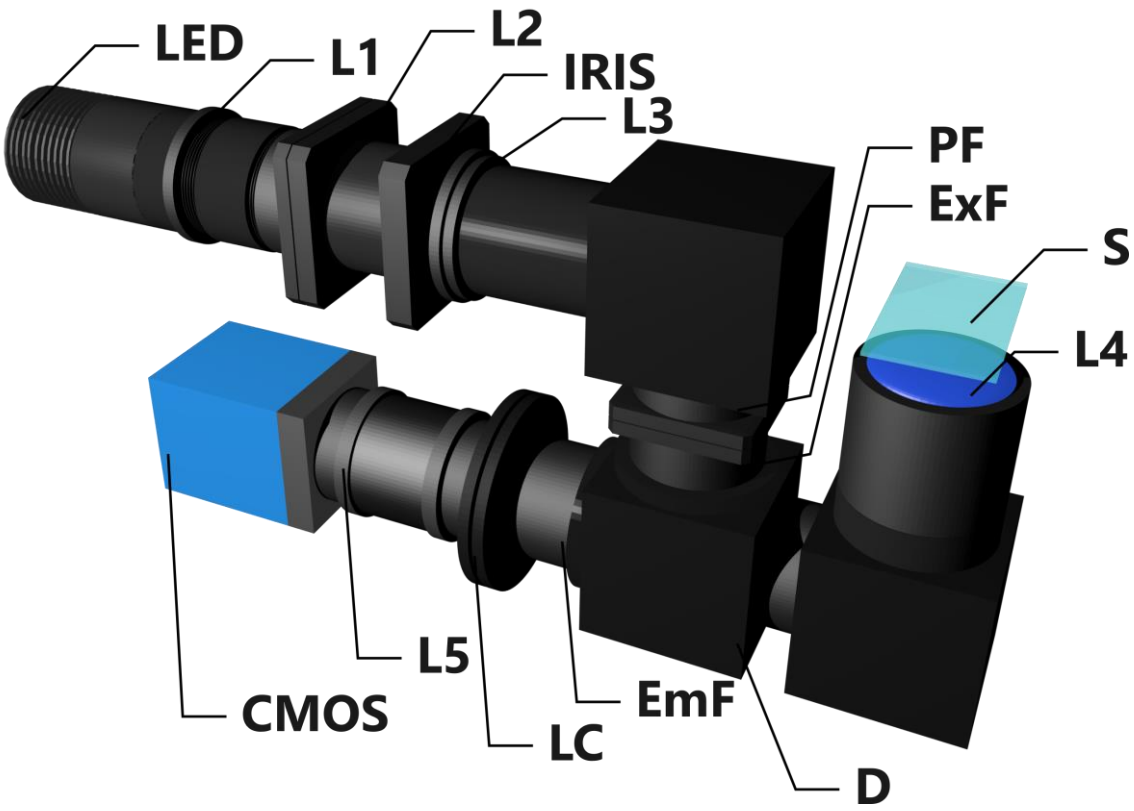

Figure 5.1 Schematic illustration of the experimental setup for the fluorescence polarization analyzer (L: lens; PF: polarizing filter; ExF: excitation filter; D: dichroic mirror; S: sample; and EmF: emission filter).

A 470 nm wavelength LED was employed as the excitation source. In order to collimate the beam, an aspheric condenser lens was used. The excitation beam was introduced into plano-convex lenses and focused on the blades of an iris diaphragm. The iris diaphragm removed the unnecessary beam to create a uniform beam profile. After passing through the iris diaphragm, the beam was collimated again by a condenser lens. The collimated beam was reflected by a prism mirror to compact the instrument, and was then introduced into a linear glass polarizing filter. The polarized excitation beam entered a dichroic block with an excitation filter and a dichroic mirror. The dichroic mirror reflected the excitation beam, and then the beam was also reflected by a prism mirror to compact the instrument. The excitation beam passed through an objective lens and was focused onto a microdevice, which held the samples to be imaged. The microdevice was fabricated using standard soft-lithography techniques with polydimethylsiloxane (PDMS) and a glass slide [13]. The PDMS included black silicon rubber to decrease the background. The sample had an emission wavelength of

approximately 520 nm. The fluorescence signals were collected by the objective lens and then introduced into the dichroic block including the emission filter. After passing through the dichroic mirror and the emission filter, the fluorescence passed through a high-transmittance LC layer (MS-β14A, Tianma Japan, Kawasaki, Japan) with a polarization filter while modulating the polarization. The high-transmittance LC layer, which employed the twisted nematic (TN) mode, was designed as a single pixel. The fluorescence signals were focused on the CMOS image sensor by an imaging lens, and were captured as images. The captured images were processed by the board personal computer (PC) using homebuilt software. The homebuilt software was designed using Microsoft Visual Studio to adjust the CMOS control. The frequency of the high-transmittance LC layer orientation and that of image sampling for CMOS were synchronized using a digital analog converter with a ratio of 1:4. The applied voltage to the high-transmittance LC layer was designed to fit the measurement conditions (60 Hz; < 8 V).

5.2.2 Black Microdevice Fabrication

The microdevice was fabricated using standard soft-lithography techniques with PDMS and a glass slide. The PDMS included black silicon rubber to decrease the background. After mixing the PDMS prepolymer including black silicon rubber and the crosslinking curing agent, which were obtained from a commercially available PDMS kit (Sylgard® 184), at a weight ratio of 10:1, the PDMS was cast on the mold. Figure 5.2 shows photos of the clear PDMS and black PDMS microdevice after curing.

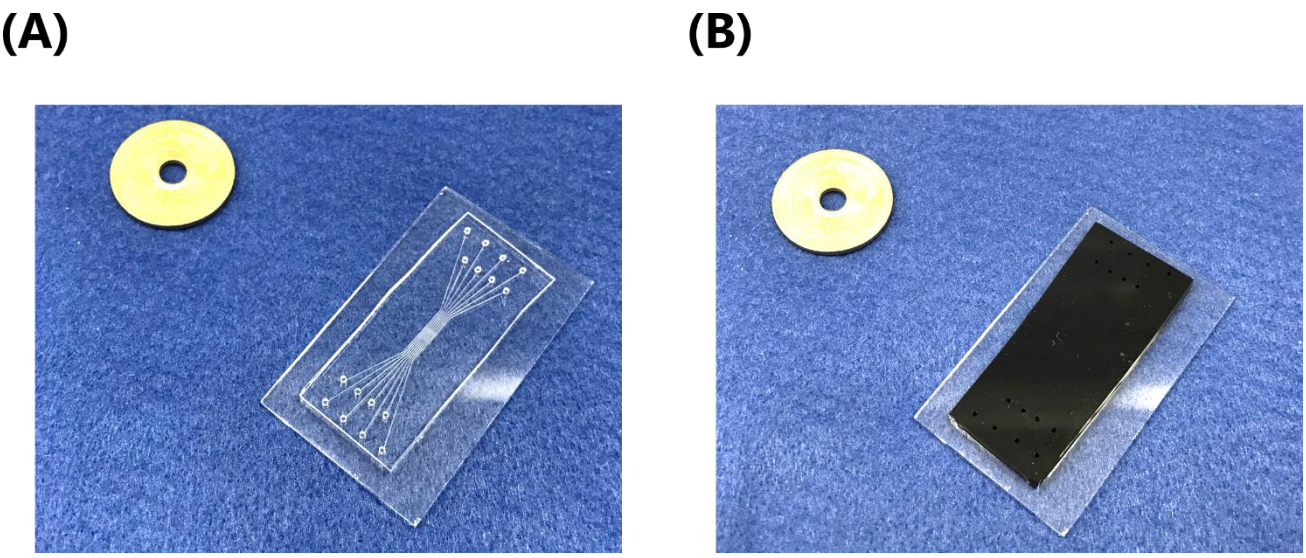

Figure 5.2 Photos of the (A) clear polydimethylsiloxane (PDMS) and (B) black PDMS microdevice.

First, simultaneous FPIAs of 96 mycotoxin samples were conducted. In this experiment, the microdevice had microchannels with individual inlets and outlets to hold eight different samples. Each microchannel was 100 μm wide and 100 μm deep with 12 microchambers. Each microchamber was a square with sides of 100 μm length. The sample filled the microchamber, and then the sample in the microchannel was exhaled by air injection from the inlet. As a result, the samples remained in each microchamber. Figure 5.3 shows a schematic illustration of the design and a fluorescence image of the 96 samples. The microdevice was able to obtain 96 samples in the same field of view.

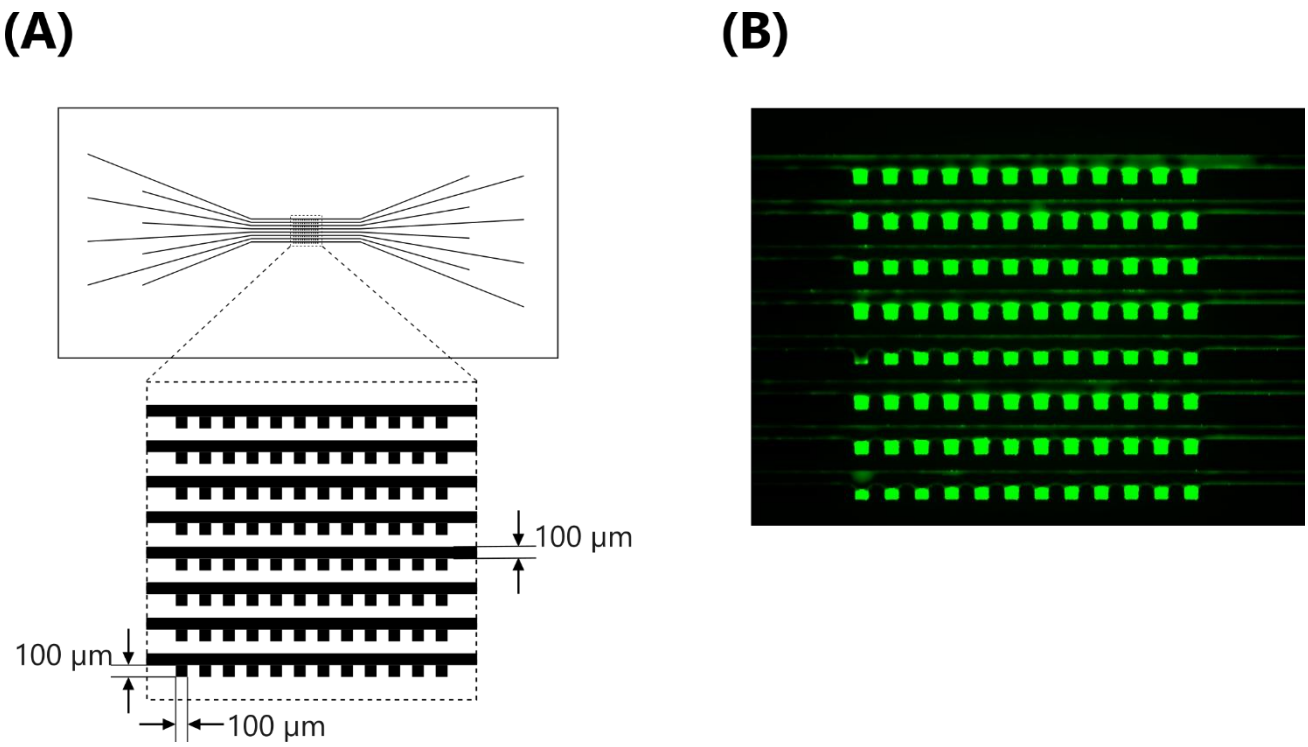

Figure 5.3 Microdevice for measurement of 96 samples. (A) Schematic illustration of the design and (B) a fluorescence image of the remaining 1 mM fluorescein in 96 microchambers. The microdevice could obtain 96 samples in the same field of view of the analyzer.

Second, high-throughput FPIAs for more than 500 samples were conducted to prove the potential for high-throughput analysis. In this experiment, the microdevice had 625 microchambers that were square with a length of 100 μm and depth of 100 μm. The microdevices were filled with the sample by interposing the sample between the PDMS and the glass. Figure 5.4 shows a fluorescence image of 625 independent samples. The excitation beam of the analyzer was irradiated with a circular shape, so the microdevice was able to obtain about 500 samples in the same field of view.

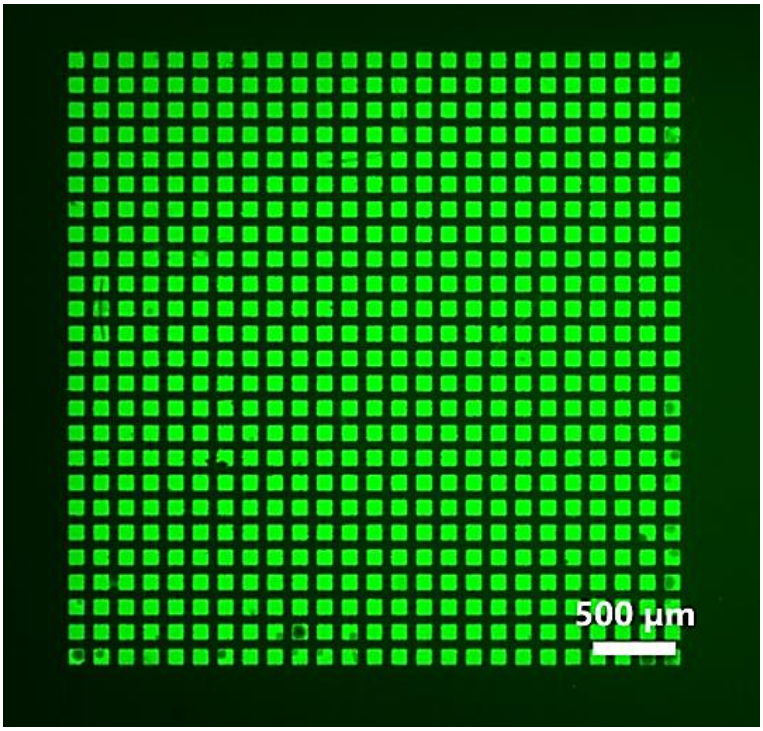

Figure 5.4 Fluorescence image of 625 independent samples. The microchambers were filled with 1 mM fluorescein. The microdevice could obtain more than 500 samples in the same field of view of the analyzer.

5.2.3 Multiple Sample Fluorescence Polarization Immunoassay for Mycotoxin

Simultaneous FPIAs of multiple samples for deoxynivalenol (DON) were demonstrated to evaluate the performance of the developed portable analyzer. The mixture of DON, fluorescein-conjugated DON, and anti-DON antibodies was incubated before sample measurement. The reactions were performed according to the instructions of the commercial DON assay kit manufacturer (Aokin AG, Berlin, Germany). First, the simultaneous FPIA measurements of 8 different DON concentrations (2.4, 4.8, 9.6, 19.2, 38.5, 76.9, 153.8, and 615.4 ng/mL) in 12 chambers (total of 96 samples) were conducted. The measurements were performed in triplicate. Second, the simultaneous FPIA measurements of single DON concentrations (from 2.4 ng/mL to 615.4 ng/mL) in more than 500 chambers were conducted. The measurements were performed in triplicate. FP measurement on a similar sample was also performed using a commercial conventional FP apparatus (FP-715, JASCO Co., Tokyo, Japan) to compare their performance.

5.3 Results and Discussion

5.3.1 Development of a Portable Fluorescence Polarization Analyzer with a CMOS Sensor

Simultaneous FPIAs of multiple samples of DON were demonstrated using the developed portable FP analyzer, a photo of which with an iPhone 7 is shown in Figure 5.5.

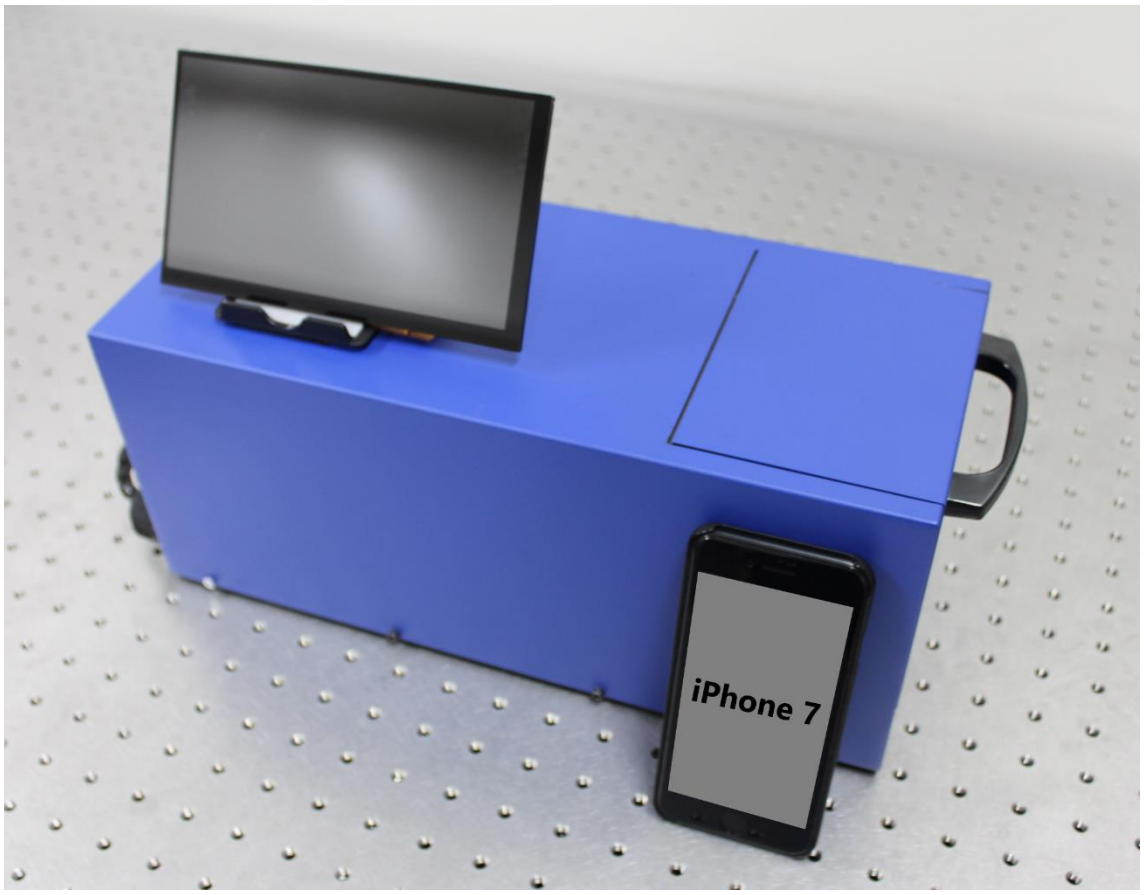

Figure 5.5. Photo of the portable fluorescence analyzer with an iPhone 7.

DON (or vomitoxin; Figure 5.6) is produced by one of the fungal pathogens of grain, namely *Fusarium graminearum*, which causes a disease known as Fusarium head blight [14]. DON has been found in grains such as wheat, corn, rye, rice, and barley worldwide, including in Japan [15]. In particular, DON has been related to two outbreaks of gastrointestinal illness in China and India [16]. In animals, DON has also been

related to immune response depression and blood levels of proteins [17]. Because of its toxicity, the Codex Alimentarius Commission determined a maximum reference value (2 mg/kg in grains for processing) in 2015. The Ministry of Health, Labour and Welfare in Japan also determined a provisional maximum value of 1.1 mg/kg for wheat, and the definitive value is under discussion. Comparing other methods, FPIA has been employed as a rapid and simple method to detect DON concentrations; however, its throughput is low [18]. FPIA demonstrations for DON have been conducted by the apparatus for single [19] or microplate readers, which require optical scanning [20].

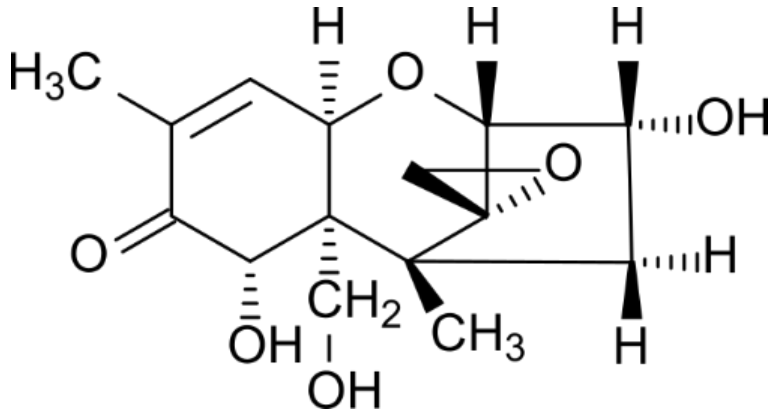

Figure 5.6 Deoxynivalenol (DON; M: 296.32).

5.3.2 Multiple Sample Fluorescence Polarization Immunoassay for Mycotoxin

Here, simultaneous multi-sample FPIAs of DON were demonstrated using the developed portable analyzer that realized FP imaging. First, the simultaneous FPIA measurements of 8 different DON concentrations in 12 chambers (total of 96 samples) were conducted. Figure 5.7 shows typical images obtained by FP imaging of the AC, DC, and *P* of the DON samples. The luminance of the *P* image was gradually changed by the FP values of each sample. Figure 5.8 shows sets of standard curves of FP against DON concentrations (from 2.4 ng/mL to 615.4 ng/mL) obtained by the portable FP analyzer and conventional apparatus. The measurements were performed in triplicate, so each plot of the portable FP analyzer showed

the total results from 288 microchambers. As expected, the relaxation of FP from the 288 microchambers was observed with increasing DON concentration, which is typical for FPIA. Both sets of results were correlated, thereby indicating that simultaneous FPIAs for 96 independent samples were possible with the analyzer. A conventional microplate reader for measurements of 96 samples requires sample scanning, which requires additional complex optical components. However, the analyzer developed here realized FP imaging for all 96 samples as a single two-dimensional image, so scanning was not necessary.

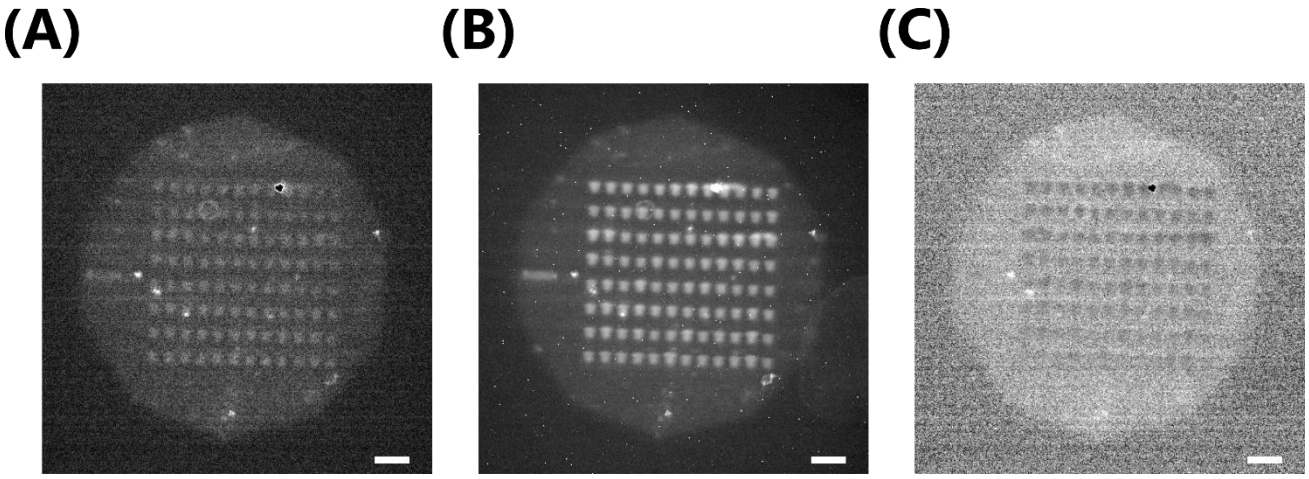

Figure 5.7 Typical images obtained by the fluorescence polarization (FP) analyzer for the deoxynivalenol (DON) FP immunoassays. (A) AC image, (B) DC image, and (C) *P* image of eight different DON concentration samples. Each sample filled 12 microchambers. The scale bars are 300 μm.

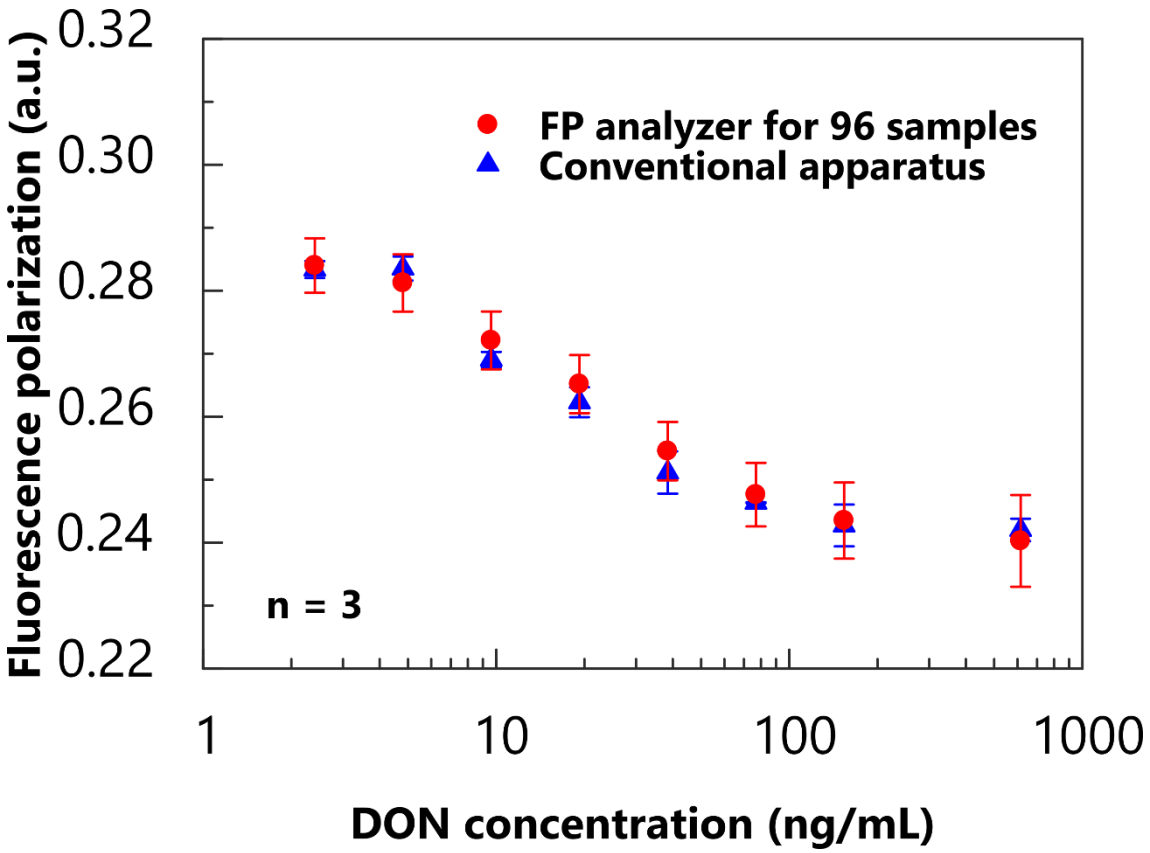

Figure 5.8 Standard curves of fluorescence polarization (FP) against deoxynivalenol (DON) concentrations obtained using the portable FP analyzer and conventional apparatus, which is designed for single sample analysis. The measurements were performed in triplicate, so each plot of the portable FP analyzer shows the total results from 288 microchambers.

Second, the simultaneous FPIA measurements of each DON concentration (from 2.4 ng/mL to 615.4 ng/mL) in more than 500 chambers were conducted. Figure 5.9 shows typical images obtained by the FP analyzer of the AC, DC, and *P* of the DON samples. Figure 5.10 shows sets of standard curves of FP against DON concentrations (from 2.4 ng/mL to 615.4 ng/mL) obtained by the portable FP analyzer and conventional apparatus. The measurements were performed in triplicate, so each plot of the portable FP analyzer shows the total results from 1500-1539 microchambers. Both sets of results were correlated, thereby indicating that simultaneous FPIA for > 500 independent samples was possible with the analyzer.

High-throughput FPIA for mycotoxins was conducted. The larger error bars of the results with the system than those of the results with the conventional FP apparatus were attributed to the detection sensitivity

for fluorescence because the number of pixels for detection was only 100. Through further optimization of the optics (lenses and filters), microdevice design (dimensions), area of the measurement detection (the number of pixels), and detection conditions (CMOS exposure time and detection cycles), among others, improvement in the detection sensitivity is possible. The results showed the features of the portable FP analyzer as high-throughput. The number of samples could be made suitable for the applications by changing the microdevice design. Additionally, the mixer structure was easy to integrate into the microdevice, so mixing for FPIA reactions was also conducted on the FP analyzer [21].

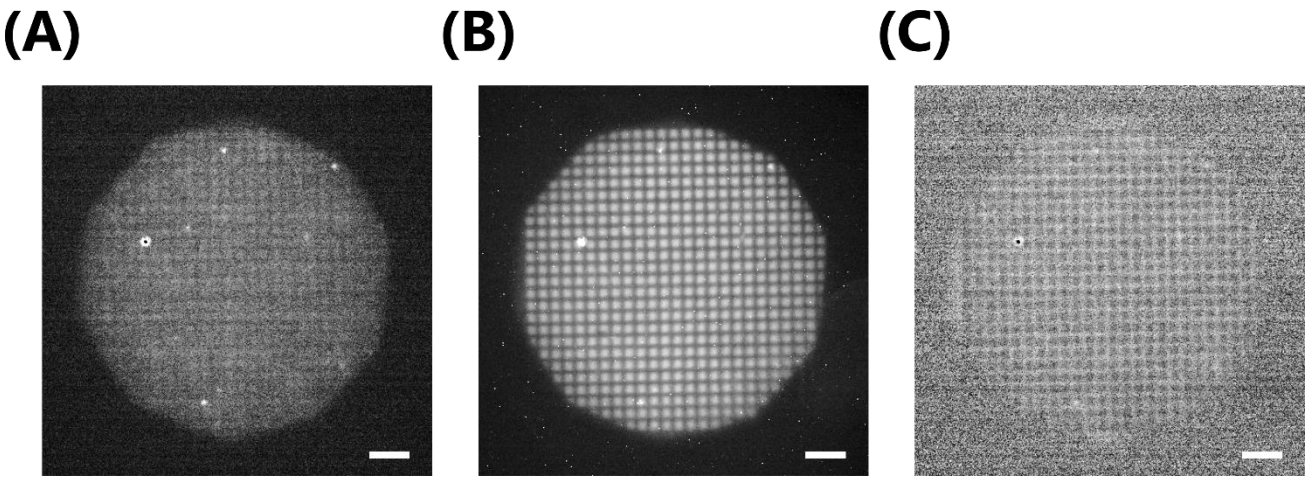

Figure 5.9 Typical images obtained by the fluorescence polarization (FP) analyzer for the deoxynivalenol (DON) FP immunoassay. (A) AC image, (B) DC image, and (C) *P* image of > 500 microchambers filled with single DON concentration samples. The scale bars are 500 μm.

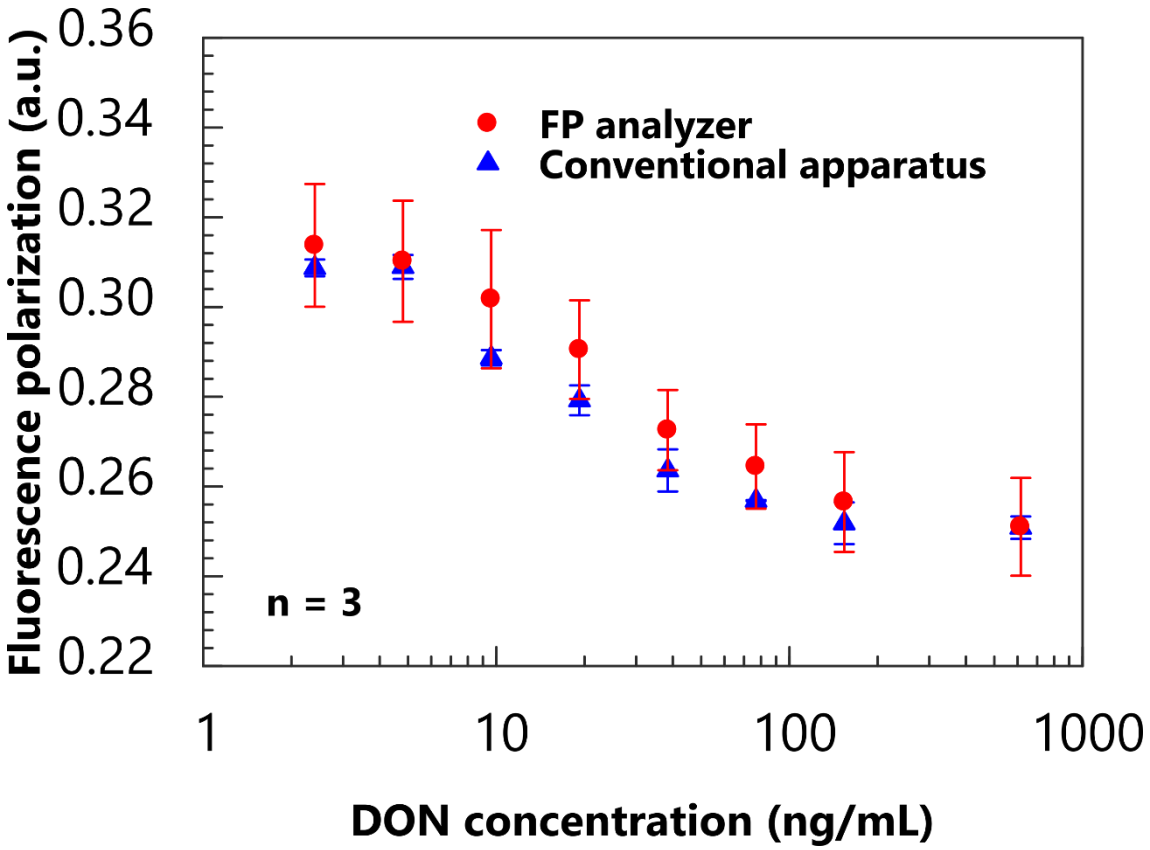

Figure 5.10 Standard curves of fluorescence polarization (FP) against deoxynivalenol (DON) concentrations obtained by the portable FP analyzer and conventional apparatus, which is designed for single sample analysis. The number of microchambers for each measurement was 500-520. The measurements were performed in triplicate, so each plot of the portable FP analyzer shows the total results from 1500-1539 microchambers.

5.4 Conclusions

High-throughput FPIAs for mycotoxins using a portable FP analyzer were conducted. First, simultaneous FPIA measurements for 8 different DON concentrations in 12 chambers (total of 96 samples) were conducted. The results indicated that simultaneous FPIAs for 96 independent samples were possible without any scanning. Second, high-throughput FPIA measurements for single DON concentrations in more than 500 chambers were conducted. The number of samples could be made suitable for the application, and a mixing process could be conducted on the FP analyzer by changing the microdevice design. Table 5.1 shows a comparative table of the abilities of the FP analyzer, conventional commercial apparatus, and microplate-based apparatus. The present analyzer had many advantages compared with the others. The FP analyzer has

a size of 65 cm (W×D×H) and costs less than $5000; however, the FP analyzer has the potential for further downsizing and price reduction by optimizing the optical components and electronics. Furthermore, sample reaction and FP detection can be conducted with the analyzer by changing the microdevice. Features such as the low cost and portability of the analyzer will contribute to on-site measurement and point-of-care testing. In particular, the on-site measurement for mycotoxins is valuable for easily checking grain growth. Additionally, the high-throughput feature of the analyzer will contribute to the study of molecular interactions. The measurement throughput of the portable FP analyzer was still low because the measurement time has not been optimized. The measurement time has the potential to be much higher through optimization of the exposure time, frequencies, and microdevice design. Recently, some studies on molecular interactions, such as protein-protein, protein-DNA, and protein-ligand binding interactions, employed FP measurement because of its simplicity [22-24]. The FP analyzer will be able to conduct high-throughput sample reaction and FP detection, so only sample injections will need to be handled by researchers. Therefore, the portable FP analyzer with high-throughput has the potential to contribute to various researchers and consumers.

Table 5.1 Comparative table of the abilities of the fluorescence polarization (FP) analyzer, conventional commercial apparatus, and microplate-based apparatus.

System	Developed FP analyzer	Conventional apparatus	Microplate reader
Appearance			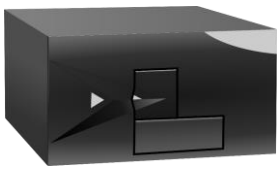
Size (W×H×D mm^3) Weight	350×150×100, 5.5 kg	297×220×420, ~20 kg	425×253×457, 14 kg
Polarizer	LC	Filter	Filter
Detector	CMOS	PMT	PMT
Number of samples	>500 at a time	1	96
Measurement throughput*	5.0 samples/s	0.5 samples/s	4.8 samples/s
Precision**	<11.0% for 1 sample [25] < 24.5% for 500 samples	< 8.1%	***
Cost	<$5000	~$10000	~$30000
Portability	✓	×	×
Mix	✓ ****	×	✓

*The measurement throughput was calculated from the ratio of the number of samples at a time to the measurement time.

**The precision was calculated from the ratio of error bars to the dynamic range of deoxynivalenol measurement. For single sample detection, the precision (< 11%) was almost the same as that of the conventional apparatus [25].

***No results were obtained for the microplate-based apparatus in the same measurement conditions.

****The mixing process can be integrated by changing the microdevice design.

References

[1] J. R. Lundblad, M. Laurance, and R. H. Goodman, *Mol. Endocrinol.*, **10**, 607 (1996)

[2] K. Kakehi, Y. Oda, and M. Kinoshita, *Anal. Biochem.*, **297**, 111 (2001)

[3] D. M. Jameson and S. E. Seifried, *Methods*, **19**, 222 (1999)

[4] T. Tachi, N. Kaji, M. Tokeshi, and Y. Baba, *Lab. Chip.*, **9**, 966 (2009)

[5] T. Tachi, T. Hase, Y. Okamoto, N. Kaji, T. Arima, H. Matsumoto, M. Kondo, M. Tokeshi, Y. Hasegawa, and Y. Baba, *Anal. Bioanal. Chem.*, **401**, 2301 (2011)

[6] Q. Wan and X. C. Le, *Anal. Chem.*, **72**, 5583 (2000)

[7] J. Choi, D. Kang, H. Park, A. J. deMello, and S. Chang, *Anal. Chem.*, **84**, 3849 (2012)

[8] J. C. Owicki, *Biomol. Screen.*, **5**, 297 (2000)

[9] J. A. Cruz-Aguado and G. Penner, *Anal. Chem.*, **80**, 8853 (2008)

[10] O. Wakao, Y. Fujii, M. Maeki, A. Ishida, H. Tani, A. Hibara, and M. Tokeshi, *Anal. Chem.*, **87**, 9647 (2015)

[11] O. Wakao, K. Satou, A. Nakamura, K. Sumiyoshi, M. Shirokawa, C. Mizokuchi, K. Shiota, M. Maeki, A. Ishida, H. Tani, K. Shigemura, A. Hibara, and M. Tokeshi, *Rev. Sci. Instrum.*, **89**, 24 103 (2018)

[12] O. Wakao, K. Sumiyoshi, C. Mizokuchi, M. Maeki, A. Ishida, H. Tani, K. Shigemura, A. Hibara, and M. Tokeshi, *Proc. of MicroTAS 2017*, 557-558 (2017)

[13] M. Maeki, T. Saito, Y. Sato, T. Yasui, N. Kaji, A. Ishida, H. Tani, Y. Baba, H. Harashima, and M. Tokeshi, *RSC Adv.*, **5**, 46 181 (2015)

[14] C. M. Maragos and R. D. Platter, *J. Agric. Food Chem.*, **50**, 1827-1832 (2002)

[15] C.M. Placinta, J. P. F. D'Mello, and A. M. C. Macdonald, *Anim. Feed Sci. Technol.*, **78**, 21-37 (1999)

[16] R. V. Bhat, S. R. Beedu, Y. Ramakrishna, and K. L. Munshi, *Lancet*., **7**, 35-37 (1989)

[17] J. P. F. D'Mello, C. M. Placinta, and A. M. C. Macdonald, *Anim. Feed Sci. Technol.*, **80**, 183-205 (1999)

[18] M. Z. Zheng, J. L. Richard, and J. Binder, *Mycopathologia*, **161**, 261-273 (2006)

[19] M. S. Nasir and M. E. Jolley, *Comb. Chem. High Throughput Screen*., **6**, 267-273 (2003)

[20] C. Li, K. Wen, T. Mi, X. Zhang, H. Zhang, S. Zhang, J. Shen, and Z. Wang, *Biosens. Bioelectron.*, **79**, 258-265 (2016)

[21] N. Kimura, M. Maeki, Y. Sato, Y. Note, A. Ishida, H. Tani, H. Harashima, and M. Tokeshi, *ACS Omega.*, **3**, 5044-5051 (2018)

[22] W. A. Lea and A. Simeonov, *Expert Opin. Drug Discov.*, **6**, 17-32 (2012)

[23] D. M. Jameson and J. A. Ross, *Chem. Rev.*, **110**, 2685-2708 (2010)

[24] M. M. Makowski, C. Gräwe, B. M. Foster, N. V. Nguyen, T. Bartke, and M. Vermeulen, *Nat. Commun.*, **9**, 1653 (2018)

[25] O. Wakao, A. Nakamura, K. Satou, C. Mizokuchi, K. Sumiyoshi, M. Maeki, A. Ishida, H. Tani, K. Shigemura, A. Hibara, and M. Tokeshi, *Proc. Of IEEE-NANOMED 2018*, **1**, 57-58 (2018)

CHAPTER 6 Conclusions and Future Prospects

In the present research, a measurement system that enables simultaneous fluorescence polarization (FP) measurement of multiple samples was developed. The system was based on the synchronization detection between the orientation of the liquid crystal (LC) molecules and the sampling frequency of an image sensor (charge coupled device (CCD) or complementary metal-oxide semiconductor (CMOS) sensor).

In Chapter 2, the FP measurement system was proposed and proven by a proof-of-concept experiment on the viscosity dependence of FP of fluorescein samples in water-ethylene glycol solution and another experiment on the FP immunoassay (FPIA) of prostaglandin E2 (PGE2) samples. The measurement principle of FP was based on the synchronization detection between the orientation of the LC layer of the LC display (LCD) and the sampling frequency of a CCD image sensor. As a result, the measurement performance was equal to that of a conventional apparatus designed for single sample analysis. The results are the first descriptions of the simultaneous FP measurement of multiple samples using FP imaging. The system has great potential for equipment miniaturization and price reduction as well as for providing simultaneous FP measurements of multiple samples.

In Chapter 3, the optimization of synchronization mismatch conditions toward improvement of the sensitivity of the FP system was conducted. Experimental and theoretical investigations on the influence of the synchrony between LC switching and CCD image sampling for measured values were demonstrated for synchronization optimization. The theoretical values with several synchronization mismatches at certain numbers of measurement cycles were calculated. In the presence of synchronization mismatches, the timings of the synchronization between LC switching and CCD image sampling were intentionally unsynchronized to reveal their respective influences. When there was synchronization mismatch, the experimental FP values obtained using fluorescein ethylene glycol solution and the theoretical FP values were changed according to the number of measurement cycles. Additionally, to establish a prediction method for the optimum conditions, FPIAs for PGE2 as model samples under the same synchronization mismatch conditions were demonstrated. The synchronization mismatch influenced the measurement performance of the system, thereby indicating that optimization of the number of image samplings is necessary to improve the measurement performance. For

instance, for the mismatch 0.99 case, the measurement cycle should be 50 cycles judging from its dynamic range and R^2 value. However, the behavior may potentially be applicable as a frequency filter for image analysis.

In Chapter 4, the system based on the synchronization principle was downsized and improved. The FP system realized simultaneous multi-sample detection; however, the measurement precision was lower than that of the conventional FP apparatus, as discussed in Chapter 2. The main drawbacks were low light transmittance of the LC layer and insufficient synchronization between the LC layer and CCD. Therefore, a new compact FP system was developed. By using a newly designed LC with high transmittance and improving synchronization, the performance of the system was significantly improved. Additionally, the cost was reduced by using an inexpensive CCD and a light emitting diode (LED) as the excitation source. In the FPIA for PGE2, the error rate of the FP system was reduced from 16.9% to 3.9%, which was comparable to the commercial conventional FP system.

In Chapter 5, in order to further downsize and reduce the cost, an improved FP measurement analyzer was developed by changing its form and components. An inexpensive CMOS sensor was used as the detector instead of the CCD camera, and the optical arrangement was changed. Additionally, the high-throughput FPIA for deoxynivalenol (DON) using the portable FP analyzer was conducted by changing the microdevice. First, simultaneous FPIA measurements for 8 different DON concentrations in 12 chambers (total of 96 samples) were conducted. The results indicated that simultaneous FPIA for 96 independent samples was possible without any scanning. Second, high-throughput FPIA measurements for single DON concentrations in more than 500 chambers were conducted. The number of samples was suitable for the application, and the mixing process could be conducted on the FP analyzer by changing the microdevice design. The portable analyzer had a size within 65 cm (W×D×H) and cost less than $5000; however, the FP analyzer has the potential for further downsizing and price reduction by optimizing its optical components and electronics.

The combination of the key features of the FP method, namely the short reaction time and ease of use, and the key features of the FP analyzer, namely portability, low cost, and high-throughput, will contribute to various research fields. The combination of these features will realize rapid and low-cost detection, so the

analyzer will contribute to on-site measurements for food samples and point-of-care testing for human liquids. In particular, on-site measurements for mycotoxins in grains is valuable in Hokkaido, which is responsible for about 50% of Japan's total production of wheat and corn. Additionally, features such as the high-throughput of the analyzer will contribute to the study of molecular interactions. The FP analyzer will be able to integrate mixing for sample reaction, so researchers will only need to handle sample injection. Moreover, in the study of molecular interactions, some expensive reagents are used. The sample volume of the DON FPIA demonstration using the FP analyzer was 1 nL, so the total cost for analysis will be significantly reduced. Further, the FP imaging has great potential for application in interactions analysis for cells. The principle of the synchronization will be advantageous for fluorescence imaging. The synchronization operation filtrates the signal of the interactions from the background, as mentioned in Chapter 3, so the interactions in cells are directly observed. Therefore, the portable FP analyzer with high-throughput has the potential to contribute to various researchers and customers.

List of Papers

[1] Osamu Wakao, Yusaku Fujii, Masatoshi Maeki, Akihiko Ishida, Hirofumi Tani, Akihide Hibara, and Manabu Tokeshi, "Fluorescence Polarization Measurement System Using a Liquid Crystal Layer and an Image Sensor," **Analytical Chemistry**, 87, 9647-9652 (2015) doi: 10.1021/acs.analchem.5b01164

[2] Osamu Wakao, Ken Satou, Ayano Nakamura, Ken Sumiyoshi, Masanori Shirokawa, Chikaaki Mizokuchi, Kunihiro Shiota, Masatoshi Maeki, Akihiko Ishida, Hirofumi Tani, Koji Shigemura, Akihide Hibara, and Manabu Tokeshi, "A Compact Fluorescence Polarization Analyzer with High-Transmittance Liquid Crystal Layer," **Review of Scientific Instruments**, 89, 024103 (2018) doi: 10.1063/1.5017081

[3] Osamu Wakao, Masatoshi Maeki, Akihiko Ishida, Hirofumi Tani, Akihide Hibara, and Manabu Tokeshi, "Sensitive Fluorescent Polarization Immunoassay by Optimizing Synchronization Mismatch Condition," **Sensors and Actuators B: Chemical**, 285, 418-422 (2019)

[4] Osamu Wakao, Ken Satou, Ayano Nakamura, Polina Galkina, Keine Nishiyama, Ken Sumiyoshi, Fumio Kurosawa, Masatoshi Maeki, Akihiko Ishida, Hirofumi Tani, Mikhail A. Proskurnin, Koji Shigemura, Akihide Hibara, and Manabu Tokeshi, "High-throughput Fluorescence Polarization Immunoassay by Using a Portable Fluorescence Polarization Imaging Analyzer," Manuscript in preparation

[5] Osamu Wakao, Yusaku Fujii, Akihiko Ishida, Hirofumi Tani, Akihide Hibara, and Manabu Tokeshi, "LCD-CCD Synchronization Detection for Fluorescence Polarization Immunoassay," **Proceedings of Micro Total Analysis System 2014**, 1, 2271-2273 (2014)

[6] Osamu Wakao, Masatoshi Maeki, Akihiko Ishida, Hirofumi Tani, Akihide Hibara, and Manabu Tokeshi, "Fluorescence Polarization Imaging for Multisample Immunoassay," **Proceedings of Micro Total Analysis System 2015**, 1, 1816-1818 (2015)

[7] Osamu Wakao, Masatoshi Maeki, Akihiko Ishida, Hirofumi Tani, Akihide Hibara, and Manabu Tokeshi, "Fluorescence Polarization-Based Multiple Samples Detection Using Microchamber Array Towards High-Throughput Molecular Interaction Analysis," **Proceedings of Micro Total Analysis System 2016**, 1, 1400-1401 (2016)

[8] Osamu Wakao, Masatoshi Maeki, Akihiko Ishida, Hirofumi Tani, Akihide Hibara, and Manabu Tokeshi, "Development of a Fluorescence Polarization-Based High-Throughput Assay System for Molecular Interaction Screening," **Proceedings of Microprocesses and Nanotechnology Conference 2016**, 1, 10P-7-82 (2016)

[9] Osamu Wakao, Ken Sumiyoshi, Chikaaki Mizokuchi, Masatoshi Maeki, Akihiko Ishida, Hirofumi Tani, Koji Shigemura, Akihide Hibara, and Manabu Tokeshi, "High-Throughput Fluorescence Polarization Measurement System Towards Molecular Interaction Analysis," **Proceedings of Micro Total Analysis System 2017**, 1, 557-558 (2017).

[10] Osamu Wakao, Ayano Nakamura, Ken Satou, Chikaaki Mizokuchi, Ken Sumiyoshi, Masatoshi Maeki, Akihiko Ishida, Hirofumi Tani, Koji Shigemura, Akihide Hibara, and Manabu Tokeshi, "Small-Size Low-Cost High-Throughput Fluorescence Polarization Analyzer for Multisample Immunoassay in Food

Testing," **Proceedings of the 12th IEEE Int. Conf. on Nano/Molecular Medicine and Engineering (IEEE-NANOMED 2018)**, 1, 57-58 (2018)

[11] Osamu Wakao, Masatoshi Maeki, Akihide Hibara, and Manabu Tokeshi, "Fluorescence Polarization Imaging for Multisample Immunoassay Using Liquid Crystal Display," **Chemical Engineering** (in Japanese), 61, 12-17 (2016)

[12] Osamu Wakao, Ken Sumiyoshi, Chikaaki Mizokuchi, Masatoshi Maeki, Akihiko Ishida, Hirofumi Tani, Koji Shigemura, Akihide Hibara, and Manabu Tokeshi, "Development of a Multisample Simultaneous Fluorescence Polarization Measurement System for Molecular Interaction Measurements," **Proceedings of the Sensor Symposium on Sensors, Micromachines, and Applied Systems** (in Japanese), 1, 02pm1-PS-235 (2017)

Patent

[1] Light polarization analyzer PCT/JP2015/063282 US Patent 9719927

Osamu Wakao, Manabu Tokeshi, Akihide Hibara

Acknowledgments

This thesis is the result of the author's research in the Bioanalytical Chemistry Laboratory, Graduate School of Chemical Sciences Engineering, Hokkaido University. Reaching this point of my life would have been impossible without the many important people who supported me along the way, and my deepest gratitude goes out to all of them.

First, I would like to express my sincerest respect and gratitude to my supervisor, Professor Manabu Tokeshi of the Division of Applied Chemistry, Faculty of Engineering, Hokkaido University for his guidance and wisdom, meaningful advice, and continuous support and encouragement as I took on the challenges of pursuing my PhD degree. He gave me not only a view of research, but also a view of life. I doubt that I will ever be able to convey my appreciation fully, but I owe him my eternal gratitude.

I am deeply grateful and proud that I am part of the Bioanalytical Chemistry Laboratory (Tokeshi Lab). I am especially grateful to Associate Professor Hirofumi Tani, Assistant Professor Akihiko Ishida, and Assistant Professor Masatoshi Maeki of the lab for all their assistance, advice, and valuable discussions. Very special thanks go out to Prof. Ishida for providing me with his precious advice, which was like a father's words. Also, very special thanks go out to Prof. Maeki for providing me with precious technical advice and for our journeys together to many academic conferences.

I would like to acknowledge Associate Professor Hirofumi Tani, Professor Toshifumi Satoh, and Professor Toshihiro Shimada of the Faculty of Engineering, Hokkaido University, and Professor Koichiro Ishimori of the Faculty of Science, Hokkaido University for accepting the responsibility of being my official co-supervisors.

For his extraordinary technical advice and support, I acknowledge Professor Akihide Hibara of the Institute of Multidisciplinary Research for Advanced Materials, Tohoku University. He provided me with

precious technical advice about the CCD synchronous detection method, which is the essence of this research, so I am deeply grateful to him.

I also acknowledge Assistant Professor Mao Fukuyama, Mr. Fumio Kurosawa, and Mr. Yusaku Fujii of Hibara Lab. Prof. Fukuyama and Mr. Kurosawa supported the development of the software and provided me with kind advice. Mr. Fujii has conducted prior research that built the foundation of my research.

I appreciated the opportunity to develop the system with the members of the development team of Tianma Japan, Ltd. I would like to thank Mr. Koji Shigemura, Mr. Ken Sumiyoshi, Mr. Seiji Suzuki, Mr. Chikaaki Mizokuchi, Mr. Ken Satou, Mr. Masanori Shirokawa, Mr. Kunihiro Shiota, Ms. Sanae Furuya, Mr. Ayuko Imai, Mr. Kazunori Masumura, and Mr. Sho Onose, who motivated me by being interested in my research. I am very proud of this in my research career.

I would like to acknowledge Professor Sergei A. Eremin of Moscow State University in Russia. He provided me with valuable reagents for the FPIA and kind advice.

I would like to acknowledge the Grant-in-Aid from the Japan Society for the Promotion of Science Fellows and the support by the JST-SENTAN program.

Through my research, I attended many academic conferences. Thanks to all the professors, students, and participants, I received great stimulation and experiences through the conference presentations and traveling for international conferences. In particular, I deeply thank each member of the Baba Lab of Nagoya University, Kitamori Lab of University of Tokyo, Sato Lab of Gunma University, and the many people that I had delightful dinners with; these are my lovely memories of the conferences.

I would also like to thank my labmates Taiga Ajiri, who worked with me in the lab like a brother and made my lab life especially happy, Keine Nishiyama, Yuusuke Nakatani, Donny Nugraha Mazaafrianto, Daiki Arai, Yuki Hanada, Koto Aoki, Ayako Kurishiba, Ryusuke Saito, Jun Sekiya, Nanako Nishiwaki, Lori Shayne A. Busa, Saeed Mohammadi, Yuka Fujishima, Fumiya Sakai, Kastuki Fukamachi, Yuto Kikuchi, Takeshi Komastu, Seiya Nakamata, Daichi Fujii, Shohei Yamazaki, Kota Kikuchi, Niko Kimura, Yuki Kudo, Saya Sato,

Ryohei Mizukami, Yi Bao, Yuri Moratelli Piske, Shingo Ikeda, Kazuki Shimizu, Ayano Nakamura, Koki Hoshikawa, Yang Yi, Issei Takata, Reo Takeda, Takuma Nishimura, Ryoga Maeda, and Chen po-sheng, and our lab secretaries Michiko Tani-San and Kokoro Haruki-San. I would like to give special thanks to Koto, who worked on prior related research. I am also extremely grateful for Ayano's devoted hard work on related research, and I wish her happiness and success in her research.

I would like to thank my friends, as they made me think of Hokkaido as my second hometown. Finally, I would like to give a big thank you to my family, as they provided me with the opportunity to study far from my original hometown, and they always support me.